Universität für Bodenkultur Wien
University of Natural Resources and Life Science, Vienna

Department of Water, Atmosphere and Environment
Institute for Hydrology and Water Management

MASTERARBEIT / MASTER THESIS

Analyses of diurnal discharge fluctuations in forested micro-watersheds

(Lehrforst Rosalia)

verfasst von / submitted by

Stecher Gabriel, B.Sc.

zur Erlangung des akademischen Grades / in partial fullfilment of the requirements for the degree of

Diplomingenieur (Dipl.-Ing.)

Wien / Vienna 06.04.2021

Supervisor: Josef Fürst, Ao.Univ.Prof. Dipl.-Ing. Dr.nat.techn.

Co-Supervisors: Reinhard Nolz, Priv.-Doz. Dipl.-Ing. Dr.nat.techn.

Mathew Herrnegger, Dipl.-Ing. Dr.nat.techn.

Affirmation / Eidesstattliche Erklärung

I hereby declare that I am the sole author of this work. No assistance other than that permitted has been used. Ideas and quotes taken directly or indirectly from other sources are identified as such. This written work has not yet been submitted in any part.

Ich erkläre eidesstattlich, dass ich die Arbeit selbständig angefertigt habe. Es wurden keine anderen als die angegebenen Hilfsmittel benutzt. Die aus fremden Quellen direkt oder indirekt übernommenen Formulierungen und Gedanken sind als solche kenntlich gemacht. Diese schriftliche Arbeit wurde noch an keiner Stelle vorgelegt.

Stecher Gabriel

Acknowledgements

An dieser Stelle möchte ich mich bei meinen Betreuern, Ao.Univ.Prof. Dipl.-Ing. Dr.nat.techn. Josef Fürst, Priv.-Doz. Dipl.-Ing. Dr.nat.techn. Reinhard Nolz und Dipl.-Ing. Dr.nat.techn. Mathew Herrnegger, die mich bei Fragen stets umfangreich beraten haben, herzlichst bedanken. Deren Anmerkungen und hilfreiche Betreuung haben stets zur Verbesserung dieser Arbeit beigetragen. Da die vorliegende Arbeit während der COVID 19 Pandemie verfasst wurde, möchte ich mich vor allem für die unkomplizierte Betreuung unter den außergewöhnlichen Rahmenbedingungen bedanken.

Ganz besonders möchte ich meiner Familie danken, die mich jederzeit unterstützt und mir mein Studium erst ermöglicht hat. Besonders möchte ich mich hier bei meinen Eltern bedanken, die mich nicht nur finanziell unterstützt haben, sondern mir auch jederzeit als wichtige Ansprechpartner abseits des Studiums zur Seite standen.

Darüber hinaus möchte ich mich bei all meinen Studienfreunden, die zu sehr guten Freunden geworden sind, bedanken. Durch sie wurde das Studium zu einer sehr schönen Zeit, die ich nie missen werde und die mich auch auf persönlicher und vielen anderen Ebenen sehr bereichert hat. Dies gilt auch für alle Freunde, Verwandte und Mitbewohnerinnen, die immer ein offenes Ohr für mich hatten, und mir während der Masterarbeit und auch in anderen Lebensphasen zur Seite standen.

Abstract

Discharge is observed at four gauging stations established from 2015 to 2018 in the hydrological research watershed Rosalia. The experimental watershed includes small sub-watersheds (9, 27, 146, 222 ha). Additionally to the discharge measurements, precipitation, relative humidity, air, water and soil temperature, soil water content, and electrical conductivity are monitored in the Rosalia at several locations. At all gauging stations, pronounced diurnal discharge fluctuations are observed. They mainly occur in low flow periods during precipitation-free days from spring until autumn. This thesis aims to analyse the observed diurnal discharge fluctuations and investigate the processes causing this phenomenon in forested micro-watersheds like the Rosalia.

Following a detailed time series analysis of relevant hydro-meteorological obervations, the HYDRUS model was setup for a transect in the headwaters of the catchment to develop a better understanding of the underlying processes causing this phenomenon. HYDRUS is a software package for simulating water, heat, and solutes movement in two- and three-dimensional variably saturated porous media.

It was found that at all gauging stations daily discharge amplitudes show a clear seasonal pattern. The largest amplitudes of up to 29 %, compared to the mean discharge, occur during the summer months. During winter, diurnal discharge fluctuations are hardly present. Diurnal discharge fluctuations are characterised by early morning maximum flows at around 6 a.m. and afternoon minimum flows at around 3:30 p.m.. Analogous analyses for soil water content and air temperature revealed a clear relationship with discharge fluctuations on a seasonal and daily temporal scale. The interrelation between air temperature, soil water content and discharge implicates evapotranspiration, with transpiration dominant, as the primary linking process causing fluctuations in diurnal discharge.The root water uptake of the riparian vegetation thereby acts as an additional boundary condition. This is also confirmed in the HYDRUS simulations. A sensitivity analysis of the root distribution showed that the riparian vegetation within a distance of 8 m from the creek is influencing the discharge. Riparian root water uptake and the corresponding transpiration proved to be the main factors

causing diurnal discharge fluctuations. Simulations also showed a mean reduction of actual transpiration by 25% along the simulated transect, when vegetation and riparian root water uptake are removed. Furthermore, four sets of parameters (van Genuchten) of soil hydraulic properties, based on ten soil samples, were estimated and used in the HYDRUS model . Based on a sensitivity analysis of the estimated soil hydraulic properties, it could be shown that these have no influence on the general occurrence of the diurnal discharge fluctuations. However, the magnitude of the simulated fluctuations changed with the different soil hydraulic properties by up to more than 50 %.

Therefore, it was proved that root water uptake of the riparian vegetation is the most important process causing the diurnal discharge fluctuations in the experimental research watershed Rosalia.

Kurzfassung

Im forsthydrologischen Versuchsgebiet Rosalia der BOKU wird seit 2015 der Abfluss in hoher zeitlicher Auflösung gemessen. Die vier Pegel, die von 2015 bis 2018 errichtet wurden, teilen das Gesamteinzugsgebiet in vier Teileinzugsgebiete (9, 27, 146, 222 ha). Zusätzlich zu den Abflussmessungen werden in der Rosalia Niederschlag, relative Luftfeuchte, Luft-, Wasser- und Bodentemperatur, Bodenwassergehalt und elektrische Leitfähigkeit gemessen.

An allen Pegeln sind ausgeprägte tageszeitliche Abflussschwankungen zu beobachten. Diese treten vor allem in Niedrigwasserperioden während niederschlagsfreien Tagen vom Frühjahr bis Herbst auf. Das Ziel dieser Arbeit ist es, die beobachteten täglichen Abflussschwankungen umfassend zu analysieren und die wichtigsten Prozesse zu untersuchen, die dieses Phänomen verursachen. Die Prozesse, die die täglichen Abflussschwankungen verursachen, werden mit Hilfe des Softwarepakets HYDRUS modellhaft abgebildet und beschrieben.

Die täglichen Abflussamplituden zeigen an allen Pegeln im Einzugsgebiet ein klares saisonales Muster. Die größten Amplituden treten in den Sommermonaten auf. Außerdem sind die täglichen Abflussschwankungen durch frühmorgendliche Maximalabflüsse und nachmittägliche Minimalabflüsse gekennzeichnet. Ähnliche Analysen für den Bodenwassergehalt und die Lufttemperatur ergaben eine klare saisonale und tägliche Beziehung mit den Abflussschwankungen. Aufgrund der Wechselbeziehung zwischen Temperatur, Bodenwassergehalt und Abfluss können die auftretenden täglichen Abflussschwankungen mit der Evapotranspiration, insbesondere mit der Transpiration erklärt werden. Die beobachteten Schwankungen werden also in erster Linie durch die Wurzelwasseraufnahme der Ufervegetation verursacht, die dann den Abfluss reduziert. Die Ergebnisse der HYDRUS-Simulation bestätigen, dass die tageszeitlichen Abflussschwankungen in erster Linie auf die Wurzelwasseraufnahme im ufernahen Bereich zurückgeführt werden können. Basierend auf einer Sensitivitätsanalyse der Wurzelverteilung konnte der abflussbeeinflussende Bereich der begleitenden Ufervegetation auf bis zu 8 m bestimmt werden. Daher kann die Wurzelwasseraufnahme und die folgende

Transpiration im Uferbereich als Hauptfaktor, der zu den täglichen Abflussschwankungen führt, bestimmt werden. Die Simulationen zeigen auch eine mittlere Verringerung der aktuellen Transpiration um 25% entlang des simulierten Hangtransekts, wenn die Vegetation und die Wasseraufnahme entlang des Ufers entfernt werden. Darüber hinaus wurden vier Parametersätze (van Genuchten) der hydraulischen Bodeneigenschaften, auf der Grundlage von zehn Bodenproben geschätzt und im HYDRUS Modell verwendet. Aufgrund einer Sensitivitätsanalyse der hydraulischen Bodeneigenschaften konnte gezeigt werden dass diese keinen Einfluss auf das grundsätzliche Auftreten der täglichen Abflussschwankungen haben. Allerdings änderte sich die Amplitude der simulierten Fluktuationen mit den variierenden hydraulischen Bodeneigenschaften um bis zu über 50%.

Daher wurde die Wurzelwasseraufnahme der Ufervegetation als der wichtigste Prozess nachgewiesen, der die täglichen Abflussschwankungen im forsthydrologischen Vesuchsgebiet Rosalia verursacht.

Content

1 Introduction

This work aims to describe and explain the diurnal discharge fluctuations in the hydrological research watershed Rosalia. Processes causing diurnal discharge fluctuations are comprehensively investigated, and the software package HYDRUS is applied to simulate and model processes leading to diurnal discharge fluctuations. HYDRUS is a software package that simulates water, heat, and solute movement in two- and three-dimensional variably saturated media.

1.1 Background and Objectives

The BOKU university forest Rosalia has been used for research and education since 1875. Based on an initiative by researchers of various disciplines, the forestry research was extended in 2013, and a hydrological research watershed was added (BOKU - Institute of Hydrology and Water Management, 2020). Since 2015, hydrological data, including discharge, air, water and soil temperature , soil water content, relative humidity, precipitation, and electrical conductivity, are observed at four locations in a high temporal resolution (10 min). At all gauging stations, distinct diurnal discharge fluctuations have been detected. These fluctuations occur only during precipitation-free times, and the associated amplitudes can be greater than 20 % of the mean daily discharge. During winter months, no such pronounced diurnal fluctuations have been observed. This pattern would indicate that processes causing diurnal discharge fluctuations are constrained by seasonal effects.

The overall aim of the thesis is a better understanding of the underlying processes causing diurnal discharge fluctuations in the Rosalia watershed, which can be transferred to similar forested micro-watersheds.

The specific objectives are:

1. Analysis of the observed high resolution time series in order to identify the magnitude of the diurnal discharge fluctuations, and their temporal characteristics. Their relationship with soil water content, air temperature fluctuations and the plant activity on a daily and seasonal time scale is to be investigated.

2. A process based description of the discharge fluctuations using HYDRUS to investigate, whether the observed diurnal discharge fluctuations are predominantely caused by the root water uptake of the riparian vegetation.

This work is organised as follows: In the introduction, the motivation and the theoretical background is presented. The next section provides an overview of the watershed as well as the hydrological observation network. This section also includes a hydrological description of the study area and the data basis for this thesis. This is followed by a comprehensive analysis of the observed diurnal discharge fluctuations. Similar analyses are also carried out for soil water content and air temperature. A thorough description of HYDRUS follows these analyses. This chapter also describes the configuration of the model. In the following section, simulation results are represented and discussed. The thesis ends with a summary and conclusions.

1.2 Diurnal discharge fluctuations

Examinations and analyses of short-term fluctuations in hydrological variables are rarely described in the hydrological literature. Systematic analyses of diurnal fluctuations in hydrological variables such as groundwater level, streamflow or soil moisture might yield useful information for the description of underlying hydrological systems. Under normal circumstances, temporal variations of streamflow rates and groundwater levels occur over different time scales, ranging from long-term (seasonally, interannually) to short term (daily or sub-daily). According to Pörtge (1996) diurnal discharge fluctuations can only be detected in watersheds with an area up to about 40 km². Other authors, however, described diurnal discharge fluctuations in catchments much larger than 40 km² (Lundquist and Cayan, 2002; Troxell, 1936; Meyboom, 1965).

Diurnal cycles of climate forcings, such as solar radiation, temperature, and humidity, cause comparable diurnal fluctuations in discharge and groundwater levels of the riparian zone along a stream, especially during dry periods. The diurnal signal of streamflow and shallow groundwater is often a result of the daily plant metabolism rhythm, which also alternates during the season due to phenological changes. Similar transpiration rates accompany the daily metabolic cycle of the vegetation. Compared to plant transpiration, soil evaporation can be neglected during dry periods (Gribovszki et al., 2008). Within a research watershed in the Czech Republic, Deutscher et al. (2016) linked sap flow measurements with diurnal streamflow and found a negative correlation between these two variables during dry, precipitation-free periods. In that study, stand transpiration acted as the most dominant factor, inducing diurnal streamflow fluctuations (Deutscher et al., 2016).

Multiple approaches were developed to estimate and study evapotranspiration rates based on streamflow recession. High-resolution discharge measurements can be used to investigate temporal patterns of evapotranspiration on the catchment scale (Dvořáková et al., 2014). Gribovszki et al. (2010) summarised and described historical studies and models that calculate evapotranspiration based on diurnal groundwater level or runoff fluctuations. These methods are generally simple to use and require few parameters and variables compared to traditional methods (e.g. Penman-Monteith, Thornthwaite, Hargreaves). While many authors discussed the temporal behaviour of diurnal fluctuations and their linkage with riparian transpiration, Széles et al. (2018) investigated the spatio-temporal differences in runoff generation mechanisms affecting diurnal discharge fluctuations during periods of low flow in a micro-watershed in Austria (66 ha). They concluded that the transpiration of riparian vegetation along the tributary streams was able to explain about 25 % of the diurnal fluctuations at the basin outlet, and 75 % of the volume associated with diurnal fluctuations was explained based on the transpiration of riparian vegetation along the main stream. Széles et al. (2018) used a solar radiation driven model to estimate the temporal variation. This yielded lag times between the daily radiative forcing and the daily evapotranspiration peak from 3 to 11 hours from spring to autumn. Additionally, observations and modelled results indicated a separation of transpiration rates in time and scale. The transpiration of the riparian vegetation dominates observed diurnal discharge fluctuations effects. Evapotranspiration from fields further away does not affect diurnal discharge fluctuations (Széles et al., 2018).

As described above, in many cases, climatic forcings, such as solar radiation and air temperature, are considered to be the primary factors causing diurnal discharge fluctuations. They regulate the plant water uptake, soil moisture content, transmission and release by plants, as well as the diurnal variation in precipitation, potential evapotranspiration, snowmelt, and freezing-thawing processes (Gribovszki et al., 2010).

The main factors resulting in diurnal discharge and groundwater level fluctuations are:

- Losses due to in-stream infiltration
- Precipitation
- Melting and freezing-thawing processes
- Evapotranspiration
- Additional causes

1.2.1 Losses due to in-stream infiltration

Because hydraulic conductivity and the viscosity of water are temperature dependent, the rate of water infiltration through seepage to the groundwater also depends on the stream's temperature. When stream water is warmest, water is mainly lost in this way. Diurnal fluctuations with large infiltration losses exhibit fluctuations similar to those caused by evapotranspiration (Lundquist and Cayan, 2002). However, this effect is negligible in forested catchments, where there is ample shading of the stream, and the water temperature is generally low (Gribovszki et al., 2010).

1.2.2 Precipitation

This mechanism mainly occurs in tropical climates, where daily, heavy afternoon rain events cause flood waves that might appear as diurnal fluctuations in the hydrograph. Thus, this type of fluctuation does not appear in temperate climate zones (Gribovszki et al., 2010).

1.2.3 Melting and freezing-thawing

Freezing-thawing induced diurnal fluctuations occur on frosty days when the maximum temperature is above freezing-point and temperature amplitudes are above 10 °C. It predominantly takes place at the end of winter and at the beginning of spring and indicates a strong relationship with air temperature. Typically, the minimum streamflow occurs during the morning hours and the maximum in the early afternoon. The freezing and thawing process is generally more noticeable in the streamflow hydrograph than in changes in groundwater levels (Gribovszki et al., 2010). Diurnal discharge behaviour induced by the temperature-dependent snow melting is caused by the melting of local snowpacks. In these cases, the hydrograph shows an asymmetric shape with a strong upward trend and a gradual recession, explained by the vertical percolation through the snow (Lundquist and Cayan, 2002). Diurnal fluctuations in discharge are also very pronounced in glacier dominated catchments during the melting season. The pattern here follows the cycle of the meteorological forcings.

1.2.4 Evapotranspiration

"In temperate climates, one of the most important diurnal fluctuation-inducing factors is the water consumption of vegetation." (Gribovszki et al., 2010). This mechanism behind diurnal discharge fluctuations is characterised by early morning maximum flows and afternoon minimum flows. These fluctuations are also often related to diurnal groundwater level signals and the daily course of relative humidity, which is mostly a function of the diurnal irradiation cycle. When plants transpire, their water demand is retrieved from soil moisture or groundwater via their root system. Hence, evapotranspiration (dominated by transpiration in forested and densely vegetated areas) is the direct link between diurnal discharge fluctuations rather than irradiation and diurnal variations of relative humidity (Gribovszki et al., 2010). Multiple authors linked daily fluctuations in streamflow to evapotranspiration (Dvořáková et al. 2014, Deutscher et al. 2016b, Barnard et al. (2010), Lundquist and Cayan 2002, Szilágyi et al. 2008).

Additionally, Dvořáková et al. (2014) suggested accompanying analyses of diurnal discharge fluctuations with examinations of soil moisture, groundwater levels, and lake levels. They recommend this, because streamflow fluctuations are generally attributable to analogous variations of soil moisture and groundwater levels. Smooth diurnal or seasonal discharge variations can also be described by sine curves, Fourier series, or other harmonic functions (Dvořáková et al., 2014). Many studies that linked diurnal discharge fluctuations with plant transpiration reported a time lag of 4 – 6h between maximum transpiration and minimum discharge. This indicates a clear hydrological relation of water draining into streams and water use by riparian vegetation (Barnard et al., 2010).

1.2.5 Additional causes

Anthropogenic activities can also cause diurnal fluctuations in groundwater levels and streamflow. These activities might be groundwater extractions to meet the changing water demand during the day resulting in fluctuations. Similarly, hydropower plants may artificially induce diurnal fluctuations. Generally, anthropogenic activities altering discharge or groundwater levels within a day cause much larger fluctuations than natural causes (Gribovszki et al., 2010).

2 The experimental research forest Rosalia

This chapter provides an introduction and overview of the environment and location of the study area. The Rosalia watershed lies within the University forest demonstration centre. This demonstration forest covers 950 ha and is managed by the Austrian Federal Forest Authority (Österreichische Bundesforste). The demonstration forest has been used for education and research since 1875. Upon an initiative of various researchers in 2013, the hydrological research watershed was implemented. This extended and complemented the previous mainly forest oriented activities. (BOKU - Institute of Hydrology and Water Management, 2020)

2.1 Characteristics and environment of the hydrological research watershed

The hydrological research watershed area covers 222 ha, and is smaller than the total demonstration forest (950 ha). Four gauges are installed within the watershed, which divide the total watershed into sub-watersheds of 9, 27, 146, and 222 ha. Within and around the watershed, hydrological data such as discharge, air, water and soil temperature, precipitation, electrical conductivity, and relative humidity are observed at several locations and streams. A detailed description of the hydrological monitoring network and its observed variables is presented in section 0. The research watershed's main objectives are to collect and provide continuous hydrological data to study water, energy and solute transport processes in the soil-plant-atmosphere continuum (BOKU - Institute of Hydrology and Water Management, 2020).

2.1.1 Location and geography of the watershed

The Rosalia mountain range is located in the east of Austria at the boundary of the provinces of Lower Austria and Burgenland, about 60 km south of Vienna (

Figure **1**). The demonstration forest is located about 13 km south–southeast of the city Wiener Neustadt and it belongs to various municipalities, including Ofenbach, Schleinz, Walpersbach und Hochwolkersdorf (BOKU - Forest Demonstration Centre, 2020).

2.1.2 Topography

The Rosalia Mountains dominate the topography in the study area. The Vienna Basin (German: Wiener Becken) is confined by the Rosalia Mountains in the South (Hörbarth, 1995). On the east side, the Rosalia Mountain range declines to the Hungarian lowlands and to the west to the Wiener Neustädter basin. Compared to the Alps, the mountain range has a relatively low elevation. The highest elevation in the watershed is 722 m.a.s.l.. The confining gauging station that defines the lowest point of the watershed is about 425 m.a.s.l. (Ulrich, 1989). The topography shows a highly articulated and a very small-scale character. Three creeks define the branched valley system within the catchment: the main stream Grasriegelgraben and two side streams: Mittereckgraben and Trenkgraben (

Figure **1**).

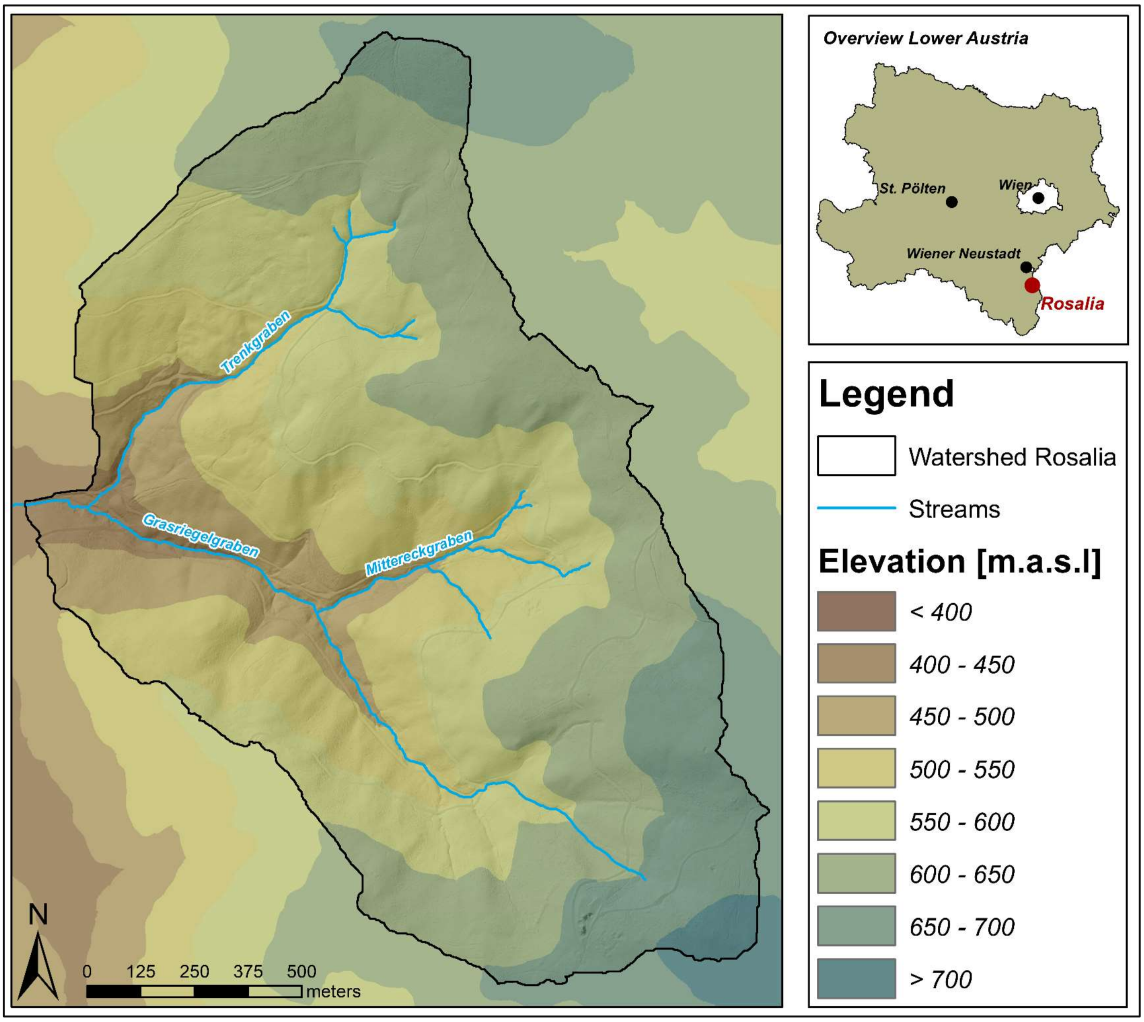

Figure 1. *Overview map of the Rosalia watershed*

The Grasriegelgraben, as the main stream, originates from the Heuberg. Further downstream and outside of the hydrological research watershed, the Grasriegelgraben flows into the Ofenbach. The Ofenbach valley has a northwest orientation and connects the study area to the Vienna Basin (Hörbarth, 1995).

In

Figure **1**, the extent of the orographic watershed is shown. Within the watershed, three main trenches occur, which contribute to the drainage of the catchment. The steepest slopes within the catchment occur along those trenches. Only about 63 % of the total catchment area has slopes less than 20°. Approximately 56% of the catchment area lies between an altitude of 500 to 600 m a.s.l. A summary of the topography is presented in Table 1.

Table 1. *Topography of the Rosalia Watershed*

Elevation [m.a.s.l]	*Area [ha]*	*Area [%]*	***Slope [°]***	*Area [ha]*	*Area [%]*
400 – 450	5.20	2.3	0 – 10	41.803	18.8
450 – 500	22.34	10.1	10 – 20	99.961	45.0
500 – 550	46.01	20.7	20 – 30	60.850	27.4
550 – 600	58.77	26.5	30 – 40	15.816	7.1
600 – 650	63.66	28.6	40 – 50	3.474	1.6
650 – 700	23.83	10.7	50 – 60	0.266	0.1
> 700	2.39	1.1	> 60	0.021	0.0

The forest service district (German: Forstdienstbezirk) Ofenbach, in which the experimental research watershed is located, has one of the highest developed road densities in Austria, with about 60 m forest road/ha (Ulrich, 1989). The total road length within the 222 ha large watershed is about 13 km. Based on this high road density, it can be assumed that peak discharges at the outflow have a faster reaction time than they would have without roads (Wesemann, 2021). This is important, especially during heavy precipitation events.

2.1.3 Geology

The Rosalia mountains, the Leitha mountains and the accompanying Wechsel-Semmering mountains are part of the Carpathian core mountain range zone. In the northeast, the Rosalia mountains are separated from the Leitha mountain range by the tertiary filled Wiener Neustädter Pforte (Gasch, 1985). The geology within the demonstration forest is generally dominated by metamorphic rocks, including a minor dolomite lens in the north. The bedrock consists mostly of coarse gneiss and mica-slate (Ulrich, 1989). The geological map (1:50.000) of the Geological Federal Institute (GBA, 1995) shows a similar bedrock in the Rosalia. Moreover, the bedrock does not show fissures. Based on a geological survey within the demonstration forest, no declining rock layers, which might cause subsurface drainage and consequently alter the orographic watershed, can be found. Therefore, it can be assumed that the hydrological watershed is identical to the orographic watershed (Ulrich, 1989).

2.1.4 Soils

Generally, the bedrock substrate is an essential factor influencing soil formation. Based on the geology, soils such as cambisols with moderate to light nutrient content get formed. Based on the forest site mapping and exploration carried out by J. Gasch in 1985, the soil types, cambisols, planosols and fluvisols, are present within the Rosalia.

According to J.Gasch, the area percentages of different soil types that appear in each sub-watershed are presented in Table 2. Generally, the soil type variation increases with the catchments' size due to more diverse soil-forming processes. Variations of cambisols are the most frequently occurring soil type. In each sub-watershed, this is the dominant soil type. The second most frequent occurring soil types are different varieties of planosols. Apart from the watershed Q1, fluvisols and cambisols soils can be found most commonly on trench bottoms.

Table 2 *Soil types in area percentage [%] of the respective sub-watershed*

Aggregated soil types	Q1	Q2	Q3	Q4
Cambisols at steep slopes	0	6	5	6
Cambisols at plains and moderate slopes	62	74	66	69
Cambisols and planosols at plains and moderate slopes	38	15	24	21
Cambisols and fluvisols at valley slopes and bottom	0	5	6	4

2.1.5 Landcover and Vegetation

Generally, the vegetation is dominated by trees of various species. The hydrological research catchment Rosalia is mostly characterised by the south-east alpine Spruce-Fire-Beech forest community and the east sub-pannonic oak forests. More specifically, the sub-montane beech forest reaches up to an altitude of about 600 m a.s.l. and the low montane forest, including spruce, fire and beech, starts at about 500 m a.s.l. (Gasch, 1985). The most dominant tree species occurring is spruce (41%), followed by beech (36%) (Stangl, 2013). Surface vegetation species consist of wood fescue *(Festuca sylvatica)* and whitish grow rims *(Luzula albida),* which is often accompanied by hair-grass *(Avenella flexuosa).* Other occurring plants are woodruff *(Galium odoratum)* and various species of fern. Less common are sedge variations, such as hairy sedge *(Carex Pilosa)* and wood sedge *(Carex sylvatica)*. Characteristically, perennial honesty *(Lunaria rediviva)* appears on the valley floors (Gasch, 1985).

2.1.5.1 Vegetation phenology

Generally, phenology describes reoccurring biological events. Vegetation phenology controls several seasonal behaviours of ecosystems, such as carbon uptake as well as energy and water fluxes, which occur between the surface and the atmosphere. Plant phenology is also sensitive to climatic conditions and climate shifts within an environment. Therefore, it can be used to investigate the impact of climate change in the terrestrial biosphere (Seyednasrollah et al., 2019). Phenology in boreal and temperate forest ecosystems such as the Rosalia forest is extensively driven by the air temperature.

The data provided by the standardised and publicly available PhenoCam V2.0 dataset (Seyednasrollah et al., 2019) is used to present the vegetation's phenological changes and seasonality of the Rosalia forest. The total dataset consists of several hundred sites worldwide to track vegetation changes by near-surface remote sensing using high-frequency digital repeat photography (15-30 min). Installed cameras record the red, green and blue (RGB) colour channels for the region of interest *(ROI)* within a picture. The G_{CC} is then calculated based on the averaged green (G_{DN}), red (R_{DN}), and blue (B_{DN}) digital number. It is a ratio that has been successfully utilised for many ecosystems and is calculated, as shown below (Seyednasrollah et al., 2019).

$$\boldsymbol{G_{CC}} = \frac{\boldsymbol{G_{DN}}}{\boldsymbol{R_{DN}} + \boldsymbol{G_{DN}} + \boldsymbol{B_{DN}}} \tag{1}$$

2.2 Hydrological observation network and observed data

This chapter provides an overview of the monitoring network and observed hydrological variables within the Rosalia forest used in this thesis. Discharge is measured at four different gauging stations dividing the total watershed into four sub-catchments (Q1, Q2, Q4, Q3) with different areas (9, 27, 146, 222 ha). Additionally, three climate stations (K1, K2, K3) that measure precipitation, relative humidity and air temperature are located within and along the watershed (Figure 2). In total, about 100 hydrological quantities with a temporal resolution of 10 minutes are observed. In the following tables, all variables detected will be presented (Fürst et al., 2020).

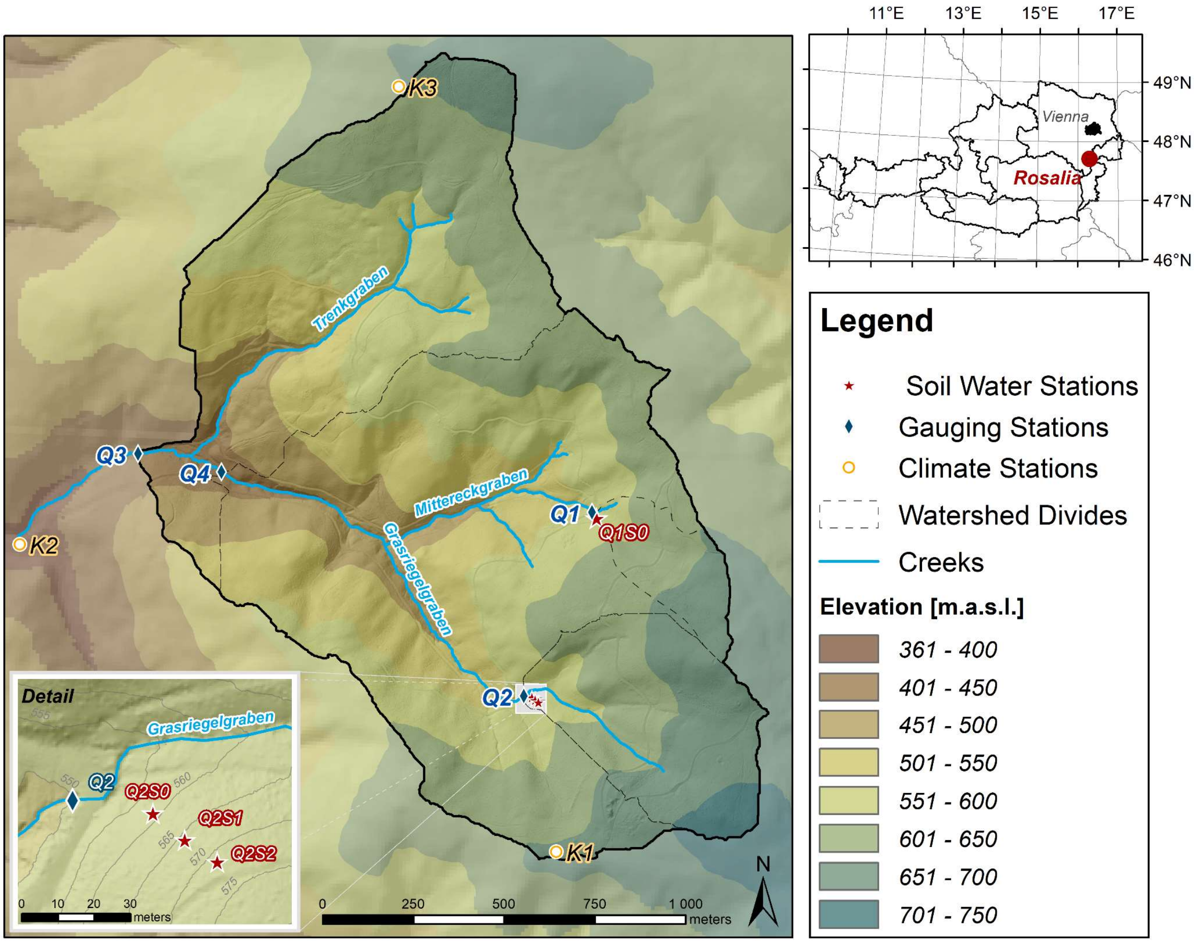

Figure 2 *Hydrological observation network – Rosalia*

2.2.1 Watershed Q1

The watershed Q1 is the head-catchment of the Mittereckgraben with the outlet at 559.8 m a.s.l. With a total area of 9 ha, Q1 is also the smallest watershed within the hydrological research watershed. At the gauging station, discharge, salinity, conductivity, water temperature, and total dissolved soilds (TDS) have been measured since June 2015. Meteorological variables observed are relative humidity, temperature and precipitation. Since July 2015, soil water content and soil temperature are observed by four sensors in different soil depths at one soil profile. The soil profile is situated along the slope upstream of the discharge gauge.

Table 3 *Hydrological observations in Q1*

	Parameter	*unit*		*observed since*
water	conductivity	µS/cm		01.06.2015
	salinity	g/kg		01.06.2015
	TDS	ppm		01.06.2015
	water level (discharge)	m		01.06.2015
	water temperature	°C		01.06.2015
air	precipitation	mm		01.06.2015
	temperature	°C		01.06.2015
	relative humidity	%		01.06.2015
	Parameter	*unit*	*depth[cm]*	*observed since*
soil	soil moisture water fraction	wfv	10	01.07.2015
	soil temperature	°C	10	01.07.2015
	soil moisture water fraction	wfv	20	01.07.2015
	soil temperature	°C	20	01.07.2015
	soil moisture water fraction	wfv	40	01.07.2015
	soil temperature	°C	40	01.07.2015
	soil moisture water fraction	wfv	60	01.07.2015
	soil temperature	°C	60	01.07.2015

2.2.2 Watershed Q2

This watershed is the second head-catchment within the hydrological research watershed. The watershed is about 27 ha large. The gauging station is located at the Grasriegelgraben at 550.0 m.a.s.l. At the gauging station, the same hydro-meteorological variables as at Q1 have been observed since June 2015. Three soil profiles exist at which soil temperature and soil water content are observed at different depths. These are located along a slope transect upstream of the gauging station. The first profile (Q2S0) has an inclined distance from the gauging station of about 16 m and was established in June 2015. Q2S1 and Q2S2 were established in the same slope transect 13 and 25 m upwards from the soil water profile Q2S0 in April 2016. This sensor arrangement provides data to observe the water movement through the slope transect in space and time.

Table 4 *Hydrological observations in Q2*

	Parameter	*unit*	*depth [cm]*	*observed since*
water	conductivity	µS/cm		01.06.2015
	salinity	g/kg		01.06.2015
	TDS	ppm		01.06.2015
	water level (discharge)	m		01.06.2015
	water temperature	°C		01.06.2015
air	precipitation	mm		01.06.2015
	temperature	°C		01.06.2015
	relative humidity	%		01.06.2015
soil Q2S0	soil moisture water fraction	wfv	10	25.06.2015
	soil temperature	°C	10	25.06.2015
	soil moisture water fraction	wfv	20	25.06.2015
	soil temperature	°C	20	25.06.2015
	soil moisture water fraction	wfv	40	25.06.2015
	soil temperature	°C	40	25.06.2015
	soil moisture water fraction	wfv	60	25.06.2015
	soil temperature	°C	60	25.06.2015
soil Q2S1	soil moisture water fraction	wfv	10	12.04.2016
	soil temperature	°C	10	12.04.2016
	soil moisture water fraction	wfv	20	12.04.2016
	soil temperature	°C	20	12.04.2016
	soil moisture water fraction	wfv	40	12.04.2016
	soil temperature	°C	40	12.04.2016
soil Q2S2	soil moisture water fraction	wfv	10	12.04.2016
	soil temperature	°C	10	12.04.2016
	soil moisture water fraction	wfv	20	12.04.2016
	soil temperature	°C	20	12.04.2016
	soil moisture water fraction	wfv	40	12.04.2016
	soil temperature	°C	40	12.04.2016

2.2.3 Watershed Q3

This measuring weir was built in 1983, but was newly equipped with sensors in September 2015. The gauging station defines the watershed outlet and covers an area of about 222 ha. It is situated at the Grasriegelgraben a few hundred meters downstream of the confluence of the Trenkgraben.

Table 5 *Hydrological observations in Q3*

	Parameter	*unit*	*observed since*
water	water level (discharge)	m	01.09.2015
air	precipitation	mm	01.09.2015
	temperature	°C	01.09.2015
	relative humidity	%	01.09.2015

2.2.4 Watershed Q4

This watershed is the second largest in the Rosalia, and the gauging station is located along the Grasriegelgraben around 510 m after the confluence of Mittereckgraben and Grasriegelgraben. The gauging station is located at 425.9 m a.s.l. and the catchment area is 146 ha. The gauging station has been in operation since 01.07.2018. In addition to the hydro-meteorological data measured at Q1 and Q2, at Q4 water quality parameters, total organic carbon (TOC) and nitrate (NO_3-N), are also observed. In contrast to Q1 and Q2, no soil water sensors are installed at this gauge.

***Table 6** Hydrological observations in Q4*

	Parameter	*unit*	*observed since*
water	conductivity	µS/cm	01.07.2018
	salinity	g/kg	01.07.2018
	TDS	ppm	01.07.2018
	water level (discharge)	m	01.07.2018
	TOC	mg/l	01.07.2018
	NO3N	mg/l	01.07.2018
	water temperature	°C	01.07.2018
air	precipitation	mm	01.07.2018
	temperature	°C	01.07.2018
	relative humidity	%	01.07.2018

2.2.5 Weather stations

The three weather stations are located at the boundaries of the research watershed. K1 is situated at the Heuberg, which is on the south end of the watershed. At the north edge of the watershed the climate station K3 was established. K2 is located on the western side, outside of the watershed on the valley bottom of the Grasriegelgraben. At the weather stations, K1 and K2, the three parameters precipitation, temperature and relative humidity, have been observed from the end of August 2015. K3 was installed in August 2018 and only measures precipitation.

***Table 7** Weather Stations*

	Parameter	*unit*	*observed since*
K1 - Heuberg	precipitation	mm	26.08.2015
	temperature	°C	26.08.2015
	relative humidity	%	26.08.2015
K2 - Mehlbeerleiten	precipitation	mm	26.08.2015
	temperature	°C	26.08.2015
	relative humidity	%	26.08.2015
K3 - Krieriegel	precipitation	mm	01.08.2018

2.3 Climatic conditions and hydrological characteristics of the watershed

The watershed is dominated by a continental climate (Figure 3) with less precipitation in winter months and convectively induced maximum precipitation during summer (Ulrich, 1989). According to Walter and Lieth (Walter and Lieth, 1967), the catchment area belongs to a humid temperate zone with a distinct, though not very long cold season, defined as climate type VI. Daily rainfall exhibited a continuous increase during the day with intense maximum precipitation in early evenings (thunderstorms). This is shown to be related to the daily convective activity patterns during the irradiation period and the decrease during the radiation period (BOKU - Forest Demonstration Centre, 2020).

2.3.1 Temperature and precipitation

Precipitation in the Rosalia clearly reaches a distinct maximum in the summer months, during which 60% of precipitation occurs (BOKU - Forest Demonstration Centre, 2020). Compared to the winter months, precipitation increases in April and decreases in October and November. In summer, precipitation is dominated by convective events with maximum daily heavy rainfall up to 130 mm. The Walter and Lieth climate diagram (Figure 3) shows precipitation and temperature characteristics for the Rosalia watershed. The Walter and Lieth diagram indicates that the Rosalia exhibits a humid climate.

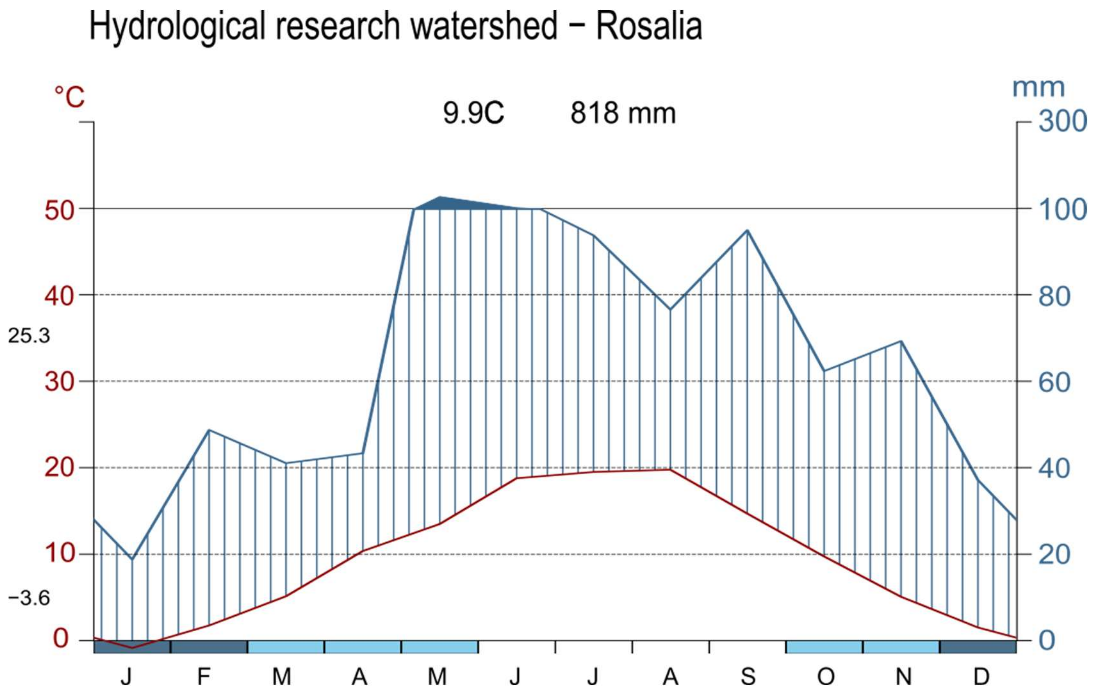

Figure 3 *Walter - Lieth climate diagram - Rosalia 2015 – 2019 (based on station K1 and K2)*

The mean monthly temperature also indicates a seasonal pattern. On average, mean maximum daily temperatures of above 25 °C occur in July and August. The lowest temperatures occur in January and December with about – 3 °C. The minimum daily temperature was observed in February and was a bit lower than −16 °C. The mean annual temperature between 2015 and 2019 was 9.9 °C. The mean annual precipitation sum of the catchment was 818 mm (2015-2019). Precipitation also showed a clear seasonal pattern. The highest precipitation occurs during May and June with 128 mm and 102 mm, respectively. Approximately 66 % of annual precipitation occurred from April until October (2015 – 2019).

2.3.2 Discharge characteristics

Discharge in the hydrological research watershed Rosalia is, compared to precipitation, relatively low. However, runoff reacts quickly to heavy precipitation events, especially during summer. Therefore, discharge variation is primarily dominated by precipitation during the vegetative period. During winter, discharge variation is mainly influenced by temperature differences. When temperatures permanently exceed 0 °C, runoff increases due to sufficient precipitation (Ulrich, 1989). These findings and further analyses are provided by Ulrich (1989) based on data obtained between 1983 and 1989.

The runoff descriptions and analyses in the following are based on the data collected since 2015. In Figure 4, the daily discharge depth is shown on a monthly basis. The mean annual discharge depth is 108 mm. Compared to precipitation, this results in a runoff coefficient of 13 %. Ulrich (1989) reported a runoff coefficient of about 18 % within the Rosalia based on data collected from 1983 to 1989.

Runoff in the Rosalia shows a clear seasonal pattern (Figure 4). Low discharge occurs predominantly from midsummer until the end of winter in February. With increasing discharge values in spring, the streamflow variability also increases. Corresponding with the sharp increase in precipitation from April to May, discharge increases similarly during those months. The highest discharge values occur in May and June. As mentioned above, during these months, the greatest precipitation sums also occur. Discharge drops in July with values starting to increase again in spring.

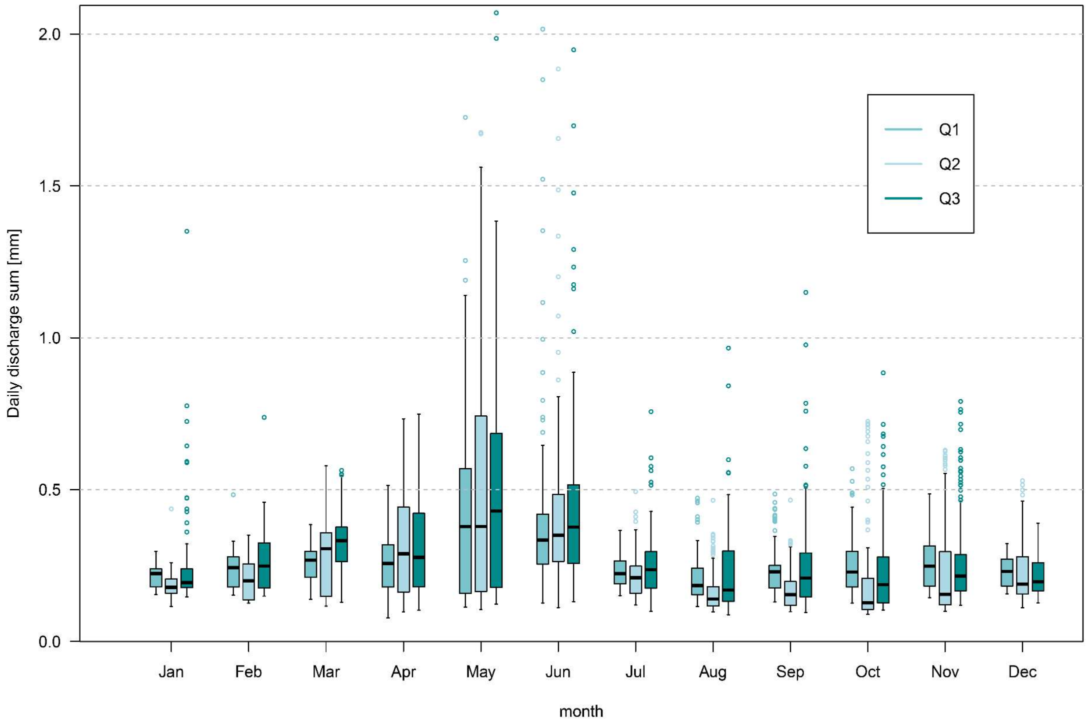

Figure 4 *Daily discharge sum (2016-2019)*

The mean discharge at Q3 is approximately 7.6 l/s. Maximum discharge recorded at gauging station Q3 was about 580 l/s. This represents a high variability in discharge, mainly due to fast streamflow response to heavy precipitation events (Ulrich, 1989). Mean discharge at gauging stations Q1, Q2 and Q4 is about 0.3 l/s, 0.8 l/s and 4.4 l/s, respectively. The small headwater catchments (Q1 and Q2) show low discharge values. 95 % of discharge is less than 0.51 l/s and 1.9 l/s at Q1 and Q2, respectively.The maximum values measured are 8.1 l/s (Q1) and 12.64 l/s (Q2). The maximum discharge recorded at Q4, which includes both headwater catchments, was 309 l/s. Like Q1 and Q2, 95 % of the discharge at Q4 is, compared to the maximum, very low with 12.05 l/s. 95 % of the streamflow recorded at Q3 was lower or equal to 16.59 l/s. Figure 5 shows the cumulative distribution function to highlight the catchment's discharge variability. The cumulative illustration of discharge also emphasises the magnitude and increase of runoff due to the increasing catchment areas within the Rosalia.

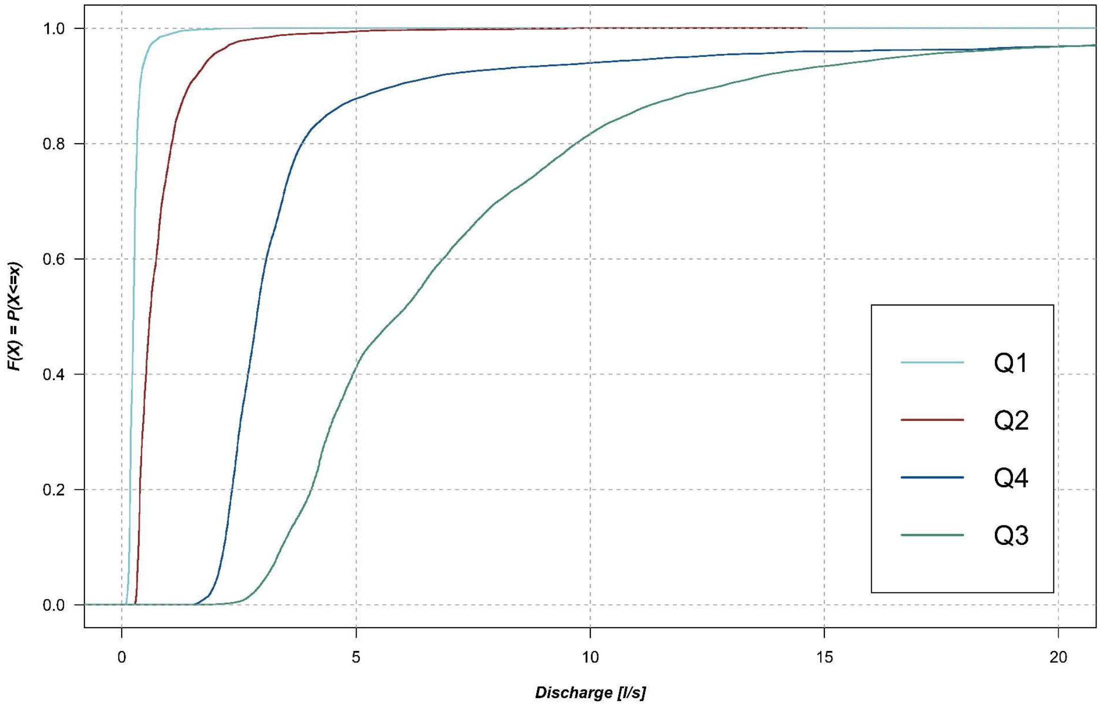

Figure 5 *Discharge - Cumulative distribution Rosalia (Q1, Q2, Q3: 2016-2019; Q4: 2018-2019) (Discharge truncated at 20 l/s)*

2.3.3 Evapotranspiration

At the present time, evapotranspiration data measured in situ is not available for the hydrological research watershed Rosalia. However, evapotranspiration is a significant hydrological variable, as is expressed by the runoff coefficient of 13 %. 87 % of rainfall input is lost to the atmosphere due to evapotranspiration, which plays a dominant role, especially in densely vegetated and forested areas. Estimations of daily and hourly areal potential and reference evapotranspiration (2007-2015) for the Rosalia based on three different methods (ASCE-Penman-Monteith; Hargreaves; and Thornthwaite) are provided following the calculation procedures described in Herrnegger et al. (2012). Figure 6 shows the mean monthly sum of estimated potential evapotranspiration (ETp). Mean annual sums of ETp differ depending on the method applied. Long-term mean annual ETp sums calculated based on Hargreaves, Thornthwaite and ASCE-PM are 800 mm, 672 mm, 851 mm respectively. Maximum monthly ETp occurs in July. As expected, the estimated ETp shows a clear seasonal pattern (Figure 6) with lowest ETp in winter and highest ETp during summer. From Figure 6 it is visible that the Hargreaves and ASCE-PM methods show noteworthy higher values in the months January to July compared to Thornthwaite. Thornthwaite only relies on air temperature, whereas ASCE-PM and Hargreaves include radiation as input, explaining the differences.

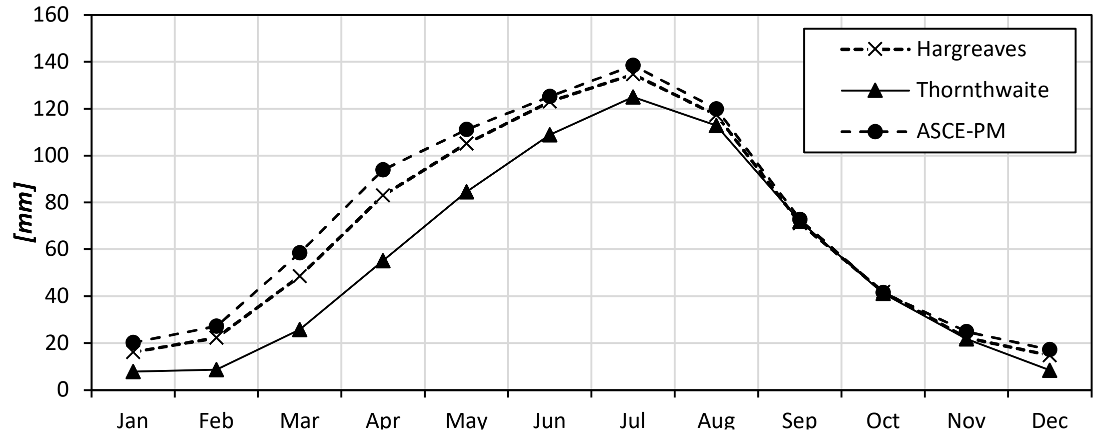

Figure 6 *Mean monthly potential Evapotranspiration (2007 – 2015)*

In order to estimate actual evapotranspiration (ETa), the mean annual sums of runoff and precipitation were compared (2015-2019). Thus, the delayed reaction of discharge resulting from precipitation is considered, as well as the uncertainties regarding the storage term in the water balance is reduced (Ulrich, 1989). Based on this approach, long-term cumulative mean daily precipitation and mean daily discharge is represented in Figure 7.

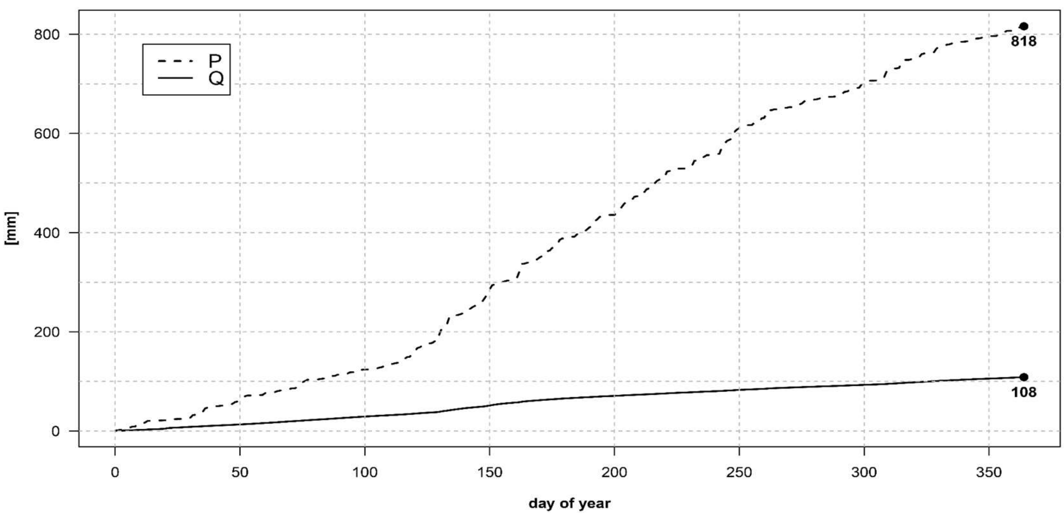

Figure 7 *Cumulative graph of mean daily precipitation and discharge in mm (2015-2019)*

Based on the difference of mean annual precipitation (818 mm) and mean annual discharge (108 mm), the mean annual ETa in the Rosalia is estimated to be 710 mm, which is equivalent to about 87% of precipitation. As mentioned above, Ulrich (1989) analysed runoff characteristics in the Rosalia. His analysis is based on observed data from 1983 to 1989. Ulrich (1989) showed that mean annual evapotranspiration reflects about 82% of precipitation. This highlights the significance of the evapotranspiration component in the water balance.

3 Analysis of observed diurnal fluctuations

Diurnal discharge fluctuations can be observed at all gauging stations in the Rosalia. Based on visual interpretation of discharge, these fluctuations only appear in precipitation-free periods from April to approximately the middle of October. Fluctuations are only clearly visible during streamflow recession and low-flow periods. Additionally, soil water content (SWC) observations also show diurnal variations during precipitation-free episodes. However, SWC fluctuations do not appear as dominantly as discharge fluctuations. As daily fluctuations of energy input trigger diurnal fluctuations in transpiration and evapotranspiration, soil water and subsurface water flow are also affected (Széles et al., 2018). Moreover, the analysis of diurnal discharge fluctuations should always be accompanied by analyses of groundwater levels or soil water content. Diurnal discharge fluctuations are often attributable to similar differences in soil water content or groundwater levels (Gribovszki et al., 2010).

In order to harmonise the observed data, including discharge soil water content, and temperature, a consistent database was established for this analysis. The starting date of this database was set to May 1st, 2016. This assures that discharge data is accompanied by soil water content observations at Q1 and Q2. At Q3 and Q4, no soil water content observations are available.

Observed diurnal fluctuations for August 2018 are exemplarily illustrated in Figure 8. In this figure, precipitation, temperature, aggregated soil water content (over respective depths) and discharge are displayed on an hourly time timescale. This illustrates the emerging diurnal discharge fluctuations and the streamflow reaction to precipitation events. All precipitation events in this time period caused a peak in discharge, which emphasises the quick runoff response within the Rosalia at all gauging stations. Additionally, diurnal fluctuations in soil water content were also pronounced during this period, especially at Q1S0. Precipitation, furthermore, led to a noticeable increase in soil water content, especially after rain-free periods, when the soil water content had already been previously depleted (15.08.2020 to 25.08.2020).

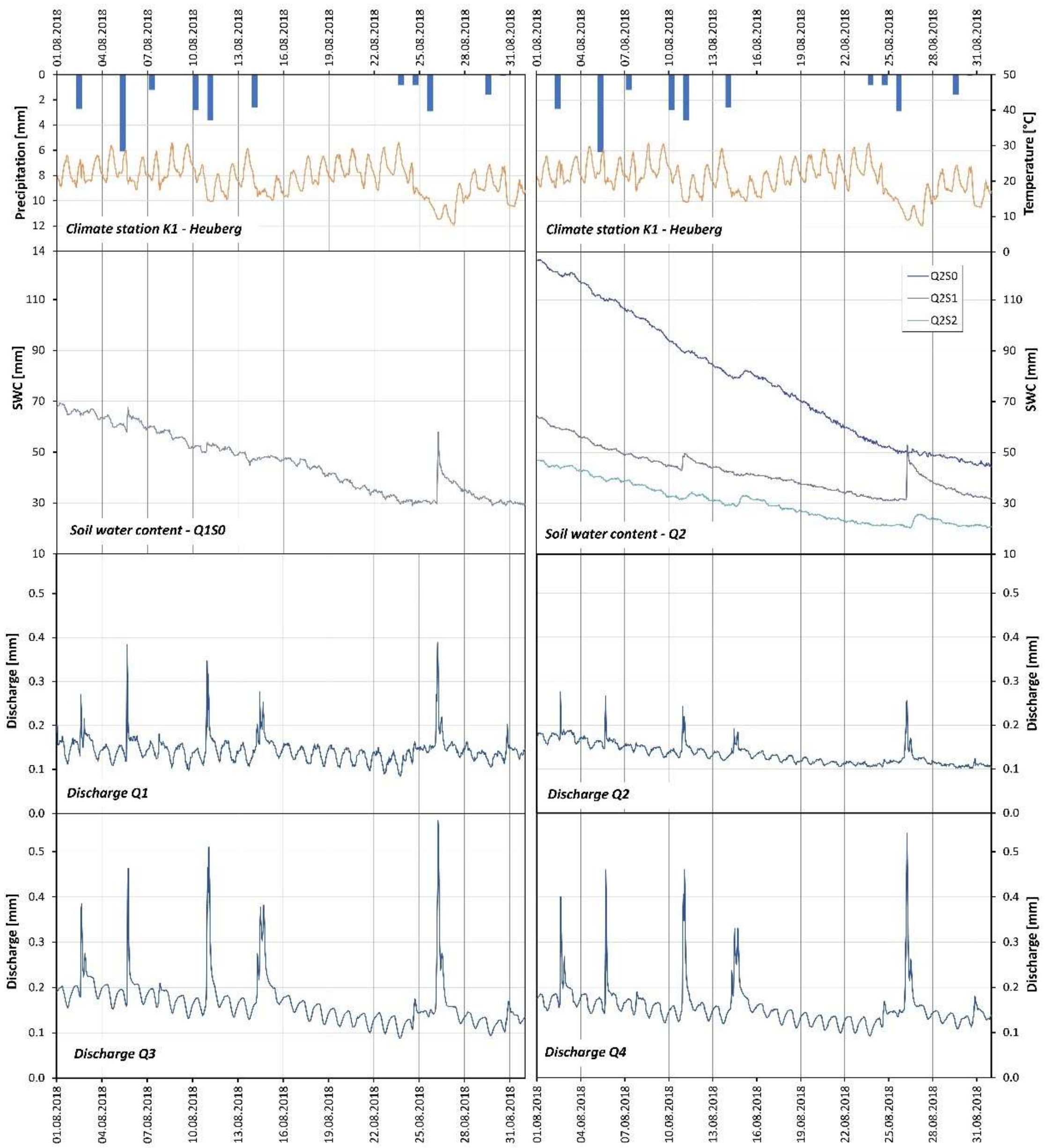

Figure 8 *Example of diurnal fluctuations in August 2018*

Precipitation does not cause a significant increase in soil water content when the antecedent soil water content is already relatively high. Temperature also follows a clear diurnal signal. It increases during the day and declines in the evenings and during the night. The diurnal discharge signal during this period is especially pronounced during the precipitation-free period between 15.08 and 23.08. After rainfall events, discharge depletes to the pre-precipitation values after about one to two days, depending on the amount of precipitation. As mentioned above, diurnal fluctuation exhibits a seasonal behaviour. The seasonality and the magnitude of diurnal discharge, soil water content and temperature values are analysed in the next section.

3.1 Analyses of seasonality

This chapter identifies the periods showing diurnal discharge fluctuations and analyses the magnitude of these. Additionally, associated diurnal fluctuations in soil water content and air temperature are analysed in the same way. This should provide a better understanding of the interaction of meteorological forcing, soil water content and discharge in precipitation-free periods.

To enable a better comparability, discharge data is represented in mm. Soil water content (SWC) measurements are also recalculated to mm for each soil profile. Because the SWC sensors do not cover the same soil depth range (0) in each soil profile, absolute magnitudes might differ. SWC data of Q1S0 and Q2S0 represent the soil water content within a 70 cm deep soil column. On the other hand, soil water content data of Q2S1 and Q2S2 show soil water content within a 50 cm deep soil profile. The recalculation of each variable to mm simplifies the diurnal discharge comparison based on their respective magnitudes. Additionally, the time, when the minimum and maximum daily discharge, soil water content, and temperatures occur are analysed. The aim of the subsequent temporal analysis is the better understanding of the process of diurnal fluctuations.

For the analysis a pre-processing step of diurnal fluctuations of discharge was necessary and only data without precipitation readings during the preceding 24 hours was selected. This yielded a consistent dataset to analyse diurnal fluctuations for periods not affected by precipitation. The absolute daily amplitudes of discharge, soil water content and temperature were then calculated based on the following equation (2).

$$\mathrm{Am}_{(q,swc,T)} = \mathrm{Max}_{(q,swc,T)} - \mathrm{Min}_{(q,swc,T)} \qquad (2)$$

3.1.1 Discharge

The daily discharge amplitudes at each gauging station are shown on a monthly basis. The distribution of amplitudes present within each month is represented as boxplots to show the variability in each month. Discharge data of the four years, covering 2016 to 2019, was used in the analysis for Q1, Q2 and Q3. Additionally, the normalised amplitudes with respect to the mean daily discharge are analysed for the gauging stations Q1, Q2 and Q3. At the gauge Q4, discharge monitoring started in July 2018. Therefore, this analysis is based on less discharge data.

3.1.1.1 Discharge amplitudes at Q1

In Figure 9, the daily amplitudes of Q1 are plotted. Q1 is the smallest catchment (9 ha) within the hydrological research watershed. Daily amplitudes occurring at Q1 show a clear seasonal pattern.

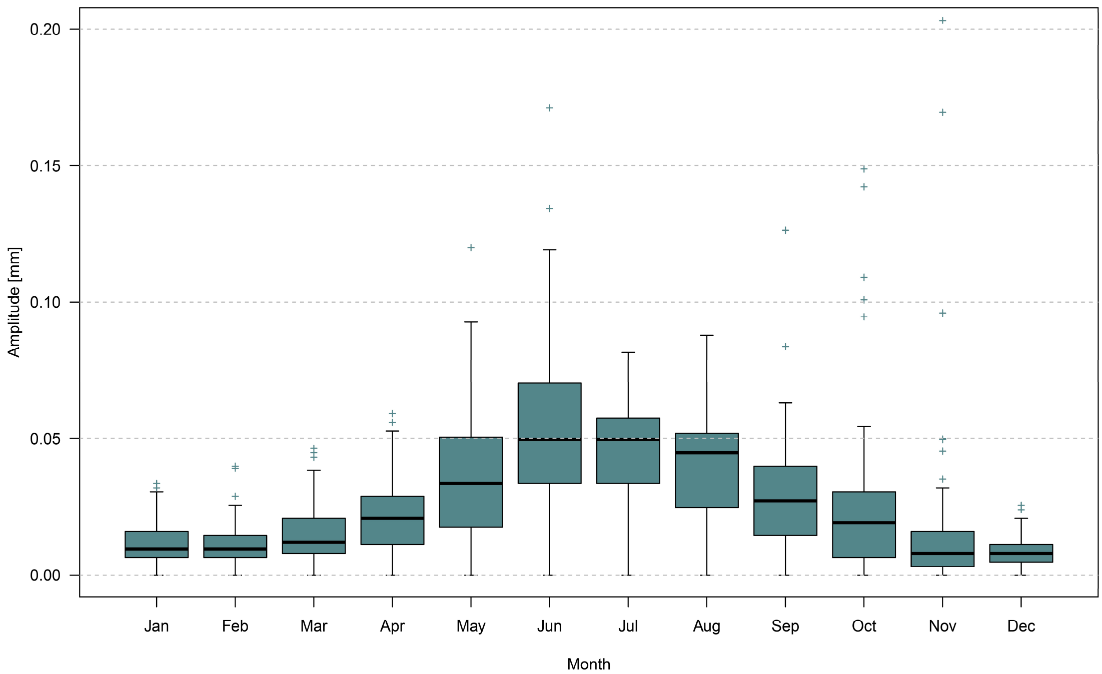

Figure 9 *Q1 - Daily discharge amplitudes 2016 - 2019*

The median of daily amplitudes shows a clear seasonal behaviour. The median of daily amplitudes is largest in June and July. During these months, the median daily amplitude is 0.05 mm. Generally, daily amplitudes are found to be low in January (median = 0.01 mm) and start to rise in March with a distinct increase in April (median = 0.021 mm) up to June. Afterwards, daily amplitudes decrease smoothly until they even out in November and December (median = 0.008 mm).

At this gauging station, the median daily amplitudes in July (0.05 mm) and August (0.045 mm) are larger than 25 % of the mean daily discharge (approx. 0.18 mm mm)

3.1.1.2 Discharge amplitudes at Q2

Figure 10 represents the seasonal appearance of daily amplitudes occurring at gauging station Q2. Gauging station Q2 characterises discharge in the Rosalia's second smallest watershed (27 ha). Seasonal differences in daily amplitudes are definitely observed.

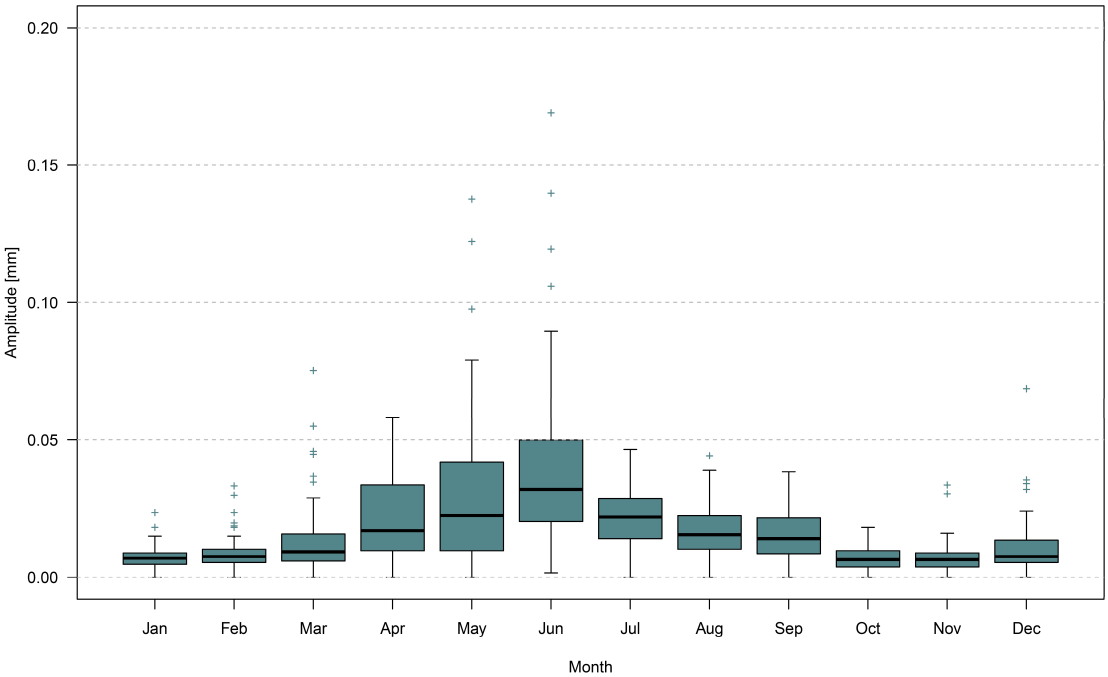

Figure 10 *Q2 - Daily discharge amplitudes 2016 -2019*

The maximum daily amplitudes at Q2 occur in June (median = 0.032 mm). Compared to the median daily amplitude of Q1 in June, the magnitude of the median is about 35 % smaller. Low values of amplitudes are observed in October, November, December, January and February. In these months, the median daily amplitudes range from 0.006 mm to 0.007 mm. Daily amplitudes in June are more than five times larger. Compared to the mean daily discharge, diurnal amplitudes in July (median = 0.022 mm) and August (median = 0.015 mm) accounted for about 10 % of mean daily discharge.

3.1.1.3 Discharge amplitudes at Q4

Due to the short time series length, daily amplitudes at the gauging station Q4 are not represented. However, a similar seasonal pattern of daily amplitudes as at Q1 and Q2 is observed. The greatest daily amplitudes occur in the summer months. Daily amplitudes in June are the highest (median = 0.089 mm). Thus, this represents the highest median daily amplitudes in June for the total catchment. During August, daily amplitudes (median = 0.033 mm) are about 24 % of the mean daily discharge. Amplitudes decrease smoothly until they stay relatively low from October to March. A substantial increase occurs in April, where daily amplitudes almost doubled compared to the months before.

3.1.1.4 Discharge amplitudes at Q3

In Figure 11, the present seasonal amplitude behaviour of discharge at the gauging station Q3 is illustrated. The gauging station defines the main outlet of the watershed, and therefore represents the discharge of the total watershed with an area of 222 ha.

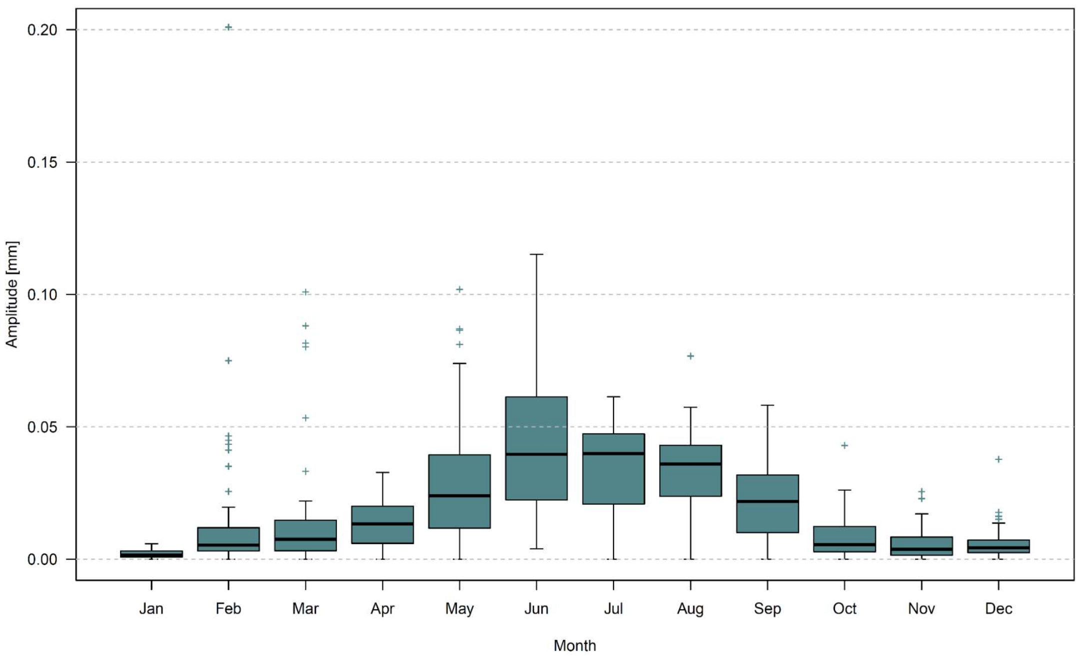

Figure 11 *Q3 - Daily discharge amplitudes 2016 – 2019*

Daily amplitudes occurring in June (median = 0.04 mm) are the greatest. They start to increase in April (median = 0.013 mm) and decrease until October (median = 0.05 mm). The months of November, December, January and

February also show small median daily amplitudes ranging from 0.004 mm to 0.016 mm. Compared to the mean daily discharge, daily amplitudes in July (median = 0.04 mm) and August (median = 0.036 mm) account for over 17 % of mean daily discharge during the respective months. This also addresses the impact of diurnal fluctuations on discharge in summer months.

3.1.1.5 Normalised discharge amplitudes

In Figure 12, the amplitudes (Q1, Q2, Q3) are represented normalised based on the mean daily discharge. This allows a comparison of the magnitudes of diurnal fluctuations between the gauging stations. In comparison to the seasonal occurrence of absolute amplitudes shown above (Figure 9, Figure 10, Figure 11), the seasonality of the normalised amplitudes does show a different pattern. Here, greatest amplitudes occur in August. Since discharge in August is generally lower than in June (Figure 4), normalised amplitudes are higher compared to June.

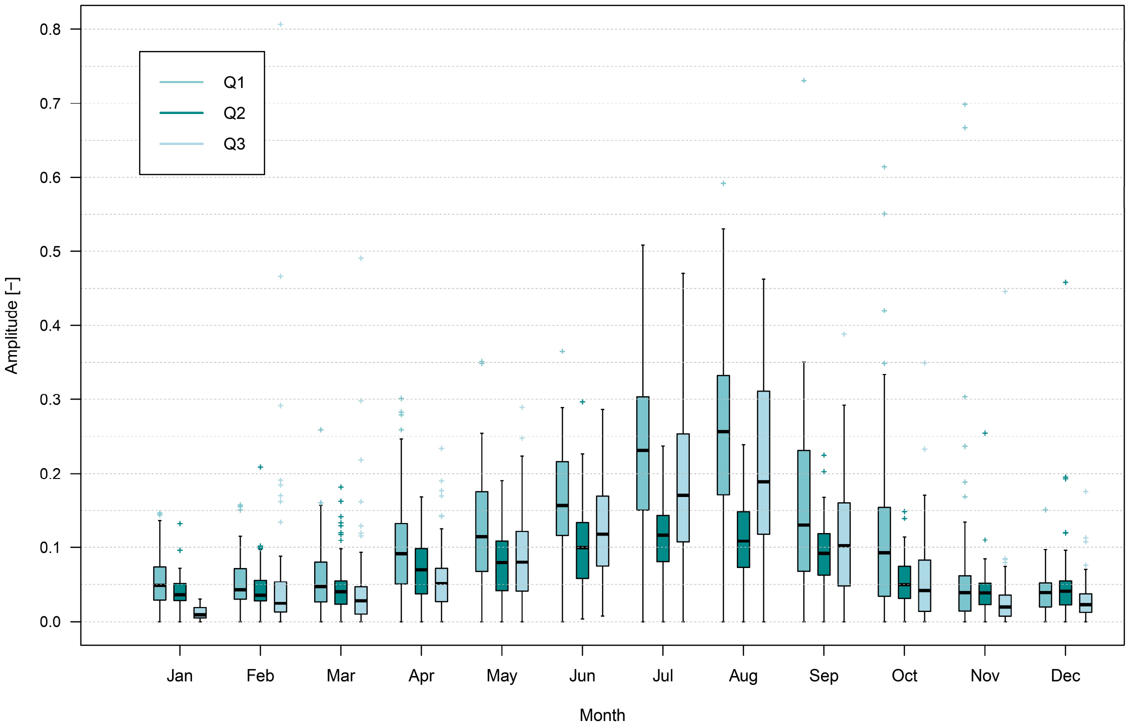

Figure 12 *Normalised discharge amplitudes (Q1, Q2, Q3) with respect to the mean discharge*

Compared to mean daily discharge, most pronounced amplitudes occur at Q1, the smallest sub-watershed. Here, daily amplitudes (median value) account for over 20% of mean daily discharge in July, and for over 25% in August. At Q2, the lowest normalised amplitudes, hardly higher than 15 %, are observed. The median of the normalised amplitudes of Q3 never exceeds 20%.

3.1.1.6 Discharge amplitude - Summary

The seasonal behaviour regarding the magnitude of diurnal discharge fluctuations was analysed for all discharge gauging stations in the hydrological research watershed Rosalia. Discharge, observed at all gauging stations, exhibits diurnal fluctuations during precipitation-free periods. The daily amplitudes show a distinct seasonal behaviour. Maximum absolute amplitudes occur throughout the watershed in June. During the winter months only very small mean daily amplitudes can be observed. The largest daily amplitudes occur at Q4 in June (median = 0.089 mm). Compared to the mean daily discharge, observed amplitudes are largest at Q1 (> 25 %). At the gauging station Q2, maximum daily amplitudes are in the range of about 10 % of the mean daily discharge. The seasonal pattern of normalised amplitudes is different, compared to the seasonal pattern of absolute amplitudes. The maximum normalised amplitudes of Q1, Q2, and Q3 occur in August.

3.1.1.7 Time of minimum and maximum daily discharge

In addition to the seasonal magnitude of diurnal fluctuations, the time when daily minimum and maximum discharge occurs is analysed. This provides a more detailed daily analysis of the diurnal discharge fluctuations in the Rosalia. When investigating diurnal discharge fluctuations, an accompanying temporal analysis is essential. For this analysis, the same consistent dataset of precipitation-free periods is used as described in 3.1. Time of the day is generally expressed as coordinated universal time (UTC), i.e., local CET is UTC plus 1 hour. Similar to the seasonal amplitude illustrations, the time of minimum and maximum discharge is plotted as boxplots in

Figure **13**. The figure gives an overview of the distribution of the time when minimum and maximum discharge occurs in every month. Since daily discharge amplitudes are most pronounced in the months from April to October (Figure 9, Figure 10, Figure 11), only these months are shown. Based on these analyses, minimum and maximum daily discharges can be detected during the entire day from 00:00 to 24:00. However, focusing on the interquartile range (IQR) and the median of the distributions, a distinct time lag, when maximum and minimum discharge is observed, can be detected at all gauging stations.

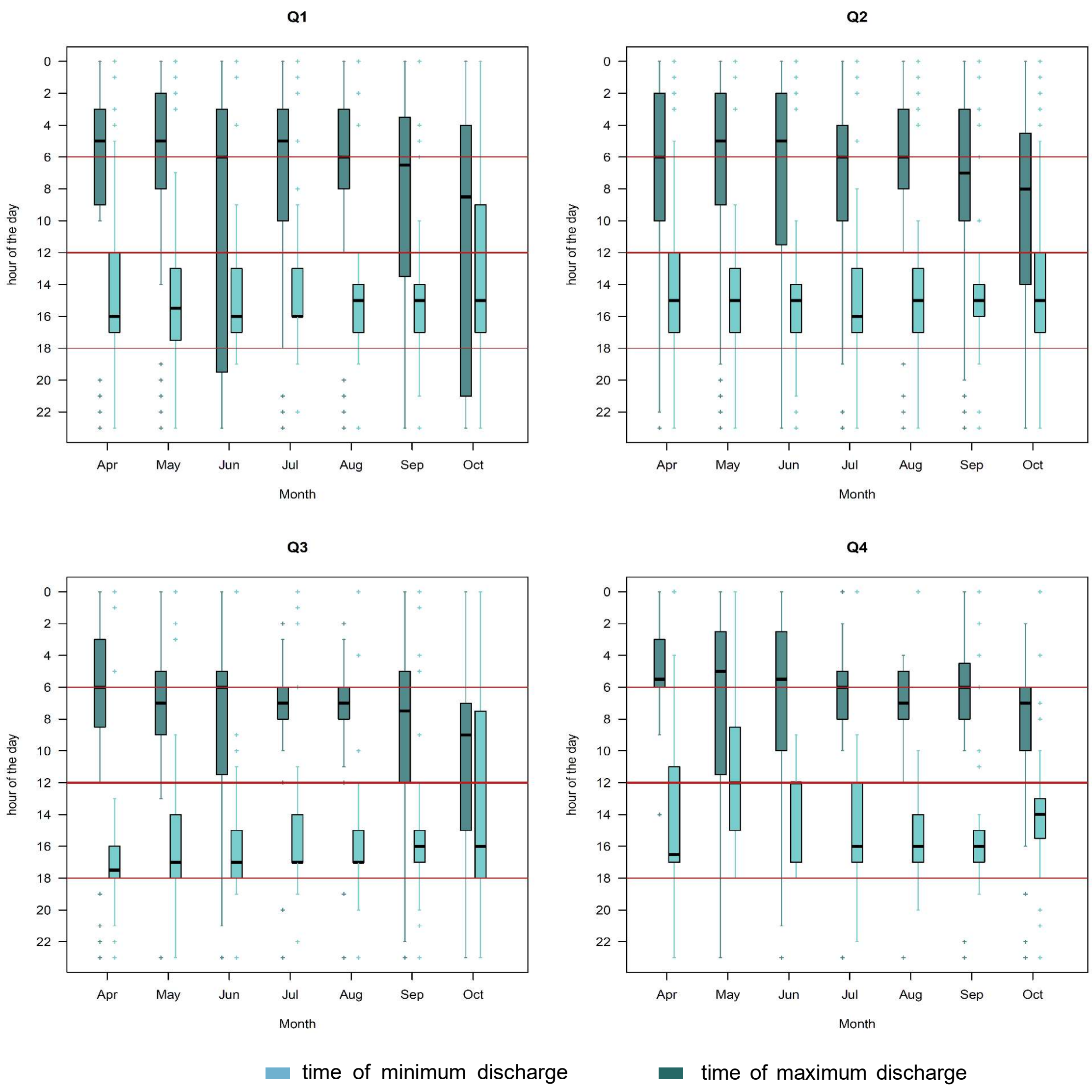

Figure 13 *Time (UTC) when minimum and maximum measured discharge occurs at gauging station*

Maximum discharge values are typically observed between 6:00 and 7:00 a.m.. Minimum daily discharge occurs about 8 to 9 hours later, at between 2:30 and 3:30 p.m. at Q1, Q2 and Q4. The seasonal analysis shows relatively constant time differences from April to September throughout the watershed. Minimum discharge at Q1 and Q2 occurs, on average, approximately between 3:00 and 3:30 p.m.. At the gauging station, Q4 minimum discharge is, on average, observed between 2:30 and 3:00 p.m.. Maximum discharge at gauging stations Q1, Q2 and Q4 can be observed around 6:00 a.m., as represented in Figure 13. At the gauging station Q3, maximum discharge occurs about one hour later at around 07:00 a.m.. Minimum discharge at Q3 can mostly be observed significantly later, at around 4:45 p.m.. The temporal analysis reveals an evident time lag between the maximum and minimum daily discharge during precipitation-free periods in the vegetative influenced season (April to October). Moreover, time delays do not show clear seasonal patterns such as those seen in the amplitudes of daily discharge fluctuations.

3.1.2 Soil water content

Diurnal discharge fluctuations are often accompanied by similar fluctuations in soil water content (SWC) or groundwater levels (Gribovszki et al., 2010). Diurnal fluctuations of soil water content similar to discharge fluctuations can also be observed in the Rosalia watershed (Figure 8, Figure 14). By visually comparing the time series of discharge and soil water content, similar behaviour on the seasonal and the daily temporal scale can be seen.

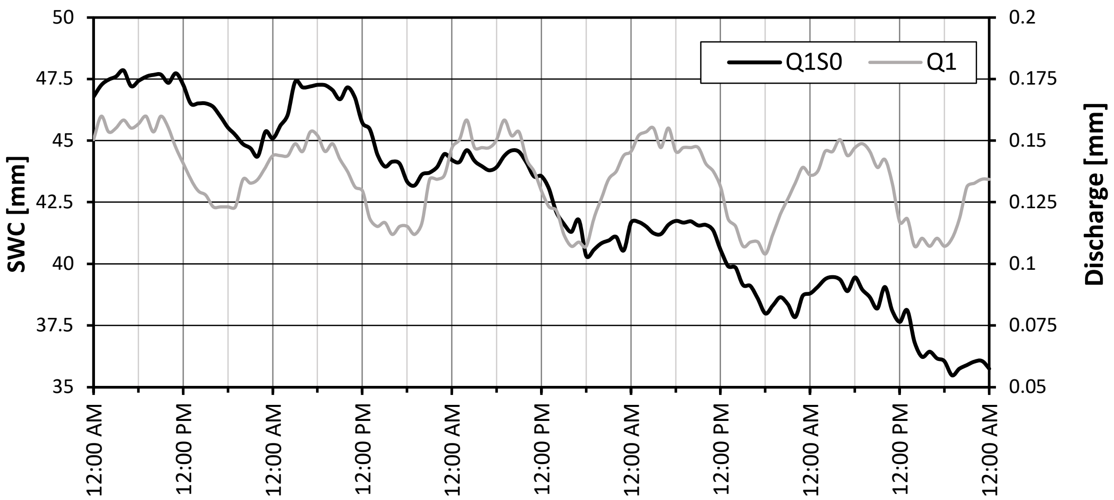

Figure 14 *Diurnal fluctuations of soil water content (Q1S0) and discharge (Q1) – 16.08.2018 – 20.08.2020*

Diurnal fluctuations of soil water content are mostly registered from spring to the beginning of autumn. These are observed mainly during soil moisture recession periods during precipitation-free episodes. In winter months, no pronounced diurnal soil water content fluctuations are observed.

Data for carrying out this analysis was selected identically to previous discharge data. So, only soil water content data with no precipitation in the preceding 24 hours was selected. The SWC database for this analysis ranges from May 2016 to the end of 2019. This ensures a temporally consistent database for all soil water content observations. The gauging station Q1 is accompanied by one soil profile (Q1S0) along the adjacent slope. At Q2, soil water content is detected at three sites (Q2S0, Q2S1, Q2S2) along the adjacent hillslope. A detailed description of all soil water content sites and sensor depths in each profile is provided in 0.

3.1.2.1 Soil water content - amplitude analyses

The soil water content analysis is carried out similarly to the diurnal discharge analyses. Daily amplitudes of soil water content are calculated based on equation (2). Firstly, the daily amplitudes will be described and investigated thoroughly; secondly, the time component of such daily diurnal signals of soil water content is analysed in the same way as before.

In Figure 15, amplitudes are plotted using the same scale of the y-axis for each soil profile. This allows for a direct comparison of the magnitude of soil water content amplitudes. The soil profiles Q1S0 and Q2S0 provide information of a 70 cm deep soil column. On the other hand, Q2S1 and Q2S2 represent a 50 cm deep soil profile. The depth difference is due to a different sensor arrangement in the respective soil profiles (2.2.1 and 2.2.2). Therefore, the absolute magnitude of the computed daily amplitude shows a clear difference. All daily soil water content amplitudes clearly show a seasonal pattern. Similar to discharge amplitudes, the largest amplitudes can be detected in June and July throughout all observations. Additionally, amplitudes in winter months show similar amplitudes with insignificant changes up to the beginning of spring.

The largest daily amplitudes are detected at Q1S0 (Figure 15). Furthermore, the most pronounced seasonal pattern can be seen at this soil profile compared to the other soil profiles. Daily amplitudes in June and July (median = 6.10 and 5.25 mm) are over three times larger than in December, January and February (median = 1.55, 1.80 and 1.90 mm). Daily amplitudes at Q2S0 show lower values and a less distinct seasonal behaviour as daily amplitudes at Q1S0. However, a clear seasonal pattern with smoothly increasing median daily amplitudes from April (2.85 mm) to June (4.7 mm) can be observed. Median daily amplitudes are above 4.5 mm in June, July, and August. Mean amplitudes in July are about two times larger than in winter months. Daily amplitudes at Q2S1 and Q2S2 are smaller than observed fluctuations in Q2S0. Furthermore, a less significant seasonal pattern at Q2S0, Q2S1 and Q2S2 is evident (Figure 15). The decrease of absolute magnitudes and the less pronounced seasonal pattern might be caused by the different sensor arrangement in each soil profile and the individual soil profile arrangement along the hillslope. This indicates that the magnitudes of Q2S1, Q2S1 and Q2S2 decrease with increasing distance from the creek (Figure 2). Nevertheless, the median daily amplitudes at Q2S1 and Q2S2 clearly show a seasonal pattern. The largest daily amplitudes are observed in June (median = 2.5 mm) at Q2S1 and in July (median = 2.5 mm) at Q2S2. The variability in observed amplitudes appears to be less evident at Q2S2 in comparison to Q2S1.

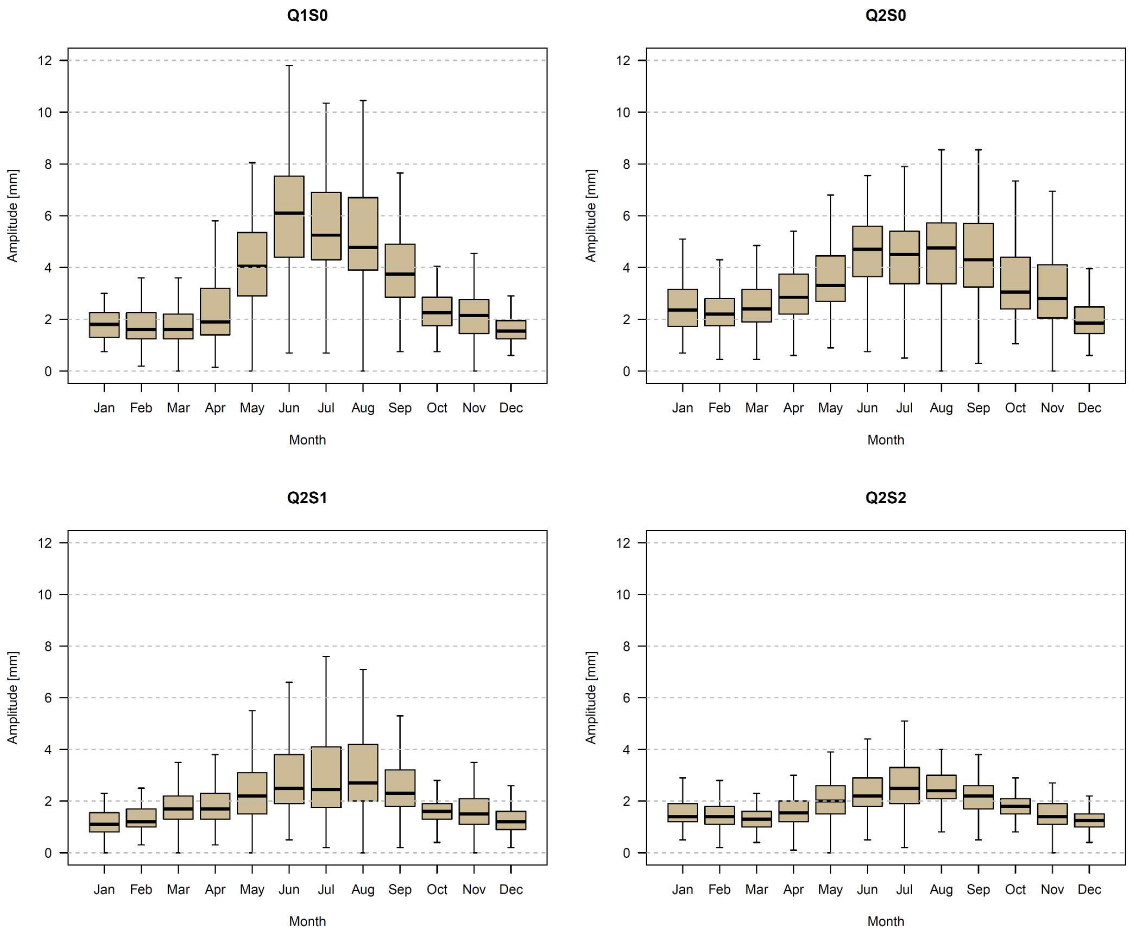

***Figure 15** Soil water content - daily amplitudes Q1S0, Q2S0, Q2S1, Q2S2 (2016-2019)*

The largest daily amplitudes are observed in June (median = 2.5 mm) at Q2S1 and in July (median = 2.5 mm) at Q2S2. Furthermore, variability in observed amplitudes seems to be less evident at Q2S2 in comparison to Q2S1.

3.1.2.2 Time of minimum and maximum soil water content

Based on the calculated daily amplitudes, the daily time of minimum and maximum soil water content is investigated here. Following 3.1.1.7, only those months, during which evident diurnal fluctuations occur, are analysed.

The daily maximum SWC can be observed mostly during nights at around 04:00 a.m. throughout all soil profiles. Minimum SWC measurements are mostly detected in the evenings between 7:00 and 8:00 p.m..

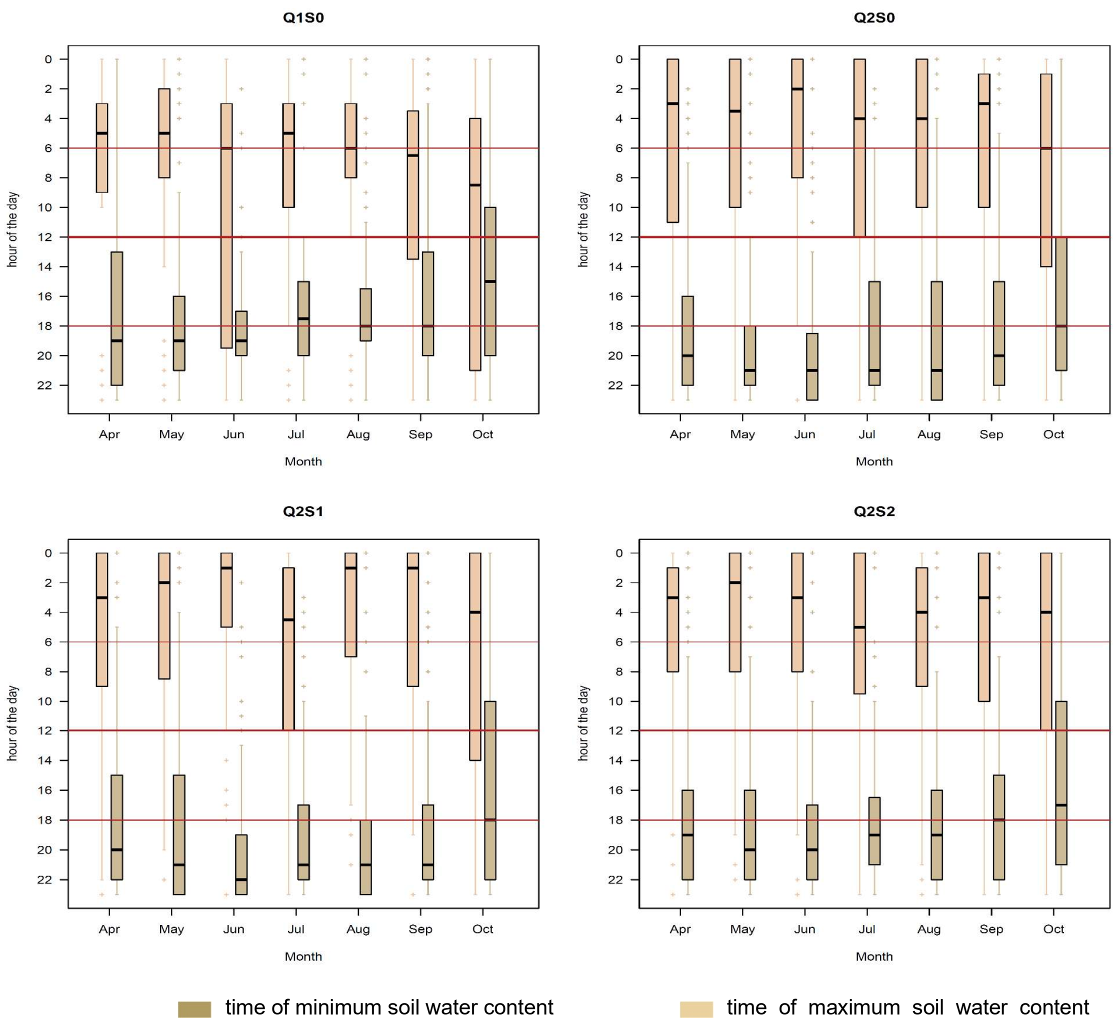

Figure 16 *Time (UTC) when minimum and maximum measured soil moisture occurs*

The mean time span between the daily maximum and the daily minimum SWC is about 15 hours within the vegetative season. However, in October, time difference decreases to about 12 hours. On average, the minimum observed SWC occurs at 5:20 p.m. and maximum daily SWC at 5:20 a.m. in October. Mostly, daily SWC amplitudes also show smaller values in October as described above. On average, at all soil profiles, minimum SWC from April to September are registered at times later than 6:00 p.m.. Maximum SWC values are mainly occurring before 6:15 a.m. from April to September. Apart from October, time differences between the minimum and maximum time of soil water content are determined to be steady from April to September. In October, where vegetation is less active, the time delay between the maximum and minimum soil water content decreases. Almost no time delay can be detected in winter and early spring months as amplitudes are also not observed.

3.1.2.3 Relationship between soil water content and discharge amplitudes

Based on the descriptions and plots above, diurnal fluctuations of soil water content (Figure 15) and discharge (Figure 9, Figure 10, Figure 11) seem to behave similarly. Both variables show a distinct seasonal pattern and a similar increase of observed amplitudes during summer months and very little or indeed no clear amplitudes in winter months. Figure 17, below, shows the relationship of median monthly amplitudes of soil water content and discharge for the respective sites.

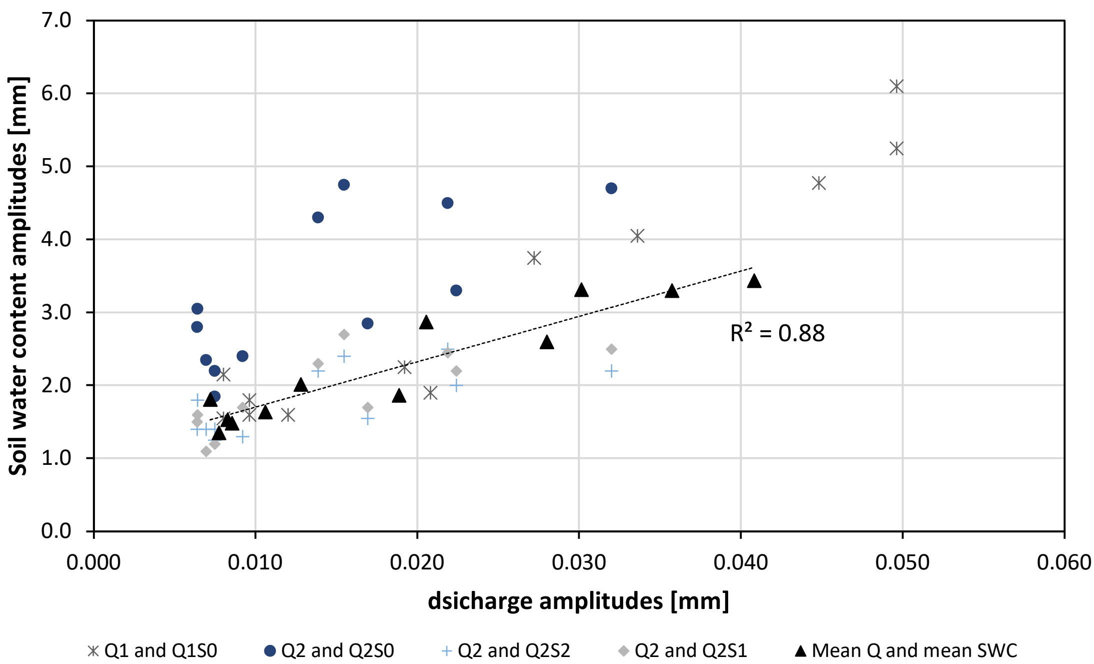

Figure 17 *Relationship of median monthly SWC and discharge amplitudes*

The coefficient of determination (R^2) of monthly median soil water content and discharge amplitudes is 0.88 on average. This clearly shows the particular relationship of discharge and soil water content amplitudes that occur over the course of the year. Discharge and soil water content amplitudes show the highest R^2 of 0.93 between Q1 and Q1S0. R^2 of the median amplitude between discharge at Q2 and the soil water content sites Q2S0, Q2S1 and Q2S2 are 0.53, 0.58 and 0.49, respectively.

3.1.3 Diurnal cyles in air temperature

The diurnal cycles of weather conditions, such as temperature, might cause diurnal discharge and soil moisture fluctuations during rainless periods (1.2). This section analyses the diurnal and seasonal cycles of temperature in the Rosalia. The diurnal signals and the time of observed minimum and maximum temperature are compared to the preceding results of discharge and SWC. In general terms, the temperature is strongly related to transpiration and evaporation processes. Therefore, this analysis might provide further insight into the processes causing diurnal discharge fluctuations in the watershed. High temperatures cause high transpiration and evaporation rates.

According to the Walter Lieth climate diagram (Figure 3), a distinct seasonal signal in temperature can be observed. Distinct diurnal signals are also evident in Figure 8, especially in precipitation free periods. Therefore, temperature data investigated here is pre-processed in an identical way to discharge and soil water content data. Only hourly temperature data in periods of no precipitation in the preceding 24 hours was selected to carry out the following amplitude analyses. The daily amplitude of temperature is computed based on equation (2). The daily amplitudes of temperatures are presented in Figure 18.

Based on the amplitude plot, a clear seasonal occurrence of daily amplitudes is detected. It can be seen that daily amplitudes exceed 10 °C in most months. In winter months, the median temperature amplitudes are between 2.5 and 4 °C. Daily amplitudes rise from March (median = 4.9 °C) to April (median = 7.95 °C). From then on, no pronounced increases of the median daily amplitudes are detected, and they remain stable with median values between 7–8 °C. During September and October, amplitudes decrease until they level out in winter.

Compared to daily amplitudes of discharge (Figure 9, Figure 10, Figure 11) and SWC (Figure 15), daily amplitudes of temperature start to rise two months earlier, in February.

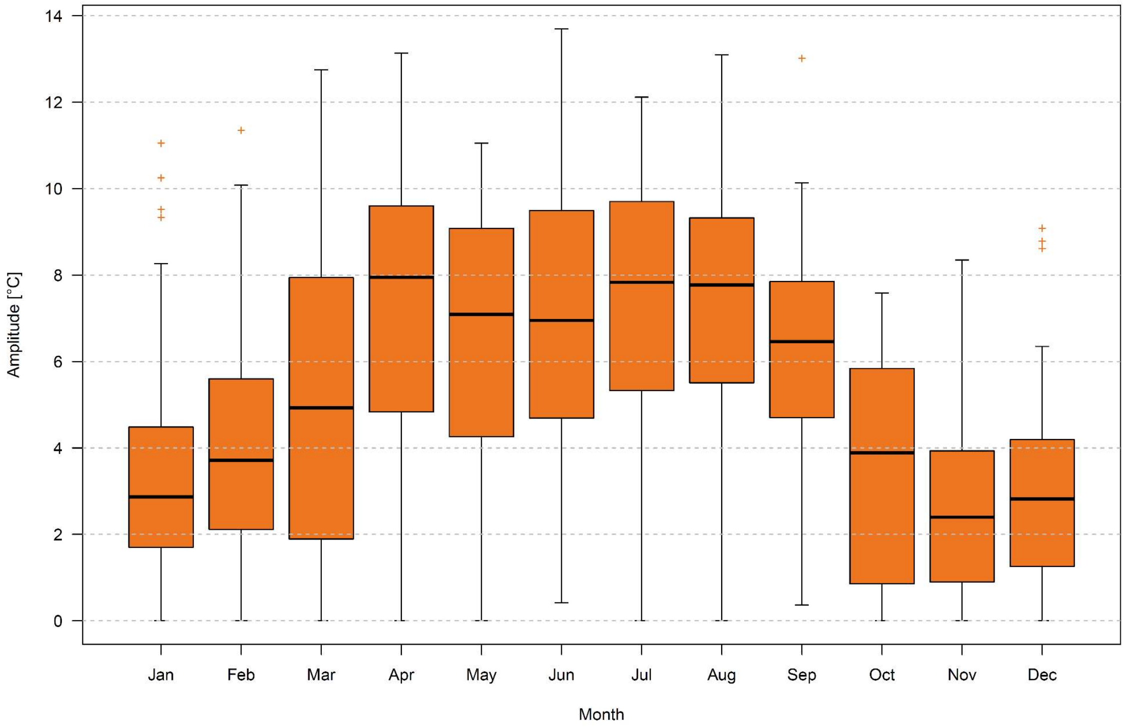

Figure 18 *Daily temperature amplitudes at climate station K1 (2016-2019)*

The calculated daily amplitudes of discharge and soil water content show clear peaks occurring in June and July and do not show steady daily amplitudes from April to August as temperature does. The mean time when maximum and minimum daily temperatures occur do not exhibit significant seasonal differences (Figure 19). As expected, maximum temperatures are observed, on average, later than minimum temperatures. Minimum temperatures occur early in the mornings between 5:30 to 6:30 a.m., and maximum daily temperatures are mostly observed between 2:30 p.m. and 3:00 p.m..The maximum daily temperatures are observed when minimum daily discharge occurs. The minimum daily soil water content is generally observed about four to five hours later than maximum daily temperatures.

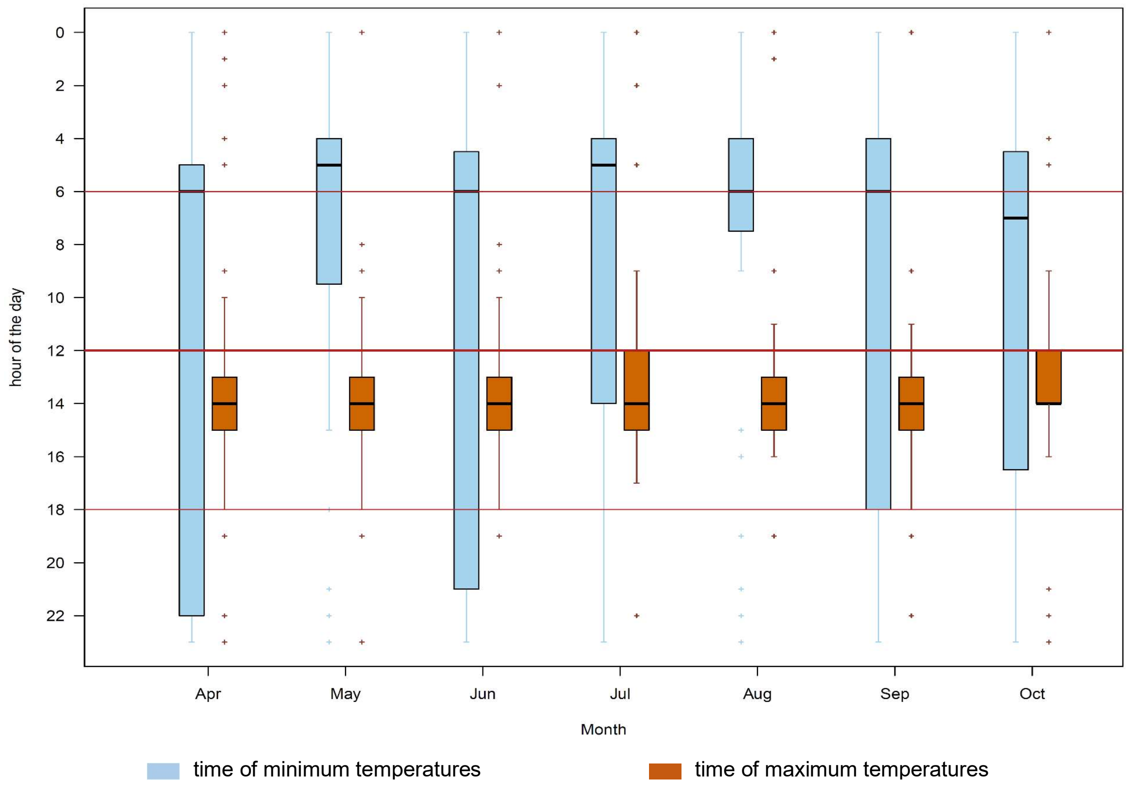

Figure 19 *Time (UTC) when minimum and maximum temperature occurs*

In Figure 20, the relationship of maximum daily temperature and minimum daily discharge and SWC is plotted (April to October). This figure visualizes the temporal relationship of the respective variables.

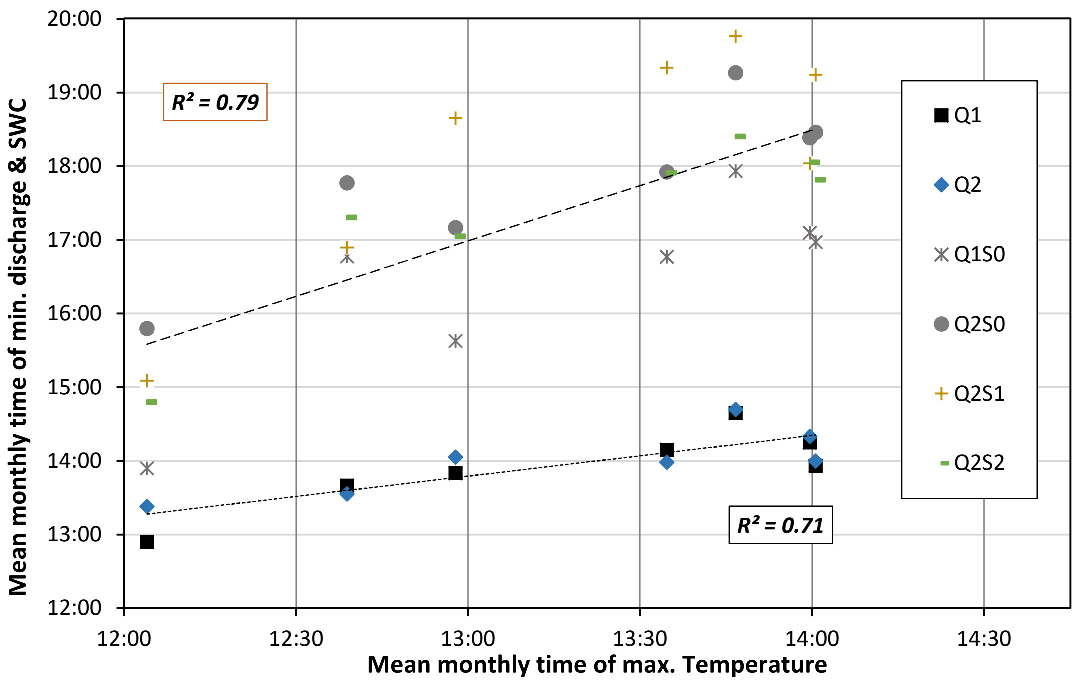

Figure 20 *Temporal relation of mean monthly time of max. temperature and mean monthly time of min. discharge (Q1, Q2) and soil water content (Q1S0, Q2S0, Q2S1, Q2S2)*

The temporal behaviour of discharge (Q1, Q2) shows a better correspondence with the maximum temperatures than the soil water content's (Q1S0, Q2S0, Q2S1, Q2S2) temporal characteristics. Minimum daily discharge appears only 30 minutes after maximum daily temperatures. Minimum daily soil water content occurs about four hours after maximum daily temperatures. This indicates a relatively slow response to maximum temperatures of soil water content compared to discharge. The illustrated linear relations in Figure 20 indicate a clear temporal relation of maximum daily temperatures with the observed minimum daily streamflow and minimum daily SWC.

3.1.4 Plant activity

Based on the dataset (PhenoCam V.2.0) the phenology of the Rosalia forest is presented. The daily data obtained ranges from 05.07.2019 to 31.08.2020, which covered just over one year's worth of data. From the daily 90th percentile G_{CC}, the mean daily G_{CC} (90th percentile) for each day of the year (doy) is calculated to illustrate the seasonally changing vegetation activity in Figure 21.

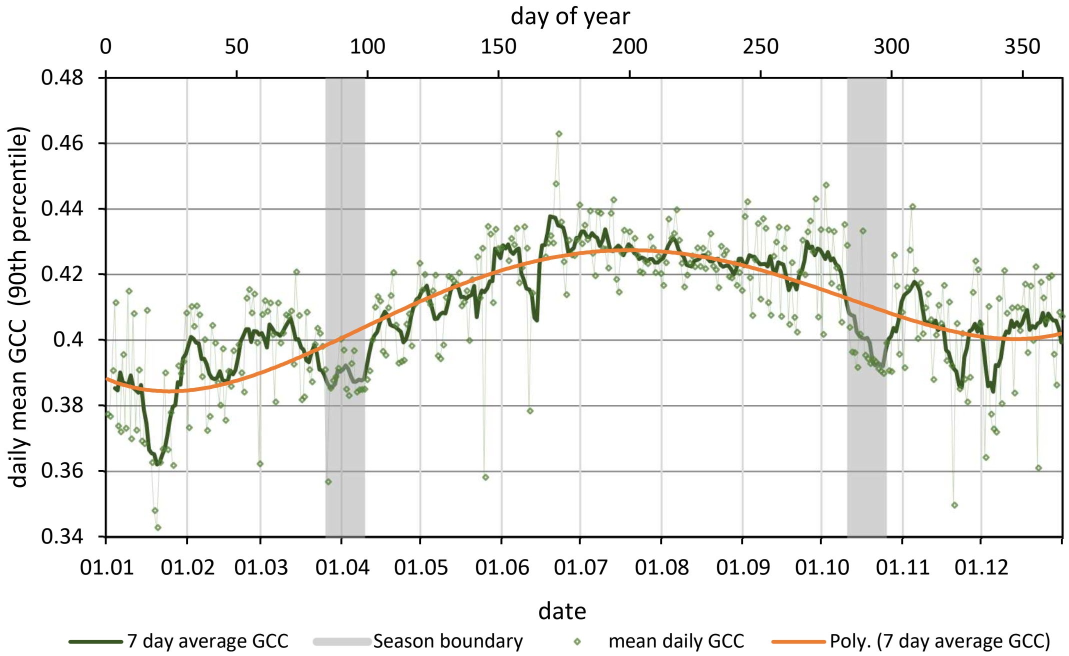

Figure 21 *Mean daily 90th percentile green chromatic coordinates (Rosalia) 2019-2020 (Seyednasrollah et al., 2019)*

The 7-day average G_{CC} is shown to illustrate more clearly the phenological changes along with the daily data. Low values occurred mostly during winter months, and high values are evident during summer months. Moreover, a dominant seasonal signal is visible. This indicates higher vegetative activity over the summer months, which goes hand-in-hand with a seasonal increase of water and energy fluxes between the surface and the atmosphere.

The grey highlighted areas in Figure 21 indicate the greenness rising and the greenness falling phenological phases, reflecting the start and end of the active vegetative season. Within these areas, the G_{CC} shows explicit low or declining values over several days. Therefore, the start of the season could be defined at the beginning of April and the end of the active plant season at the beginning of October. This results in about 200 days of active vegetation. Since similar seasonal patterns can be found in the amplitude analyses of discharge and soil water content, the relationship with the G_{CC} is analysed on a seasonal scale.

3.1.4.1 Relationship of discharge amplitudes and vegetation

The water balance in the hydrological research watershed is dominated by evapotranspiration, since 87% of observed precipitation is lost to the atmosphere (2.3.3). Therefore, vegetation, especially riparian vegetation, might withdraw a significant amount of water through root water uptake. This may be the leading cause of diurnal fluctuations. Furthermore, the distinct seasonal occurrence of daily amplitudes at all watersheds shows a similar pattern compared to the plant phenology. The G_{CC} is used here as a proxy to describe the plant activity throughout the year (phenology). Therefore, the monthly median values of the G_{CC} and discharge amplitudes are plotted in Figure 22 to determine if there is a relationship.

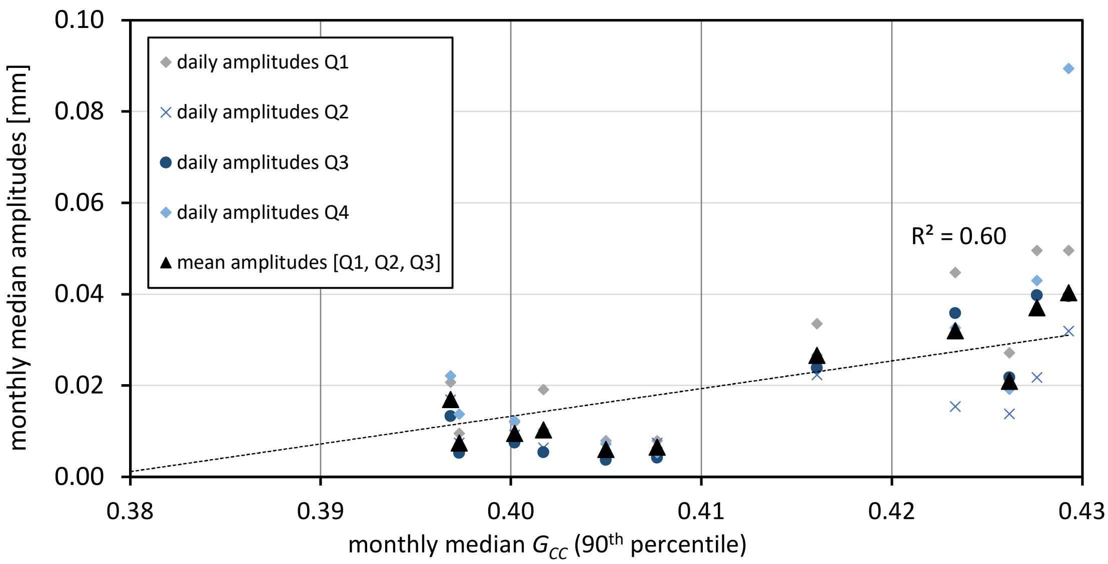

Figure 22 *Relation of monthly median discharge amplitudes and the monthly median green chromatic coordinate G_{CC}*

The graph illustrates the correlation between median monthly amplitudes and median monthly G_{CC} for each respective gauging station. Additionally, the mean amplitudes of all respective daily amplitudes are presented. A high R^2 of 0.60 can be found. The individual coefficient of determination values between the plant phenology and discharge amplitudes at each discharge station are 0.65, 0.48, 0.51 and 0.41 at Q1, Q2, Q3 and Q4, respectively.

The relationship suggests that the plant activity and the observed diurnal discharge fluctuations are related on a seasonal scale because the root water uptake of trees and other plants is related to plant phenology (G_{CC}). Therefore this could be an influencing factor of diurnal discharge fluctuations.

3.1.4.2 Relationship between soil water content amplitudes and vegetation phenology

The median of monthly discharge and soil water content amplitudes correlate well with plant activity. However, the relationship between monthly median soil water content amplitudes and the G_{CC} is even more significant compared to the discharge amplitudes. The R^2 of the seasonal plant activity (G_{CC}) and observed amplitudes in precipitation-free periods is, on average, 0.74. Figure 23 illustrates this relationship for each soil profile individually.

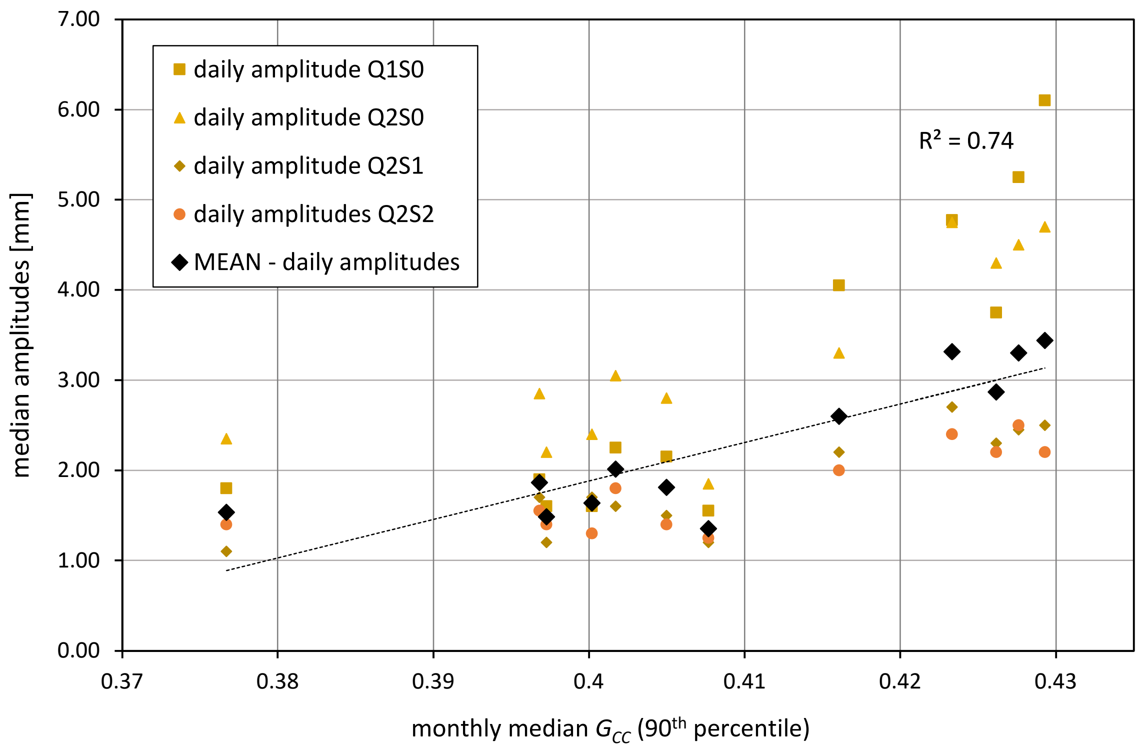

Figure 23 *Relation of median monthly SWC amplitudes and the median monthly green chromatic coordinate (G_{CC})*

The strong relationship shown reflects a strong interrelation of plant activity and detected amplitudes of soil water on a seasonal scale. The strong relationship suggests that processes causing daily soil water content amplitudes on a seasonal scale are driven by plant activity.

3.2 Diurnal fluctuations of hydrological variables - summary

The seasonal occurrence of diurnal discharge fluctuations was scrutinised in Chapter 3. As suggested by multiple authors, this analysis is accompanied by similar investigations of soil water content and climate variables, in this case, temperature. All studied variables exhibit a pronounced seasonal occurrence of diurnal fluctuations in precipitation-free periods. Additionally, the daily discharge amplitudes show a seasonal relationship with plant activity (G_{CC}). An even more pronounced correlation was found between daily soil water content amplitudes and seasonal plant activity. This indicates a strong interrelationship of plants, soil water content and discharge.

Furthermore, the time of recorded minimum and maximum daily discharge, soil water content and temperatures is analysed, compared and contrasted. This showed a clear temporal relationship between maximum daily temperatures and observed daily minimum discharge and soil water content. The results suggest a strong relationship between climatic forces, such as temperature, with the diurnal fluctuations of discharge and soil water content. Based on the seasonal occurrence and the daily temporal behaviour of discharge amplitudes, the diurnal discharge fluctuations are attributable to root water uptake of the riparian vegetation. These results are supported by findings in the literature (Dvořáková et al., 2014, Deutscher et al. 2016b, Barnard et al., (2010), Lundquist and Cayan 2002, Szilágyi et al. 2008). As plants abstract water to meet their daily water demand, discharge and soil water content is depleted diurnally, following the daily cycle of plant metabolism. This water volume is then transpired via the plant. Therefore, evapotranspiration, primarily transpiration, of the riparian vegetation can be determined as the foremost process inducing the diurnal discharge fluctuations.

4 Process based modelling of diurnal discharge fluctuations

The analyses carried out above clearly indicate that diurnal fluctuations of discharge and soil water content during dry periods can be attributed to root water uptake by plants. The diurnal fluctuations of discharge and soil water content show a seasonal pattern corresponding to the seasonal pattern of plant activity (G_{cc}), suggesting that they are caused by evapotranspiration. Furthermore, in densely vegetated catchments, evapotranspiration has been shown to be dominated by transpiration (Gribovszki et al., 2010). Multiple authors linked daily fluctuations in streamflow to evapotranspiration (Dvořáková et al., 2014, Deutscher et al. 2016b, Barnard et al., (2010), Lundquist and Cayan 2002, Szilágyi et al. 2008).

In this chapter, the processes causing the diurnal discharge fluctuations are investigated and simulated with HYDRUS (Simunek et al., 2018). The simulated water fluxes will yield a better understanding of the interaction between discharge and evapotranspiration. Based on the simulation results, the influence of riparian vegetation water uptake on discharge, especially during dry periods, is assessed. The equations representing soil water movement in the unsaturated and saturated zone will be described thoroughly here. For a more detailed description of all HYDRUS model routines, readers are referred to the HYDRUS Technical Manual – Version 3 (Simunek et al., 2018).

4.1 The HYDRUS 2D model

The HYDRUS 2D/3D software package (v.3.02) was used to carry out the analyses. HYDRUS is able to simulate water movement alongside heat and solute transport in two- and three-dimensional saturated and unsaturated porous media. Furthermore, HYDRUS is able to take into consideration flow regions defined by irregular boundaries. Water flow can occur in horizontal and vertical planes. Within the model, prescribed flux and head boundaries, atmospheric boundary conditions, free drainage boundary conditions and simplified representation of nodal drains can be assigned (Simunek et al., 2018).

The unsaturated (vadose) zone is an essential part of the hydrological cycle, and its importance has long been recognized. The zone plays a crucial role in multiple processes of hydrology, including groundwater recharge, runoff, erosion, soil water storage, evaporation, and infiltration. Initial studies of the vadose zone focused mainly on water supply and management of the root zone of agricultural soils to yield maximum crop production (Simunek et al., 2018). Simunek et al. (2018) also pointed out that interests in the vadose zone have increased in recent years due to growing concerns regarding adverse effects on the environment by agricultural, industrial and municipal activities.

The most widely used equation for predicting water flow in variably saturated porous media is the Richards equation. HYDRUS solves the Richards equation numerically for saturated-unsaturated water flow. The equation also incorporates a sink term to account for root water uptake by plants. This deterministic approach will most likely continue to be used in the near future for predicting and resolving water transport processes in the vadose zone (Simunek et al., 2018).

4.1.1 Governing flow equation

HYDRUS incorporates two different flow equations, the uniform flow and the flow in a dual-porosity system. The latter assumes that water in the matrix does not move (intra-aggregate pores or rock matrix) and that water flow is limited to fractures (e.g., macropores). On the other hand, the uniform flow equation considers two- and three-dimensional isothermal uniform Darcian flow of water through the matrix (Simunek et al., 2018). The uniform flow equation was used for the modelling task in this thesis.

4.1.1.1 Uniform flow equation

In addition to considering a two- and three-dimensional isothermal uniform Darcian water flow in a variably saturated porous medium, it is assumed that the air phase plays a negligible role in the liquid flow process. Based on these assumptions, the main flow equation is represented by the following modified Richards equation (Simunek et al., 2018):

$$\frac{\partial \theta}{\partial t} = \frac{\partial}{\partial x_i}\left[K\left(K_{ij}^A \frac{\partial h}{\partial t} + K_{iz}^A\right)\right] - S \tag{3}$$

θ is the volumetric water content [L^3L^{-3}], h is the pressure head [L], S is the sink term [T^{-1}], x_i (i = 1,2,3) are the spatial coordinates [L], t is the time [T], K_{ij}^A are the components of a dimensionless anisotropy tensor $\mathbf{K}^4$, and K is the unsaturated hydraulic conductivity function [LT^{-1}]:

$$K(h, x, z) = K_s(x, z)\, K_r(h, x, z) \tag{4}$$

K_r is the relative hydraulic conductivity [LT^{-1}] and K_s the saturated hydraulic conductivity [LT^{-1}].

4.1.2 Root water uptake

The following equation describes the sink term due to plant water uptake, which represents the volume of water removed per unit volume of soil. Feddes *et al.,* (1978) defined S as:

$$S(h) = \alpha(h)\, S_P \tag{5}$$

The stress response function $\alpha(h)$ is a dimensionless function of the soil water pressure head (0 ≤ α ≤1) and S_P is the potential water uptake rate [T^{-1}]. In Figure 24, an example of the stress response function is shown. The values of the represented vegetation types are taken from the HYDRUS database of suggested parameter values for the Feddes et al. (1978) model (Simunek et al., 2018).

The stress response function is defined by four pressure heads, depending on the plants. Close to saturation, water uptake is assumed to be zero (i.e., wetter than some arbitrary "anaerobiosis point", $\boldsymbol{P_0}$). On the other hand, the water uptake is also zero when pressure heads are smaller than the wilting point ($\boldsymbol{P_3}$). Optimal water uptake is assumed to be between $\boldsymbol{P_{Opt}}$ and $\boldsymbol{P_{2L}}$ or $\boldsymbol{P_{2H}}$. Between $\boldsymbol{P_0}$ and $\boldsymbol{P_{Opt}}$, water uptake increases linearly with h. Conversely, water uptake decreases linearly between $\boldsymbol{P_{2L}}$ ***or*** $\boldsymbol{P_{2H}}$ to $\boldsymbol{P_3}$. During periods of no water stress ($\alpha(h)$ = 1) the water uptake rate is equal to the potential water uptake rate S_P (Simunek et al., 2018).

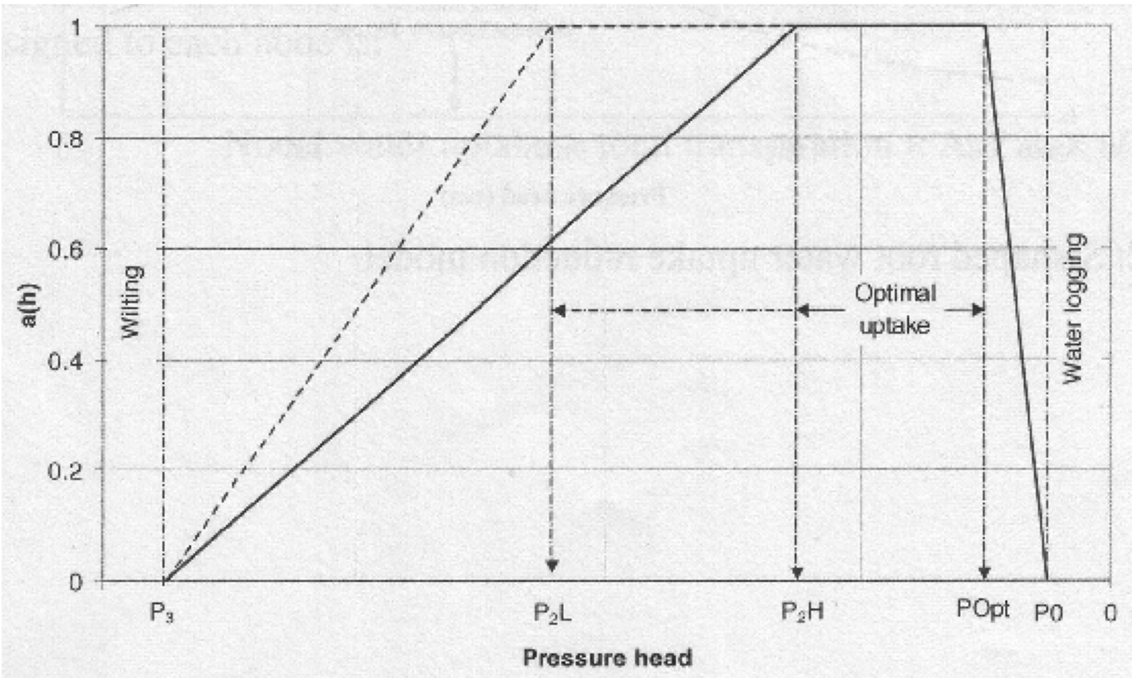

Figure 24 *Example diagram of the stress response function* (Simunek et al., 1999)

4.1.3 Unsaturated soil hydraulic properties

Generally, the unsaturated soil hydraulic properties θ(h) and *K*(h) are highly nonlinear functions of the pressure head. In the modelling environment of HYDRUS one can choose to use different analytical models for hydraulic properties, including Brooks and Corey (1964), Vogel and Cislerova (1988), Kosugi (1999), van Genuchten (1980), and Durner (1994).

For the HYDRUS simulation in this thesis, the soil hydraulic function of van Genuchten (1980) was used. To determine a predictive equation of soil water retention parameters, van Genuchten used the statistical pore-size distribution model of Mualem (1976). The expressions used, as determined by van Genuchten are shown below (Simunek et al., 2018).

The six independent parameters shown above include θ_r, θ_s, α, n, K_S and l. l

$$\theta(h) = \begin{cases} \theta_r + \dfrac{\theta_s - \theta_r}{[1 + |\alpha h|^n]^m} & h < 0 \\ \theta_s & h \geq 0 \end{cases} \quad (6)$$

$$K(h) = K_s S_e^l [1 - (S_e^{1/m})^m]^2 \quad (7)$$

$$m = 1 - 1/n, \quad n > 1 \quad (8)$$

represent the pore connectivity parameter, which was, on average, estimated to be 0.5 for various different soils (Simunek et al., 2018). The parameters, *m* and *n* (pore size distribution) are empirical coefficients that affect the shape of the soil water retention curve (Bursey, 2008).

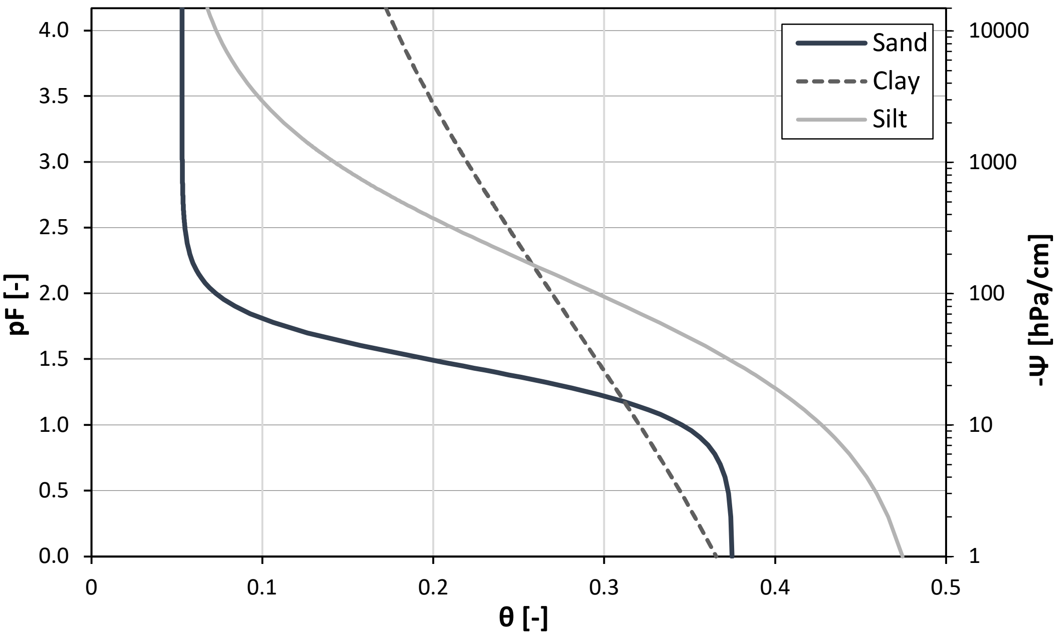

Figure 25 *Example of soil water retention curves for typical soil textures (Sand, Silt, Clay)*

In Figure 25, the plotted soil water retention curves for three textural classes (Sand, Silt, Clay) can be seen. The soil hydraulic parameters of these soil water retention curves were obtained from the HYDRUS database, which includes various soil hydraulic parameters estimated using the USDA textural triangle (Simunek et al., 2018).

4.2 HYDRUS model setup for a slope transect at Rosalia

The HYDRUS 2D model was set up by generating a representative hillslope for the Rosalia to investigate the water fluxes within the saturated and unsaturated soil matrix. The modelled hillslope represents natural conditions close to the gauging station Q2. Since this thesis focuses on the interaction of discharge and the riparian vegetation, the main area of interest is the riparian area along the creeks. A description of the HYDRUS model configuration is presented, including the geometry, soil hydraulic parameters, root water uptake parameters, initial conditions and boundary conditions.

4.2.1 Study site - hillslope Q2

The selected study site (hillslope) within the experimental research watershed Rosalia is located close to gauging station Q2. Figure 26 gives an overview of the soil transect represented in the model.

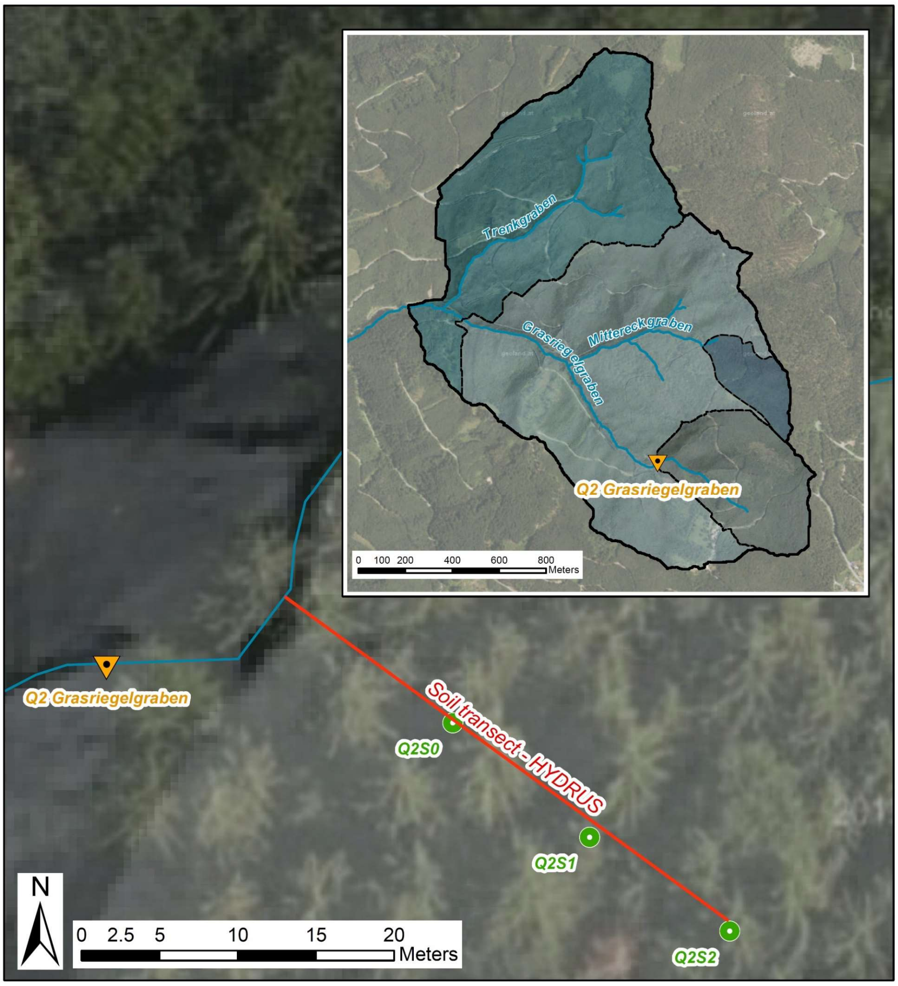

Figure 26 *Study site – Soil transect at the hillslope Q2*

4.2.1.1 General HYDRUS configuration

The main processes used to analyse the diurnal interaction of vegetation and the discharge are the water flow (4.1.1.1) and the root water uptake (4.1.2). The domain type and units used have to be defined within HYDRUS. In this study, the domain type was set as a 2D – vertical plane. Within the model, the hillslope is represented by one soil material. The simulation period covers one month. The minimum and the initial time step is 0.0024 h. Furthermore, the simulation is terminated if 10 computation steps yield no changes smaller than the iteration criteria (water content tolerance: 0.001 [-], pressure head: 1 cm).

4.2.1.2 Model domain and mesh generation

The domain represented in the model is shown in Figure 27. The surface topography was derived from a high-resolution (1x1 m) digital elevation model. So, the domain captures the actual hillslope of the Grasriegelgraben a few meters upstream of the gauging station Q2. The soil transect and the locations of the soil profiles containing the sensors is shown in Figure 27.

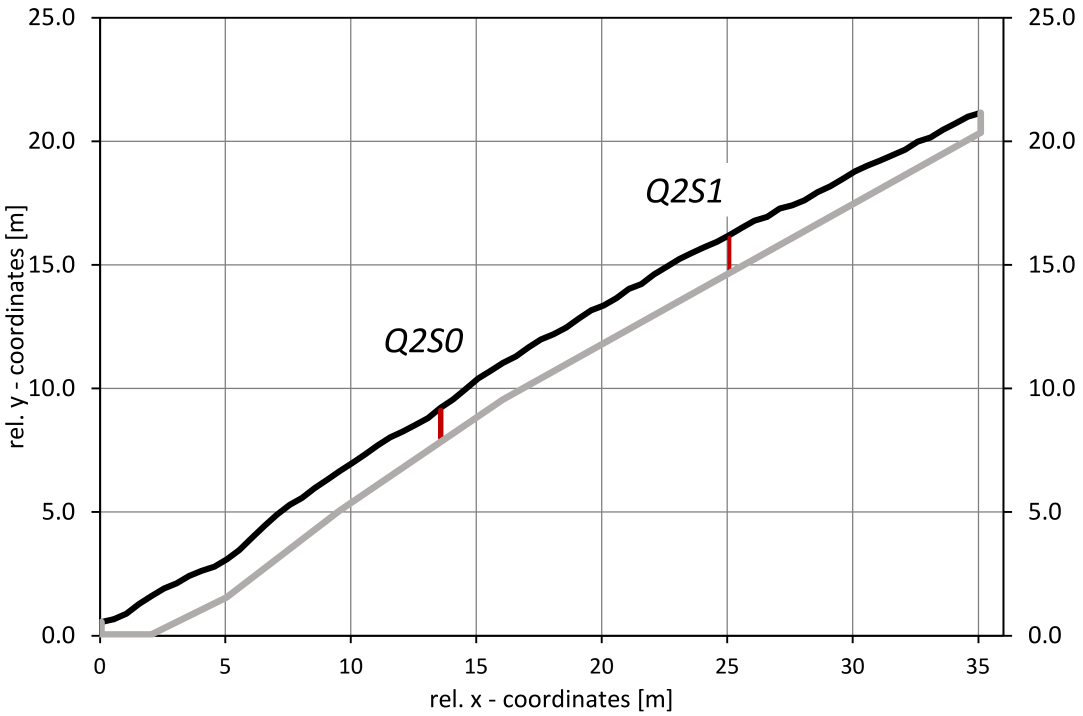

Figure 27 *Model domain and soil water profiles (Q2S0, Q2S1)*

The finite element mesh was created within the geometric domain (Figure 27). It consists of 8640 nodes. To begin with, the mesh was established with a discretization of 15 cm for the total modelling domain and was refined to 4 cm in the vicinity of the creek. Such a refined high-resolution mesh was required in this area in order to capture the processes between the stream and the riparian vegetation in detail. The generated triangular mesh in the vicinity of the creek (3 m) is represented in Figure 28. Additionally, the assigned boundary conditions are illustrated. They will be described in more detail in 4.2.1.6.

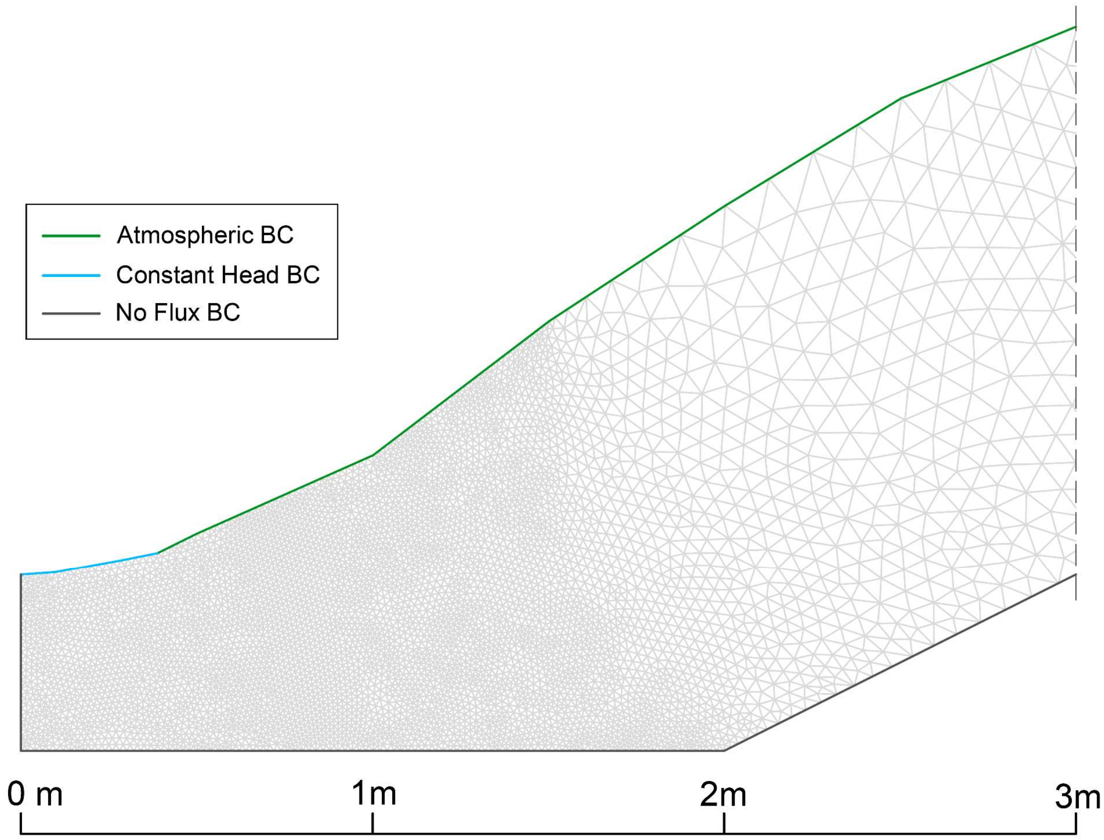

Figure 28 *Mesh of the model domain (detail of lower part)*

4.2.1.3 Soil hydraulic properties

As stated above, the van Genuchten (1980) function was used in this study to describe the soil hydraulic properties. Two different approaches have been used in the thesis to estimate the five parameters needed for the van Genuchten model. Both approaches are based on soil sample analysis. First, the soil hydraulic parameters (SHP) were estimated based on the USDA textural triangle's classes of one soil sample excavated in June 2015. Within the scope of this thesis, the water retention curves of nine undisturbed soil samples were estimated additionally (HYPROP - Analyses). They have been excavated in

October 2020, along the hillslope. Therefore, soil hydraulic properties of ten soil samples were analysed.

4.2.1.3.1 Estimation based on texture

The soil hydraulic parameters for the van Genuchten model were estimated based on the neuronal network prediction (Schaap et al., 2002) function within HYDRUS. They were derived based on the textural analyses of one soil sample which was excavated during the soil profil establishment at Q2S0 in June 2015. HYDRUS incorporates the Rosetta Lite DLL (Dynamically Linked Library), which was independently developed at the U.S. Salinity Laboratory (Schaap et al., 2002). This program predicts the soil hydraulic parameters and the saturated hydraulic conductivity in a hierarchical way using soil textural information. The percentage of each textural class of sand, silt and clay (SSC) of the soil sample (Q2S0) were determined to be 42%, 45% and 13%, respectively. The predicted soil hydraulic parameters for the van Genuchten model are presented in Table 8. Using these parameters (Table 8), the soil water retention curve is illustrated in Figure 29.

Table 8 *Soil hydraulic parameters (van Genuchten) based on texture*

θr [-]	θs [-]	α [1/cm]	n [-]	m [-]
0.0497	0.3983	0.0081	1.5424	0.3516

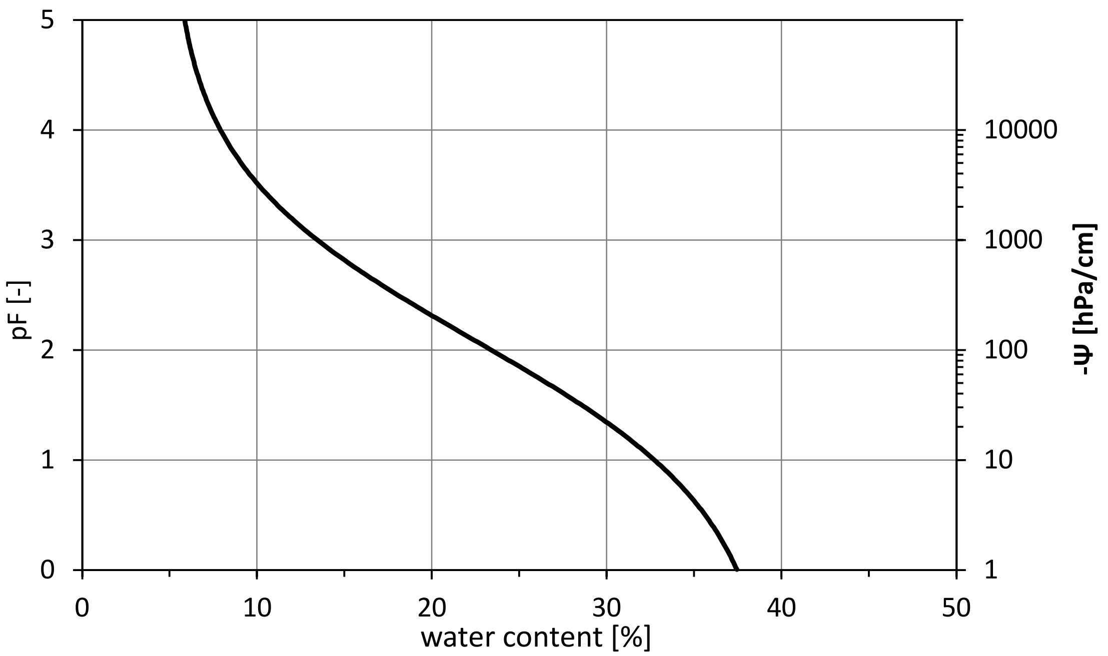

Figure 29 *Soil water retention curve estimated based on texture*

The soil hydraulic parameters were derived from only one soil sample (Q2S0). As these soil hydraulic parameters are applied to the total modelling domain, large uncertainties of the predicted soil hydraulic parameters are to be expected.

4.2.1.3.2 HYPROP analyses of soil samples

To improve the reliability of the soil hydraulic parameters estimated based on texture, nine additional soil samples were collected and analysed in October 2020. These soil samples were collected in the vicinity of the installed water content measurement profiles along the hillslope. Furthermore, the soil samples of each profile were collected at the respective sensor depths of 10, 20 and 40 cm. These soil samples were then analysed using the HYPROP 2 hydraulic property analyser (UMS, 2015).

The HYPROP 2 device is a fully automated measurement and evaluation device. It derives soil hydraulic properties of soil samples according to Schindler's evaporation method (Schindler et al., 2010). The soil water tension and the unsaturated hydraulic conductivity were measured with tensiometers at two different depths of the soil sample. Furthermore, the volumetric water content was measured by recording the weight loss of the soil sample. Using this information, the water retention curves were created (UMS, 2015). The soil hydraulic parameters of each soil sample obtained are represented in Table 9.

Table 9 *Soil hydraulic parameters (van Genuchten) derived by HYPROP analyses*

Soil Profile	depth [cm]	sample	θr [-]	θs [-]	α [1/cm]	n [-]	m [-]
Q2S0	10	Q2S0_10	0.2990	0.7790	0.0255	1.6800	0.4048
Q2S0	20	Q2S0_20	0.1480	0.5420	0.0278	1.6150	0.3808
Q2S0	40	Q2S0_40	0.0580	0.5540	0.0283	1.3650	0.2674
Q2S1	10	Q2S1_10	0.0920	0.4540	0.0285	1.4420	0.3065
Q2S1	20	Q2S1_20	0.0300	0.3850	0.0455	1.2940	0.2272
Q2S1	40	Q2S1_40	0.0250	0.5060	0.0764	1.3080	0.2355
Q2S2	10	Q2S2_10	0.0370	0.5050	0.1595	1.1450	0.1266
Q2S2	20	Q2S2_20	0.2680	0.8120	0.0527	1.3100	0.2366
Q2S2	40	Q2S2_40	0.0090	0.5300	0.0494	1.2320	0.1883

The resulting parameter sets indicate considerable variability between the soil samples, highlighting the spatial variability and heterogeneity of soil hydraulic properties along the hillslope. Especially at Q2S0_10 and Q2S2_20, the saturated water content (θs) and the residual water content (θr) show large discrepancies compared to the respective parameters from other soil samples. The resulting soil water retention curves of each soil sample are illustrated in

Figure **30**.

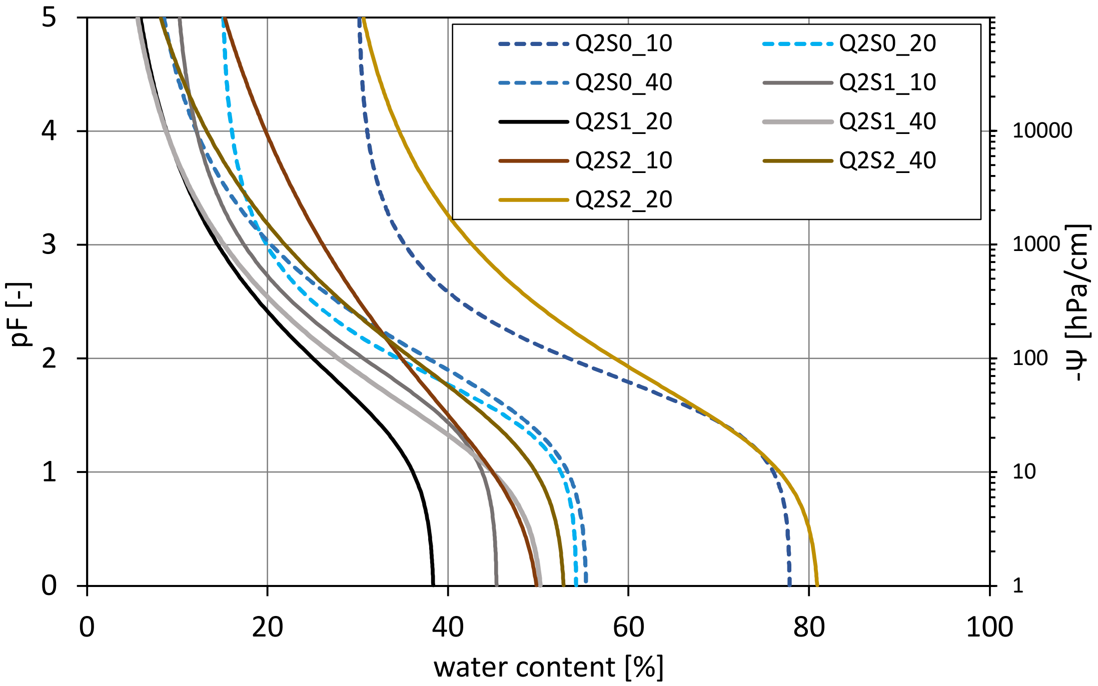

Figure 30 *Soil water retention curves derived from HYPROP*

The figure above clearly illustrates the parameter variability (Table 9) described above. The large differences in the soil water retention curves of Q2S0_10 and Q2S2_20, when compared to all other soil samples, might be explained by disrupted soil samples or measurement errors. However, a thorough analysis of the variability of the derived parameters would exceed the scope of this thesis. Therefore, the resulting parameters of the soil samples at Q2S0_10 and Q2S2_20 were omitted.

Based on the remaining analysed soil samples (Table 9) and the corresponding soil water retention curves, three parameter sets were derived using a curve fitting approach. Those three parameter sets capture the variability and heterogeneity of the analysed soil samples. The three parameter sets include minimum and maximum values corresponding to the measured soil water content values. The minimum and maximum curves represent the enveloping curves of the measured soil water retention curves. Furthermore, a third parameter set was calculated using the mean values of the measured soil water retention curves.

The parameters were calculated, minimising the root mean square error (RMSE) as the objective function for each respective parameter set. The calculated soil hydraulic parameters are listed in Table 10.

Table 10 *Soil hydraulic parameters used in the simulation*

	θr [-]	θs [-]	α [1/cm]	n [-]	m [-]
HYDRUS	0.0497	0.3983	0.0081	1.5424	0.3516
Minimum Parameters	0.0587	0.4101	0.0066	1.6092	0.3786
Mean Parameters	0.1042	0.5214	0.0077	1.6621	0.3984
Maximum Parameters	0.1709	0.5857	0.0083	1.6718	0.4019

The derived soil hydraulic parameter sets were then used as input for the soil hydraulic model in HYDRUS. Based on the different input parameter sets, the impact of changing soil hydraulic properties of the saturated and unsaturated zone on resulting water fluxes were assessed. These supplementary results are presented in chapter 4.3. Corresponding soil water retention curves are plotted in Figure 31. They also include the estimated soil hydraulic properties based on the textural classes (SWC – HYDRUS) described above.

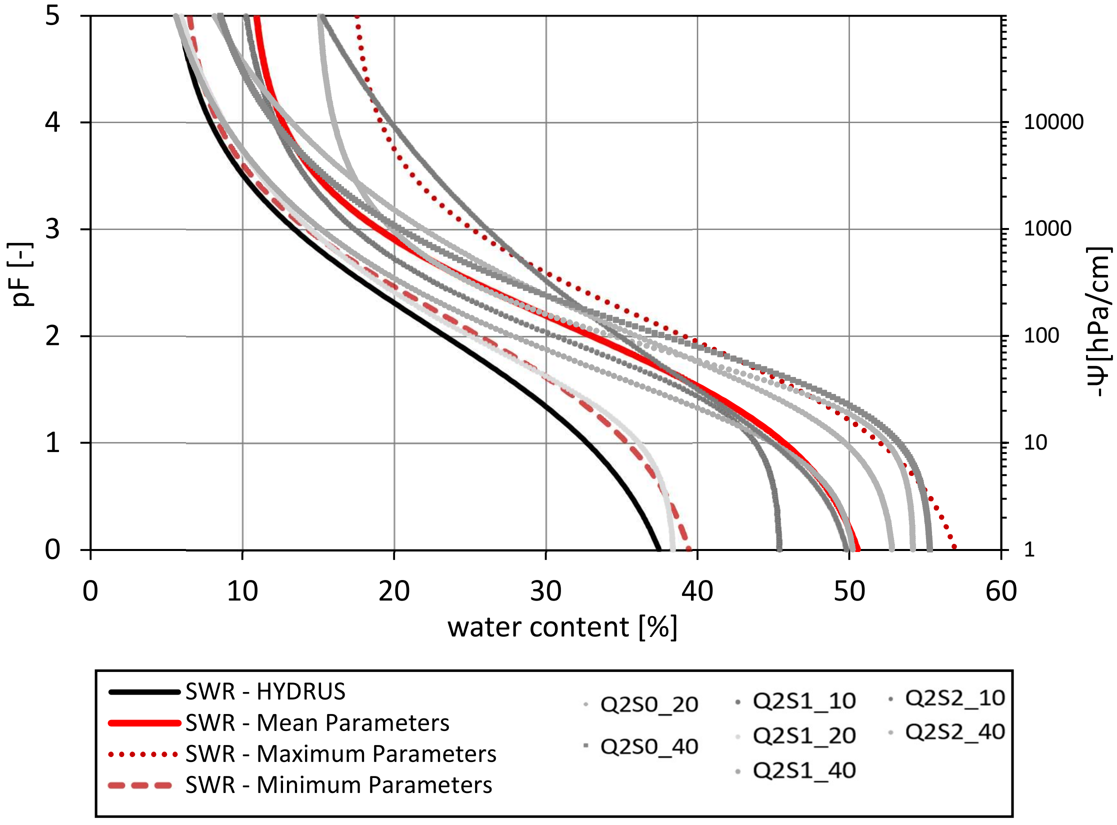

Figure 31 *Soil water retention curves based on HYPROP*

4.2.1.4 Root water uptake and root distribution

HYDRUS incorporates a database of suggested parameter values for the stress response function for various plant types (Simunek et al., 2018). The hillslope is mainly populated by beech tree. Parameters for these are however not provided in the HYDRUS database. Therefore, parameters suggested by Seeger et al. (2017) were implemented in the model. The parameters for beech communities were derived based on soil water isotopes measurements and a HYDRUS model optimisation towards observed soil moisture. The parameters (pressure heads) used are listed in Table 11.

Table 11 *Stress response functions - Parameters*

P_0 [cm]	P_{0pt} [cm]	P_{2H} [cm]	P_{2L} [cm]	P_3 [cm]
0	-25	-700	-2300	-18500

The parameters P_{2H} and P_{2L} of the stress response function are defined as a function of the potential transpiration rate. Therefore, two parameters (P_{2H}, P_{2L}) for the optimal response function ($\alpha(h)$ = 1) are defined within HYDRUS. P_{2L} is used when the potential transpiration rate is rather low (r_2L = 1 mm/d) and P_{2H} when rather higher (r_2H = 5 mm/d) (Simunek et al., 2018). The actual stress response function for both potential transpiration rates (r_2L, r_2H) based on the parameters (P_0, P_{opt}, P_{2H}, P_{2L}, P_3) is represented in Figure 32.

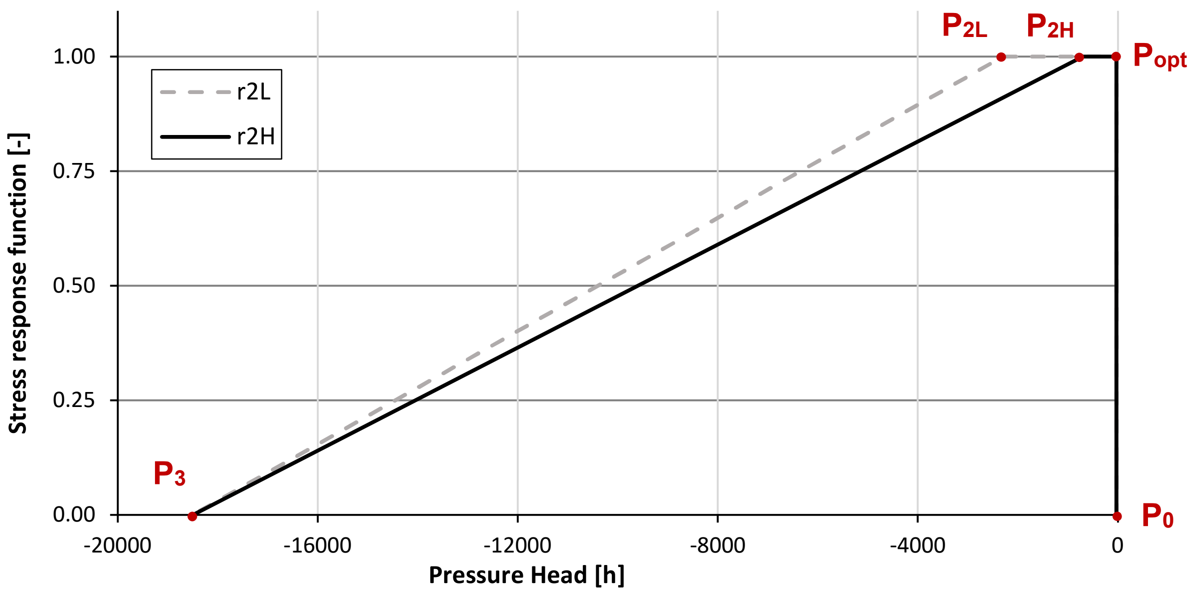

Figure 32 *Stress response function α(h) – beech trees*

As a next step considering root water uptake, the spatial distribution of the roots had to be defined. By manually selecting the nodes of the created mesh, the spatial distribution of roots was assigned. HYDRUS provides the option to assign a linear decreasing root distribution with depth on the selected nodes to represent a more realistic root distribution (Simunek et al., 2018). Moreover, a slope of the horizontal root distribution can be specified.

Schmid and Kazda (2001) investigated the vertical distribution of European beech and Norway spruce of pure and mixed tree stands. They determined maximum root depths of about 1 m for both species. Moreover, they found that neither root growth nor root diameter is correlated with soil depth. The maximum root density of beeches did occur in 10 to 20 cm depth. Below 20 cm, the number of roots decreases continuously, and large roots (diameter > 20 mm) only occurred above 50 cm (Schmid and Kazda, 2001).

Based on the functions available in HYDRUS and the analyses of Schmid and Kazda (2001), the following root distribution was implemented in HYDRUS. A schematic illustration of the assigned root distribution is presented in Figure 33.

Generally, a vertical root distribution that linearly decreases with depth was assigned in the model. The maximum rooting depth was determined to be between 50 and 60 cm. This does not represent the real root distribution optimally but is a reasonable estimation based on the options available in HYDRUS to approximate the existing root system.

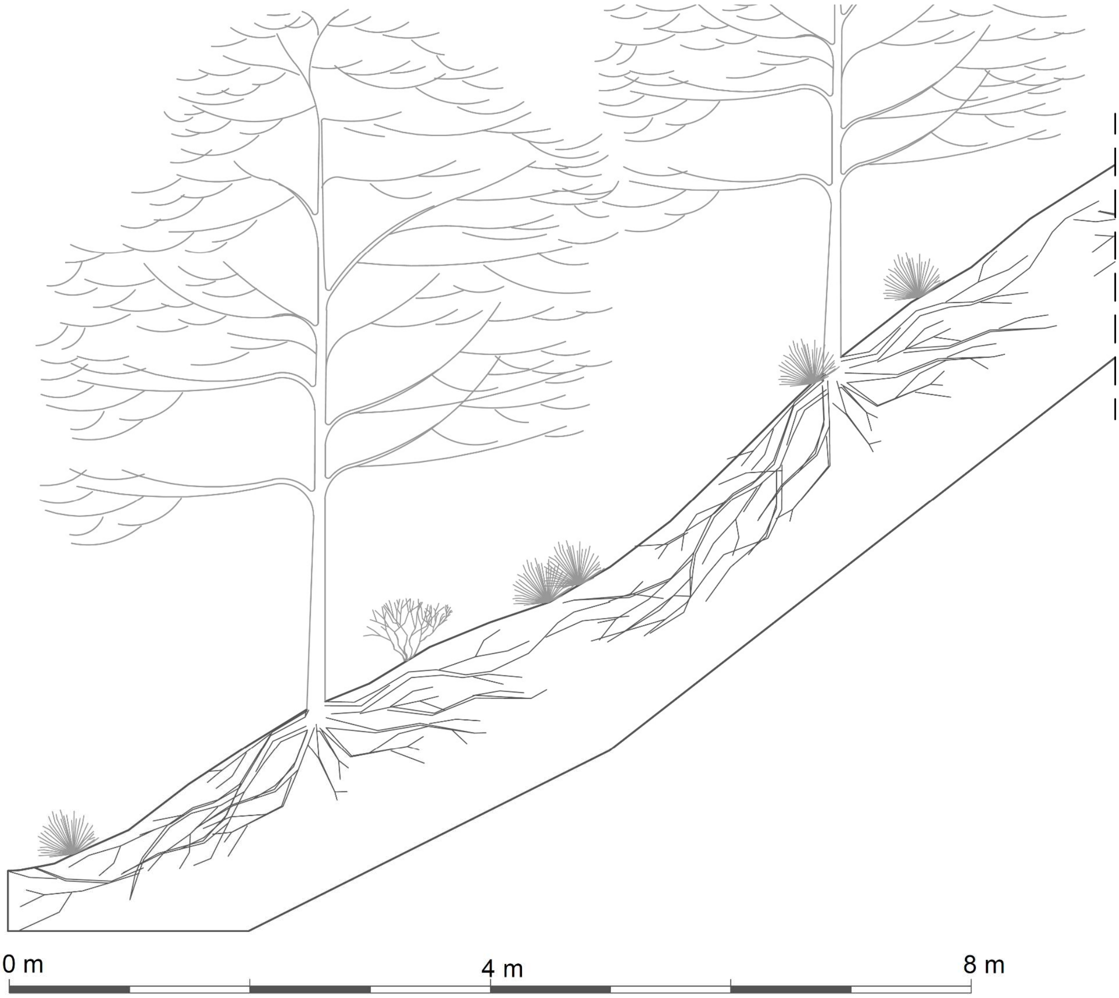

Figure 33 *Schematic illustration of the root distribution*

4.2.1.5 Preparation of HYDRUS Input

In HYDRUS, the time variable boundary conditions can be specified in the respective dialogue window. Here, fluxes applied to the atmospheric boundary are defined. Hourly input values of precipitation, potential evaporation and potential transpiration were used in this study. First, the precipitation values from the Q2 rain gauge (2.2.2) were aggregated to hourly values. Further, the interception of precipitation has to be considered. The interception was assumed to be 1 mm per event. In this way, a consistent precipitation time series for the study site Q2 was established. The input of the potential evaporation and the potential transpiration is also required. Based on the potential values, the model calculates the actual transpiration and actual evaporation depending on the available soil water. As mentioned in 2.3.3, no evaporation measurements are available for the study area. However, hourly values of reference (potential) evaporation (Penman – Monteith) have been calculated for the Rosalia experimental watershed for 2007 to 2015 (Herrnegger et al., 2012). Using these time series, long-term mean hourly values for potential evapotranspiration rates from April to October were calculated and used in this study. The estimated potential evapotranspiration was then split into potential transpiration and potential evaporation. As HYDRUS 2D is unable to partition the potential evapotranspiration, Simunek et al., (2018) suggested using either a crop coefficient or the Leaf Area Index (LAI) and the corresponding soil cover fraction (SCF) for the partitioning. The latter was used in this study. This approach is also implemented in HYDRUS 1D. Here, potential transpiration and evaporation are calculated as follows.

$$T_p = ET_p(1 - e^{-k*LAI}) = ET_p * SCF \quad (9)$$

$$E_p = ET_p * e^{-k*LAI} = ET_p * (1 - SCF) \quad (10)$$

where ET_p, T_p, E_p, are the potential evapotranspiration, potential transpiration and potential evaporation, respectively. *LAI* is the leaf area index [-], *SCF* is the soil cover fraction [-], and *k* is a constant which is between 0.5 and 0.75. *k* indicates the radiation extinction depending on the sun angle, distribution of plants and the arrangement of the leaves (Šimůnek et al., 2009). For this thesis *k* was assumed to be 0.75 (Simunek et al., 2018)

This approach requires the LAI. The leaf area index was downloaded from the PROBA V (Baret and Weiss, 2018) time series website (ESA, 2020) containing ten daily LAI values from October 2013 to November 2020. Based on LAI time series, long-term mean weekly LAI values were derived and further used in the partitioning approach of potential evaporation and potential transpiration. The mean weekly LAI and the partitioning of potential evaporation and transpiration is shown in Figure 34.

The obtained LAI index does show a clear seasonal pattern. Largest values occur in the first week of June (3.8). At the beginning and the end of the growing season, LAI is 1.4 (Beginning April) and 1.8 (End of September).

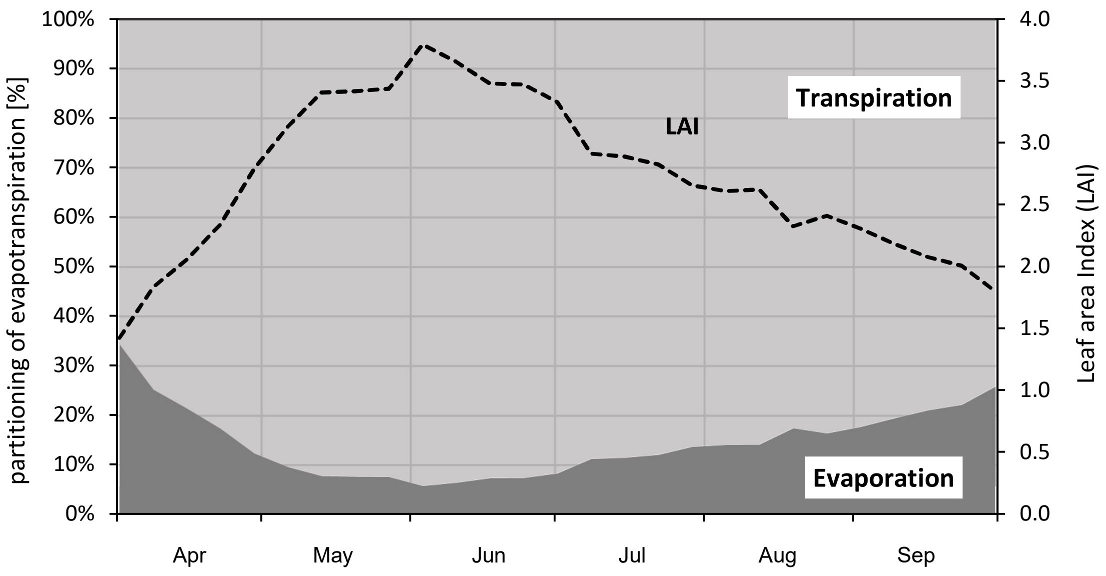

Figure 34 *Partitioning of potential evaporation using LAI on a weekly basis*

4.2.1.6 Boundary and initial conditions

The assignment of boundary and initial conditions is a crucial task. Therefore, one has to estimate the most realistic settings and further analyse the consequences of different configurations (Cloke et al., 2003). Model settings, regarding initial and boundary conditions (BC), determine the presence or absence of particular flow processes along a hillslope. Cloke et al. (2003) investigated various configurations of boundary and initial conditions and described related consequences on the resulting fluxes. When modelling hillslope-riparian areas, the resulting fluxes are highly sensitive to the assigned boundary conditions. Minor changes of the boundary conditions could affect simulated water flow throughout the model domain. Various studies that investigated hillslope flow processes and the interaction with streams could be found in literature. Based on a literature review, no consistent representation of the lower hillslope BC could be retrieved. In the respective studies, the following BC representing the lower hillslope have been used. Rassam (2020) defined the lower BC as a combination of seepage and constant head. Other authors used seepage face and no flux (Richard et al., 2013), free drainage (Liao et al., 2016) and a gradient boundary flow (Mujtaba et al., 2020) to define the lower boundary condition. This shows that the lower BC representing the boundary between stream and soil matrix should fit the local conditions and should therefore be assigned individually, as per the local conditions (Cloke et al., 2003). As such, testing of different settings and configurations during model development had to be conducted.

Therefore, during model development for this study, multiple boundary condition configurations (free drainage, seepage, constant head) were tested. Based on this preliminary investigation, the boundary condition (BC) representing the small stream (lower hillslope BC) is highly sensitive for assessing the interaction of root water uptake and observed diurnal fluctuations of the stream. Finally, the BC representing the boundary between the stream and the adjacent soil matrix was determined to be a constant head. The constant head was assumed to be 4 cm, which reflects the water level of the stream quite well. Along the boundary, the head pressure (4 cm) decreases linearly with the height differences along this boundary to 0 cm where the BC ends. This is illustrated in the grey box of Figure 35.

The BC representing the subsurface boundary of the model domain also had to be determined. This boundary condition is prone to high uncertainty due to lack of information of the subsurface conditions. Cloke et al., (2003) also pointed out that one can never achieve a complete conceptualisation of every single point at all boundaries of a domain. As such, it is very common to assign a no flux boundary condition (impermeable bedrock) to the lower BC (Cloke et al., 2003). Furthermore, other studies (Richard et al., 2013, Mujtaba et al., 2020, Bursey, 2008) did also assign a no flux BC. Due to lack of information of the subsurface model domain a no flux BC was also used in this study.

Additionally, a no flux BC was used for the vertical uphill BC. Therefore, this configuration does not allow any water draining into the model domain from further uphill. This might lead to uncertainties of the resulting subsurface water flow along this boundary. Further possible subsurface water inflows, replenishing the soil water content along this boundary cannot be represented by this boundary condition. The error that might arise from this assumption is considered to be negligible, because only few meters upslope, the transect is interrupted by a former forest road.

The upper BC representing the surface of the domain was determined as atmospheric BC. The BC is defined by the water fluxes based on the input, including potential transpiration and evaporation rates, and precipitation, as described in 4.2.1.5. The modelling domain and the assumed BC configurations used in this study are shown in Figure 35 below.

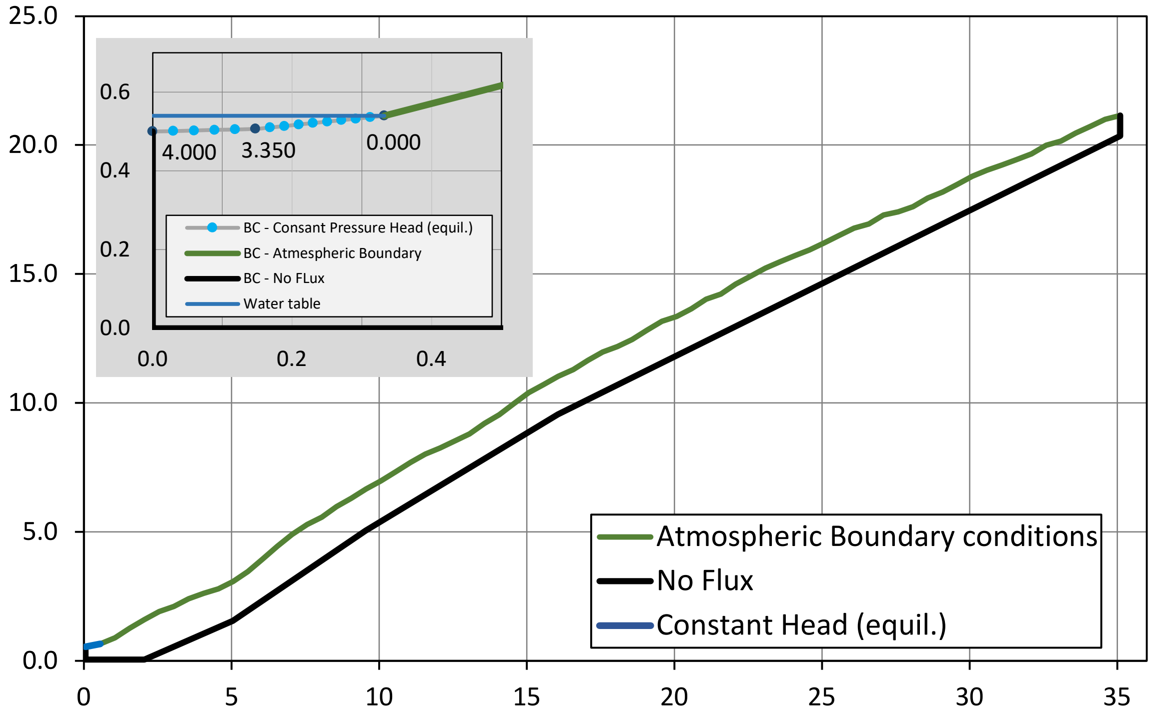

Figure 35 *HYDRUS - Boundary Conditions*

Finally, the initial conditions had to be specified. This could either be done by specifying initial water content or pressure heads within the domain. For the modelling task in this thesis, initial conditions were represented by a pressure head distribution. Three commonly assumed initial conditions are; (i) hydro-static curvilinear water table, (ii) hydrostatic inclined water table and (iii) hydrostatic pressure below a linear water table with non-hydrostatic conditions above. Each approach might affect the resulting water fluxes (Cloke et al., 2003). Bursey (2008) estimated the initial conditions based on previous model simulations and then utilised the resulting conditions in the soil matrix for the simulation. In this study, a combination of both approaches was used. First, a hydrostatic pressure head was implemented in HYDRUS. After the model run, the resulting pressure heads and its inclination could be determined. Based on this previous run, the finally used initial conditions could be specified based on the derived inclination and location of the pressure head. Moreover, each simulation period (month) was extended by one preceding week. This allows a more realistic representation of initial conditions, because initial conditions (pressure heads) naturally dispersed through the soil. This yields a more realistic estimation of the pressure head throughout the model domain.

4.3 HYDRUS simulations

The model configuration was used for analysing the interaction of a small stream and the riparian vegetation. The model was run to simulate 1-monthly periods. The phenomenon of diurnal discharge fluctuations appears on a high temporal resolution of hours and days. Therefore, the model was run on a time step of 1 hour.The resulting water fluxes are anticipated to yield a better understanding of these processes. Because the primary focus of this study is to gain a better understanding of the interaction of root water uptake and discharge, the modelled water fluxes occurring at the stream-soil matrix boundary are of primary interest in the analyses following below. In order to evaluate the model, these water fluxes were then compared with observed discharge values. According to the model configuration, simulated fluxes can only take place along the atmospheric and the constant head boundary.

The selected periods (months) for the model simulations should exhibit low flow periods with observed diurnal discharge fluctuations. Due to the given circumstances, August 2018 was selected for setting up the model and first test simulations. August 2018 shows a representative low-flow period with little precipitation and pronounced observations of diurnal discharge fluctuations. The model was then used also to simulate further periods (months). This was done in order to validate the model configuration and examine whether periods with various discharge and hydrological conditions can also be represented. Therefore, the months from May to September 2018 were also stimulated. All months show diurnal discharge fluctuations for particular periods.

The hydrological condition of these months is illustrated and described in the following section. In Figure 36, the mean daily discharge and the daily precipitation sums are illustrated for the period of May to September 2018.

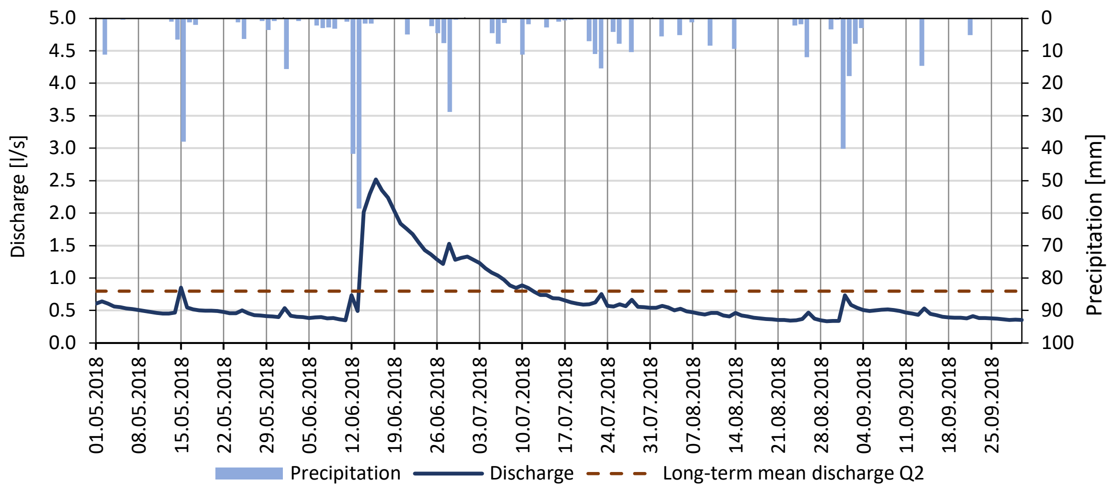

Figure 36 *Mean daily discharge and daily precipitation sums at Q2 (May-September 2018)*

Discharge during this period was mostly lower than the long-term mean discharge. Low flow periods occurred in May, August and September 2018. During the third week of June, discharge exceeded the long-term discharge (0.8 l/s) significantly. Maximum recorded discharge was about 2.5 l/s. This was a result of a severe precipitation event on 14th June 2018. The recorded daily precipitation sum was about 60 mm. The peak discharge was followed by a distinct recession period lasting until end of August 2018. As stated above, diurnal discharge fluctuations are only observed during discharge recession and low-flow periods. During heavy discharge events, other processes are dominating the discharge behaviour. Furthermore, high resolution (10 min) discharge data obtained for June 2018, showed data gaps before and after the heavy precipitation event, leading to uncertainties in the observed values. Therefore, the configured model was applied to the months of May, July, August and September 2018.

The results for each simulation period are represented and described below. Each chapter includes a short hydrological description, followed by a representation of the model input and a discussion of results. The simulated water fluxes presented here include actual transpiration, actual evaporation and the simulated boundary flux. It has to be noted that within the HYDRUS model environment, water fluxes into the soil domain are represented by negative values. Water fluxes leaving the model domain are positive. Due to the general model configurations (4.2.1.1) the resulting fluxes from the simulation are computed in cm per time. Therefore, fluxes in a two-dimensional model domain have the units cm²/h. In order to analyse the simulated fluxes between the stream and the soil matrix further, the water flux values were recalculated to l/s. This was achieved by multiplying the simulation output [cm²/h] with the length [cm] of the total contributing creek system. Based on a GIS analysis, the creek system of the Grasriegelgraben till the gauging station Q2 was approximated to be 1000 m (Fürst et al., 2020). Considering, the left and right side of the creek, the total contributing length is 2000 m.

The simulated fluxes are compared against the observed discharge. This indicates whether the observed discharge and the simulated boundary flux do behave accordingly or show discrepancies. In order to provide a further quantitative comparison of the simulated boundary flux and the observed discharge, the daily amplitudes during precipitation-free periods are calculated for both time series. This reveals whether the simulated fluxes explain the observed diurnal discharge fluctuations and whether they can be attributed to root water uptake. Additionally, selected low flow periods are represented in separate plots to visually assess the temporal accordance of daily maximum and minimum discharge as well as boundary fluxes.

A sensitivity analyses of the root distribution within the vicinity of the creek was performed. By stepwise reduction of the roots from the creek, the hypothesis can be assessed whether the phenomenon of diurnal discharge fluctuations is predominantly caused by root water uptake of the riparian vegetation. Furthermore, the distance of riparian roots from the creek affecting the discharge can be assessed.

Furthermore, a sensitivity analyses of the boundary flux to the different soil hydraulic parameters was carried out. To investigate the impact of varying the soil hydraulic paramters on the simulated boundary flux, the soil hydraulic parameters represented in Table 10 were used in the simulation as well. The resulting boundary fluxes are then compared with each other.

4.3.1 May 2018

Accumulated precipitation in May 2018 was about 74 mm. 38 mm, about half of the monthly sum, was recorded on only a single day (15.05.2018). The observed monthly sum is only 57% of the long-term mean precipitation for May (129 mm). Precipitation was recorded on 13 days in May 2018. Apart from the intense precipitation event on the 15th of May, daily precipitation exceeded 10 mm only once (02.05.2018). Discharge was always below the long-term mean discharge of 0.8 l/s. The mean discharge of May 2018 was 0.51 l/s or 5.01 mm. Therefore, discharge was equivalent to about 7 % of precipitation. As described in 2.3.2 the long-term runoff coefficient is 13 % (2016-2019).

The prepared input data, as described in 4.2.1.5, is illustrated in Figure 37. Potential transpiration rates are found to be much higher than potential evaporation rates. In May, potential transpiration accounts for about 92 % of total potential evapotranspiration.

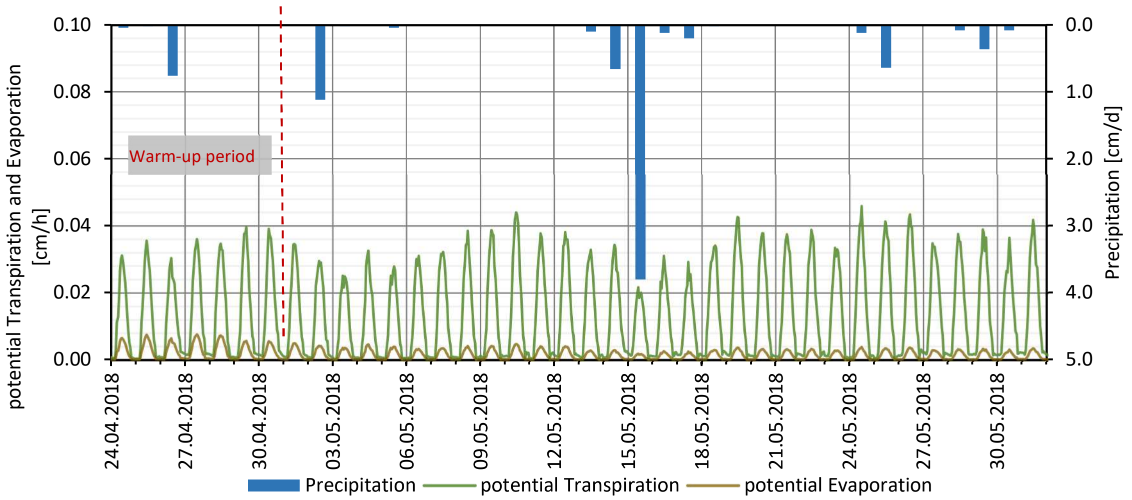

***Figure 37** HYDRUS input data - May 2018*

Based on the input data and the model configuration, the simulated water fluxes are presented in the following figures. In Figure 38, the simulated fluxes, including actual transpiration, actual evaporation and the boundary flux are shown. The simulation results show that actual transpiration rates vary due to water availability and root water uptake. This causes soil water to decrease, and consequently, maximum daily transpiration rates to decrease, especially during periods of no precipitation. This steady decrease can be observed in the periods with no precipitation at the beginning and end of May. Actual evaporation rates also show variability throughout the simulation period due to soil water availability.

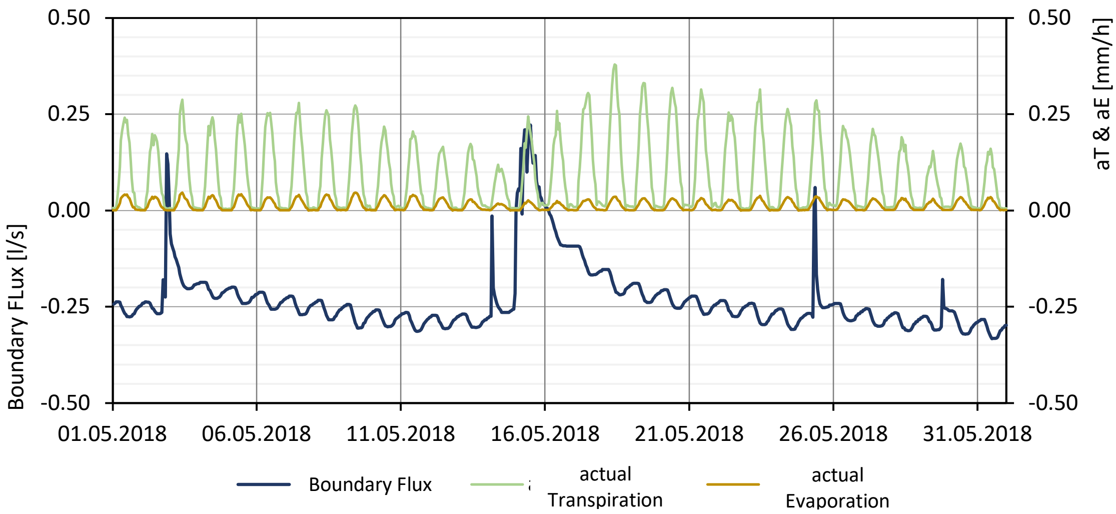

Figure 38 *Simulation results – water fluxes May 2018*

The simulated boundary flux, which is of primary interest in this study, shows noticeable diurnal fluctuations during periods of little or no precipitation. Generally, positive peaks occur due to heavy precipitation events, which indicates subsurface flow towards the stream. After the peak on the 15th of May, the boundary flux shows a recession. Moreover, the boundary flux shows an exponential recession during dry periods. As a next step, the simulated boundary flux is compared to the observed discharge for May 2018 (Figure 39).

The simulated boundary flux shows a pattern similar and parallel to the observed discharge. The simulated values follow the peaks and mimic the general discharge pattern closely. Furthermore, the apparent diurnal fluctuations of the boundary flux appeared to represent the diurnal discharge fluctuations effectively. The general shift between discharge and the boundary flux is due to the simulated flux represents the water flux, altering the discharge and causing the diurnal discharge fluctuations. The mean amplitudes of the diurnal discharge fluctuations on precipitation free periods are about 0.069 l/s. Therefore, the observed mean daily amplitudes in May 2018 are about 13 % of the mean discharge.

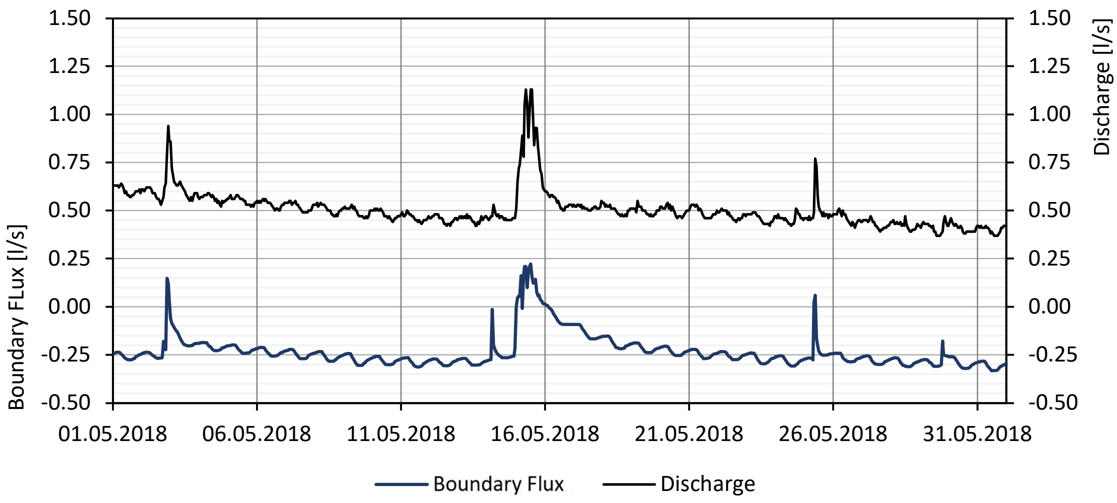

Figure 39 *Comparison of simulated boundary flux and observed discharge - May 2018*

The daily amplitudes of the simulated boundary flux range from 0.04 l/s to 0.14 l/s. The mean daily amplitudes of the simulated flux on precipitation free days is about 0.054 l/s. These differ only slightly from the observed amplitudes. This strongly indicates that the simulated boundary flux does explain the observed diurnal discharge fluctuations. Comparing the maximum discharge on 15th of May with the simulated boundary flux reveals that the boundary flux shows a more pronounced recession. Discharge seems to decrease faster compared to the simulated boundary flux.

In Figure 40, the observed and simulated data is plotted on a finer time scale. In this plot, the dry period from the 19th to the 29th of May 2018 is illustrated. For a better visual interpretation and evaluation of the simulated boundary flux, the observed discharge is plotted on the second y-axis. This allows a relative comparison of the observed and simulated fluxes. In this illustration, the timing of the minimum and maximum observed and simulated data can be better compared. It can be seen that the simulated flux mimics the observed diurnal discharge fluctuations thoroughly. Also, the small increase on the 25th of May can be seen clearly.

Additionally, the times of the simulated and observed maximum and minimum values correlate well. Maximum daily discharge is observed in early mornings. Minimum daily discharge is observed in the early afternoon. Corresponding to these discharge fluctuations, minimum boundary fluxes (loss of discharge) and maximum daily values of the simulated flux can be seen. Therefore, it can be noticed that large values of the simulated boundary flux (loss from discharge) lead to a reduction of discharge during the day and to the diurnal discharge fluctuations. This strongly indicates the impact of root water uptake on the stream discharge in the experimental research watershed Rosalia.

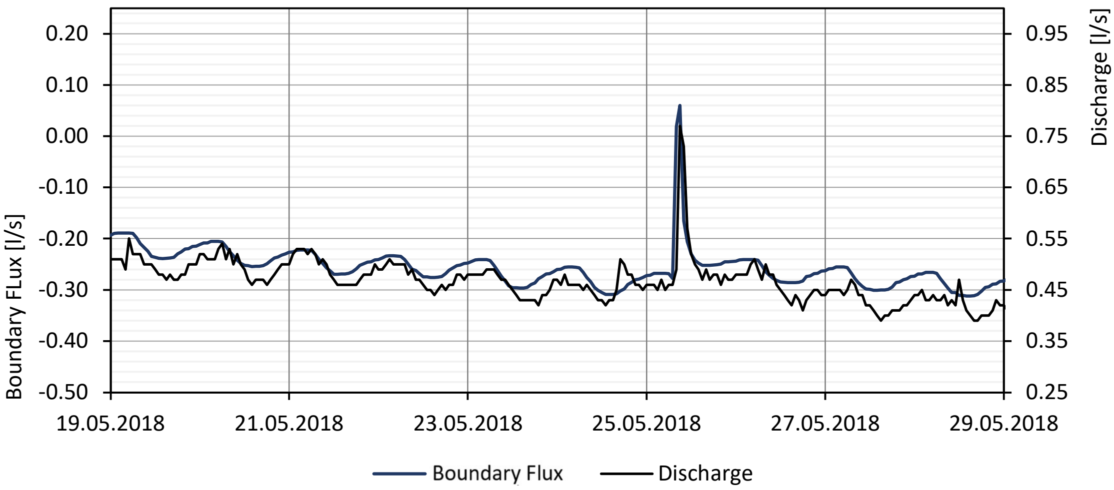

Figure 40 *Comparison of simulated boundary flux and observed discharge – 19.05.2018-29.05.2018*

4.3.2 July 2018

The general hydrological conditions in July 2018 differed from those in May 2018. The total precipitation of about 88 mm was akin to the long-term mean precipitation (95 mm). Precipitation was observed on 15 days. The maximum daily precipitation was 15.4 mm.

Discharge in July was dominated by a recession after the peak discharge (2.5 l/s) in June. In July, mean discharge was 0.78 l/s (7.8 mm), which is close to the mean long-term discharge (0.8 l/s). Therefore, discharge is equivalent to about 9 % of precipitation. As was seen in the month of May, this is significantly lower than the long-term average (13 %). Based on the partitioning of potential evapotranspiration, potential transpiration accounts for about 89 % of it, and potential evaporation accounts for about 11 % (Figure 41). The simulation results are presented analogously to May in Figure 42. Similarly, to May 2018, actual transpiration rates do decline in precipitation-free periods.

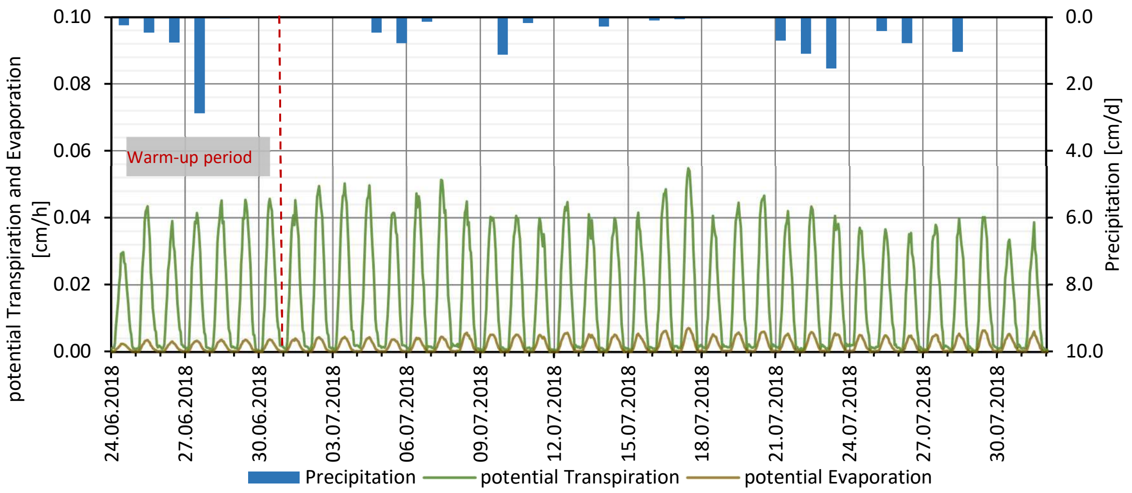

Figure 41 *HYDRUS input data - July 2018*

The boundary flux between the stream (constant head boundary) and the soil matrix clearly shows diurnal fluctuations, which are especially pronounced during precipitation free periods.

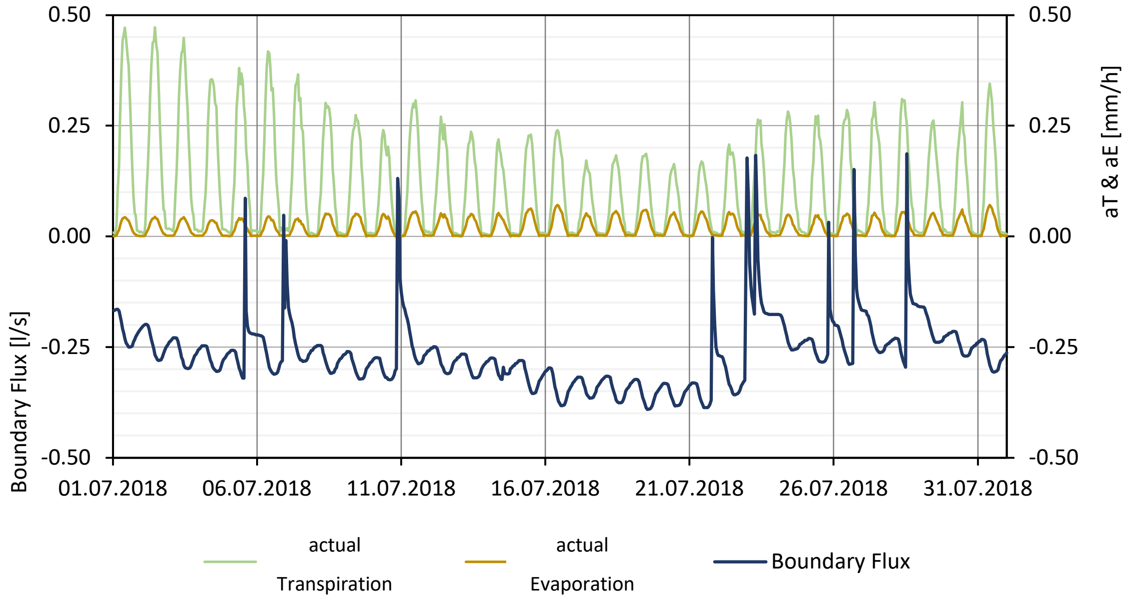

Figure 42 *Simulation results - water fluxes July 2018*

The simulated boundary flux also shows several peaks with positive fluxes (Figure 42). As described above, positive fluxes do represent inflow to the stream. Correspondingly, as before, the simulated boundary flux is compared to the observed discharge in Figure 43.

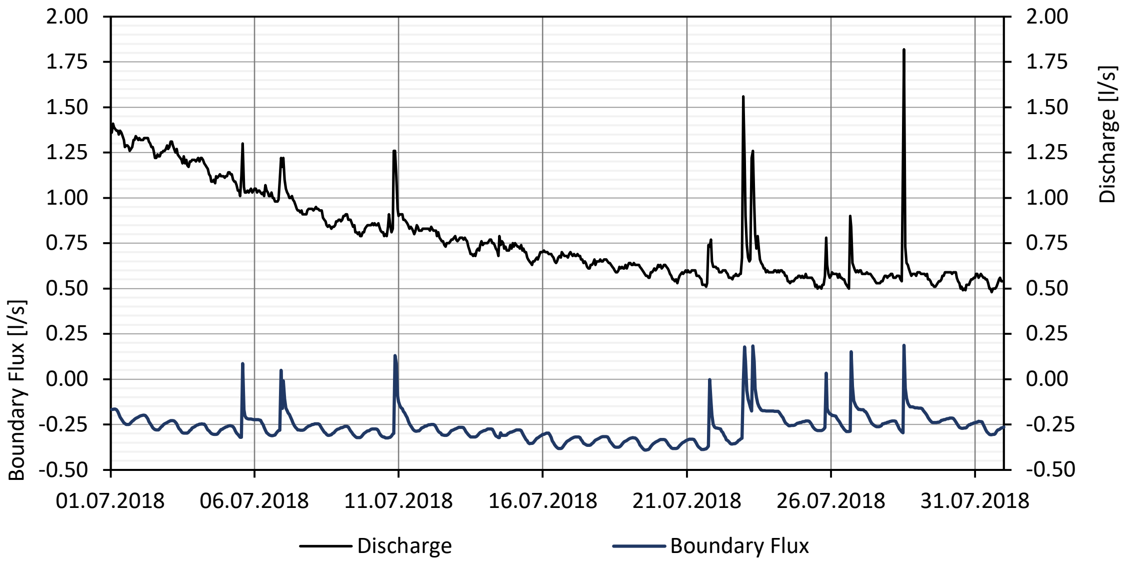

Figure 43 *Comparison of simulated boundary flux and observed discharge - July 2018*

In contrast to the simulation of May 2018, the general decreasing trend of the observed discharge is not well represented by the boundary flux. As mentioned above, July 2018 is dominated by a substantial recession period. Due to the model configuration (4.2.1.6), the general recession of the hydrograph cannot be captured by the boundary flux sufficiently, since the constant head boundary condition represents steady discharge conditions. However, the diurnal fluctuations of the discharge are adequately reproduced by the simulated boundary flux.

Peaks in the hydrograph are generally captured quite well by the simulated boundary flux. Simulated amplitudes in precipitation-free days range from 0.05 l/s to 0.16 l/s. The mean daily amplitudes based on the simulated boundary flux are 0.073 l/s. Mean daily amplitudes observed are about 0.10 l/s.

Figure 44 compares the measured discharge and the simulated boundary flux for a selected dry period. The time of minimum and maximum daily discharge values and the simulated boundary flux match very well. Maximum discharge occurs in early mornings followed by a decrease up to early afternoon. The simulated boundary flux and observed discharge show a similar pattern as in the previous simulation period.

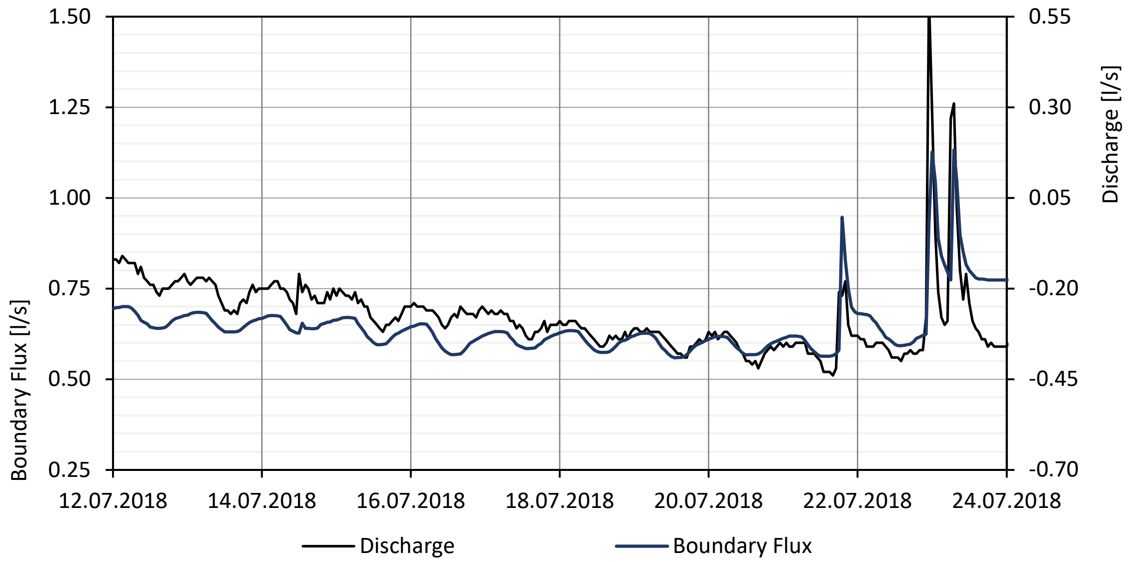

Figure 44 *Comparison of simulated boundary flux and observed discharge – 12.07.2018 – 24.07.2018*

4.3.3 August 2018

Comparing the observed precipitation of August 2018 (50 mm) with the long-term mean precipitation of August (77 mm), August 2018 was relatively dry. The maximum daily precipitation in August was 12 mm. Thirteen days with precipitation were recorded. Precipitation sums exceeded 5 mm/d on 7 days. The mean discharge in August 2018 was 0.42 l/s (4.17 mm). This is only about 50% of the long-term mean discharge (0.8 l/s). Furthermore, the relatively low discharge in August 2018 results in a run-off coefficient of 8.3 %.

In Figure 45, the input data is plotted, including precipitation, potential transpiration and potential evaporation. Based on the partitioning of potential evapotranspiration, about 84 % of potential evapotranspiration is accounted to be potential transpiration.

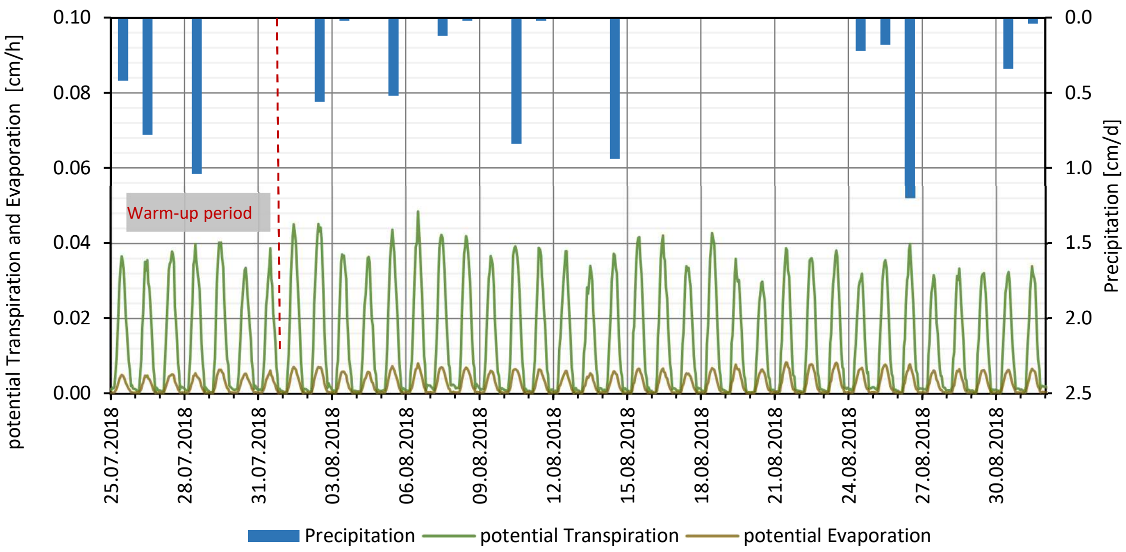

Figure 45 *HYDRUS input data - August 2018*

Based on the input data and the model configuration, the simulated water fluxes are represented in the following figures. In Figure 46, the simulated actual transpiration, actual evaporation and the boundary flux are shown.

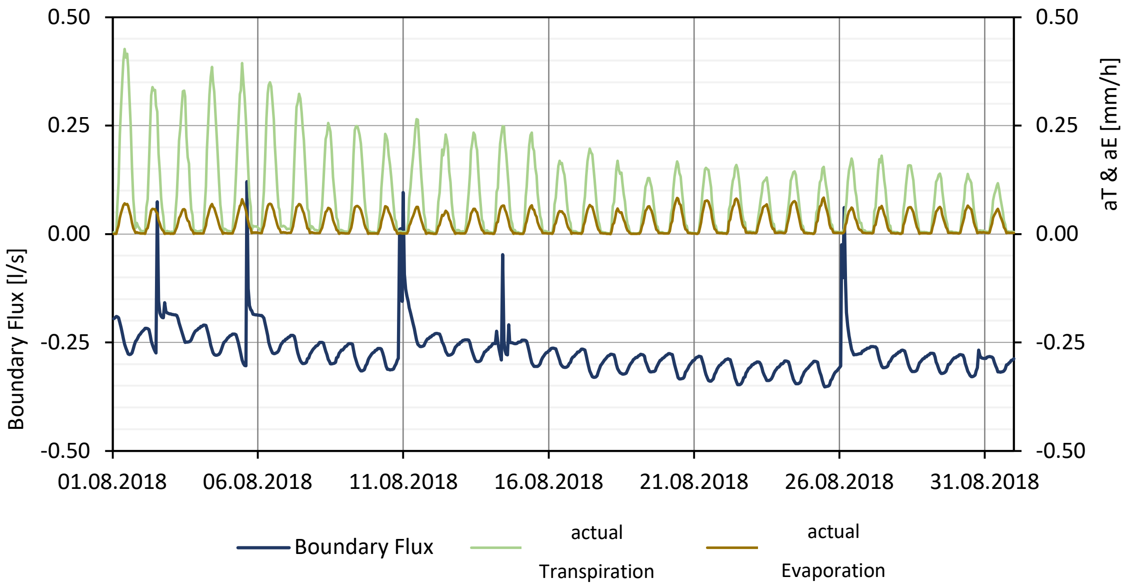

Figure 46 *Simulation results - water fluxes August 2018*

Daily actual evaporation patterns did not change significantly over the modelling period. On the other hand, actual transpiration generally decreased over time due to soil water depletion, especially during dry periods. However, it increased slightly after precipitation events based on increasing water availability in the soil matrix. The boundary flux clearly showed diurnal fluctuations. As mentioned before, negative values reflected infiltration in the soil domain. Negative boundary fluxes represented abstractions from the constant head boundary, which represented the stream in this model configuration. The constant boundary flux, however, also showed positive values over the modelling period. Positive values indicate infiltration from the model domain towards the stream. In the selected model period, this occurred four times as a result of subsurface flow due to strong precipitation events. As a next step, the simulated boundary flux was compared to the observed discharge for August 2018 (Figure 47).

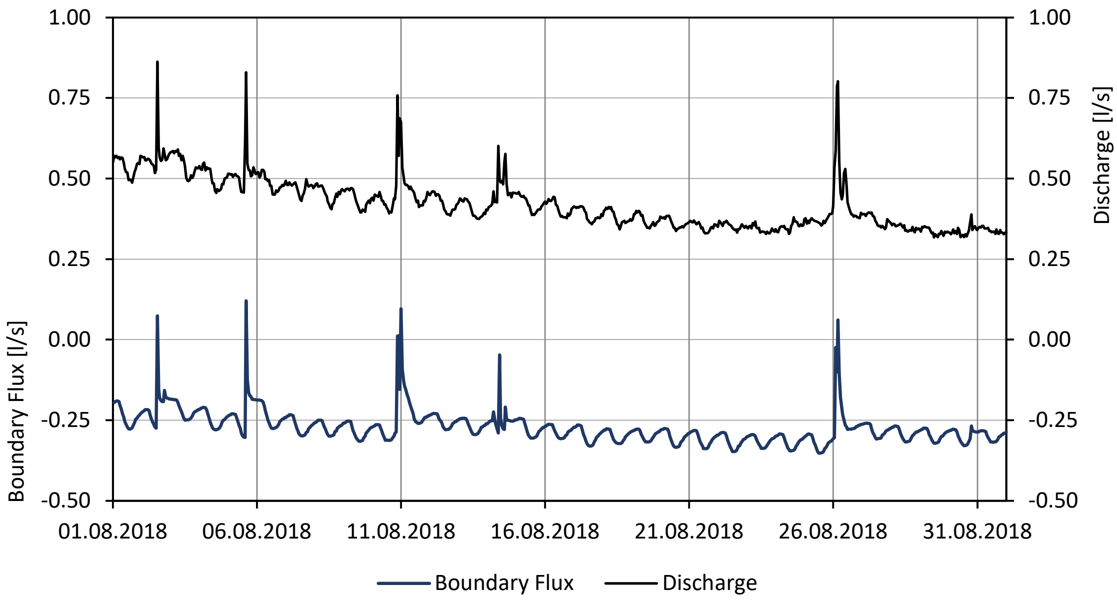

Figure 47 *Comparison of simulated boundary flux and observed discharge - August 2018*

The modelled boundary flux shows a similar pattern as the observed discharge. The simulated values follow the peaks and the general trend of the observation closely. Further, the noticeable diurnal fluctuations of the boundary flux represent the diurnal discharge fluctuations adequately.

The mean daily amplitudes in precipitation free periods are about 0.07 l/s. Therefore, observed mean amplitudes in August 2018 are about 17 % of the mean discharge. Simulated amplitudes of the boundary flux range from 0.03 l/s to 0.13 l/s. The mean daily amplitudes of the simulated boundary flux in precipitation free days is about 0.06 l/s. They differ slightly from the observed. This strongly indicates that the simulated flux explains the observed diurnal discharge fluctuations. In Figure 48, the observed discharge and the boundary flux are plotted on a finer time scale. In this plot, the dry period from the 14th to 24th of August 2018 is portrayed. The simulated flux mirrors the observed diurnal discharge fluctuations thoroughly. Also, the small peak on the 14th of August can be clearly observed.

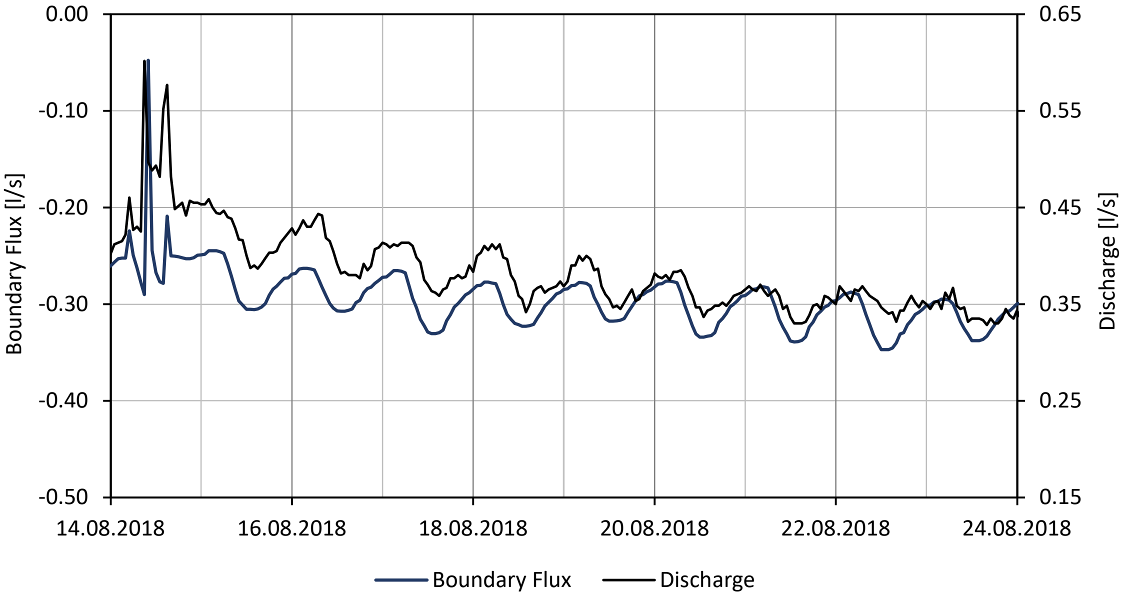

Figure 48 *Comparison of Simulated boundary flux and observed discharge – 14.08.2018 – 24.08.2018*

In addition, the simulated and observed maximum and minimum values also show a strong correlation. Maximum daily discharge is observed in early mornings (~ 6:00 a.m.), with the corresponding minimum boundary flux. On the other hand, minimum daily discharge is observed in the early afternoon (2:00.p.m.), when corresponding boundary fluxes are largest (loss of discharge). Therefore, large values of the simulated boundary flux (loss from discharge) lead to a reduction of discharge during the day and explain the diurnal discharge fluctuations. This strongly indicates the impact of root water uptake on the stream discharge in the experimental research watershed Rosalia.

4.3.4 September 2018

In September 2018 about 89 mm of precipitation were observed. This is slightly less than that of the long-term precipitation (95 mm). 40 mm were observed on the 2nd of September, and on the following day (3rd of Septemeber), 18 mm were observed. Therefore, about two-thirds of the observed monthly precipitation was recorded within two days. Subsequent precipitation events during September 2018 never exceeded 15 mm. Precipitation was observed on 9 days. Discharge exceeded the long-term mean discharge (0.8 l/s) at the beginning of September only due to the strong precipitation events. Mean monthly discharge of September 2018 was 0.45 l/s (4.31 mm), which was significantly lower than the long-term discharge of 0.8 l/s. The runoff coefficient was about 5 %. This represented the lowest runoff coefficient of all simulated months.

In Figure 49, the input data, including precipitation, potential evaporation and potential transpiration, is presented. Based on the partitioning of potential evapotranspiration, 79% of potential evapotranspiration is attributed to potential transpiration.

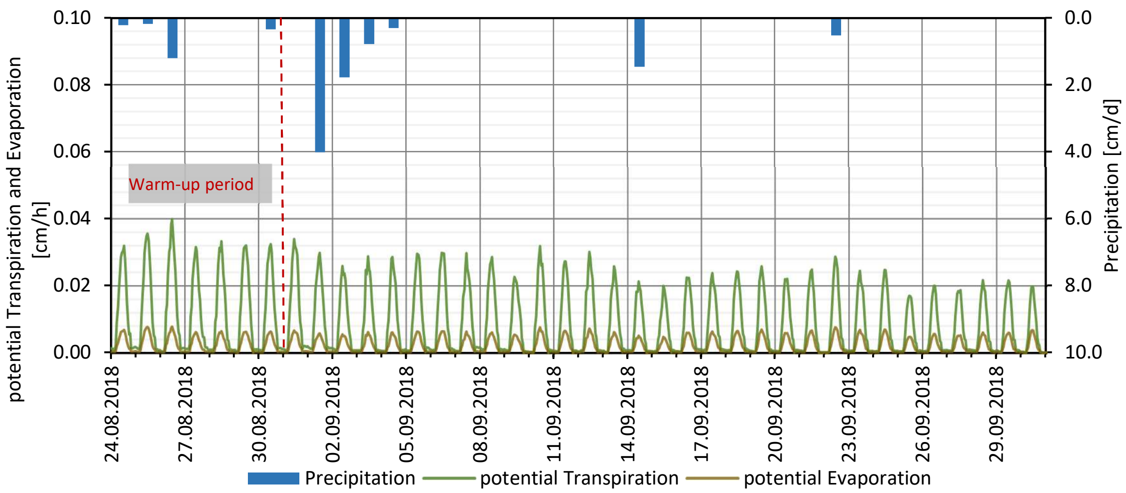

Figure 49 *HYDRUS input data - September 2018*

The simulation results are presented in Figure 50. Actual transpiration rates also show similar simulation results, as described above. A decrease can be observed during precipitation-free periods due to declining water content in the soil matrix. The boundary flux exhibits pronounced diurnal fluctuations in precipitation-free periods. At the beginning of September, positive boundary flux values are simulated leading to subsurface inflow to the stream based on heavy precipitation events. Other peaks of the simulated flux can be seen on the 14th and the 22nd of September 2018.

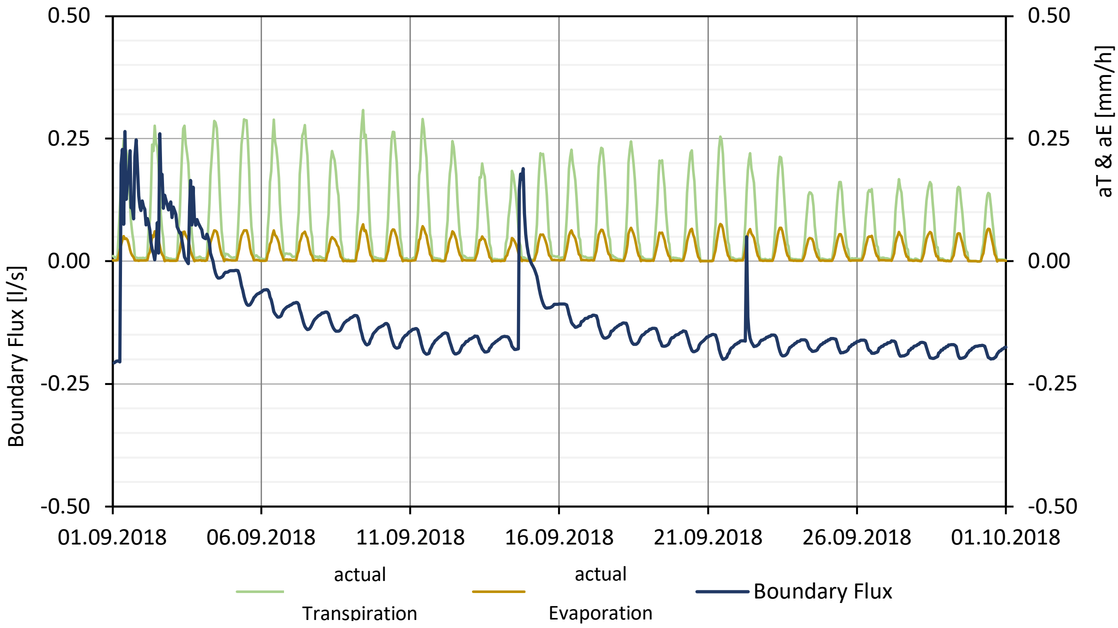

Figure 50 *Simulation results - water fluxes September 2018*

In Figure 51, the simulated flux and the discharge is plotted. The overall trend of the observed discharge and the boundary flux seems to be alike. Peaks in discharge are quite well represented in the simulated flux. The observed diurnal fluctuations are adequately mimicked by the simulated boundary flux throughout the simulation period. The diurnal discharge fluctuations seem to get less pronounced at the end of September, leading to reduced daily discharge amplitudes over time. This is also represented in the simulated boundary flux. Observed mean daily discharge amplitudes in precipitation-free days are 0.045 l/s. The mean daily amplitudes of the simulated boundary flux are 0.042 l/s. This indicates a very good representation and explanation of the diurnal discharge fluctuations with the simulated boundary flux.

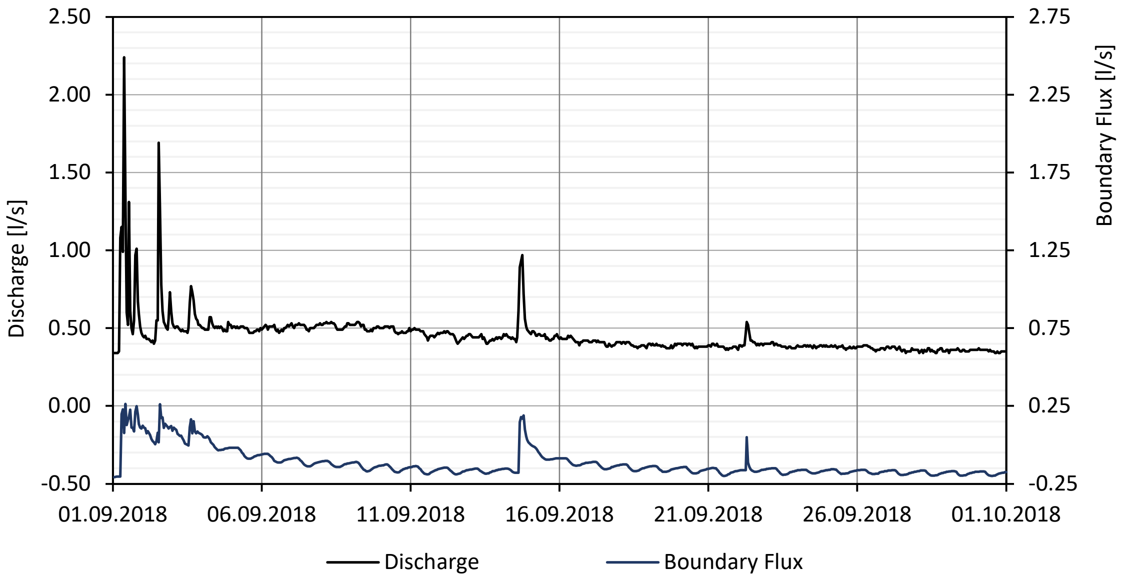

Figure 51 *Comparison of simulated boundary flux and observed discharge - September 2018*

In Figure 52, discharge and the simulated boundary flux are represented for a selected low flow period, also including a small peak. The time of minimum and maximum daily discharge values and the simulated boundary flux correspond quite well. Maximum discharge occurs in the early morning, followed by a decrease by the early afternoon. A similar behaviour can be seen for the simulated boundary flux. Furthermore, the peak discharge recorded on 14th September 2018 is also adequately mirrored by the boundary flux.

Figure 52 *Comparison of simulated boundary flux and observed discharge – 11.09.2018 – 22.09.2018*

4.3.5 Actual evapotranspiration and sensitivity of the boundary flux to root distribution

So far, the results indicate that the established model configurations are able to describe the diurnal discharge fluctuations by the simulated boundary flux. It is still necessary to show whether the observed, as well as the simulated diurnal fluctuations, are primarily attributable to the root water uptake of the riparian vegetation. Therefore, the initially assumed root distribution (Figure 33) was gradually altered in the creek's vicinity.

The stepwise removal of roots was carried out in one-meter slices (scenarios) until the simulated boundary flux did not show any changes due to further alteration of the root distribution. This was implemented in HYDRUS by selecting the mesh-nodes for each scenario and assign no root water uptake for each scenario. No other HYDRUS configurations were changed. This resulted in 8 root distribution scenarios. A schematic illustration of each scenario, showing the stepwise (one meter) alteration of the initial root distribution (Figure 33), is presented in Figure 53. These scenarios were implemented in HYDRUS individually for each simulation period. As the effect of the different root distributions showed similar patterns of the simulated boundary fluy in all simulation periods, only simulated boundary fluxes for August 2018 are illustrated (Figure 54).

To compare the resulting boundary fluxes of each scenario, the simulated boundary flux from the initial model configuration and the observed discharge are plotted in Figure 54 . This illustrates a general decrease of the boundary flux with increasing distance of riparian roots. As can be seen, the respective boundary flux decreases considerably with each scenario. Furthermore, the general pattern of the simulated boundary fluxes also changes. The pronounced diurnal fluctuations can only be seen in scenario 1. The remaining scenarios show only slight diurnal fluctuations. Therefore, the diurnal fluctuation and the occurring daily amplitudes are decreasing gradually with increasing distance of the roots from the creek. This highlights the importance of root water uptake and the root distribution of the riparian vegetation when assessing the processes that lead to diurnal discharge fluctuations.

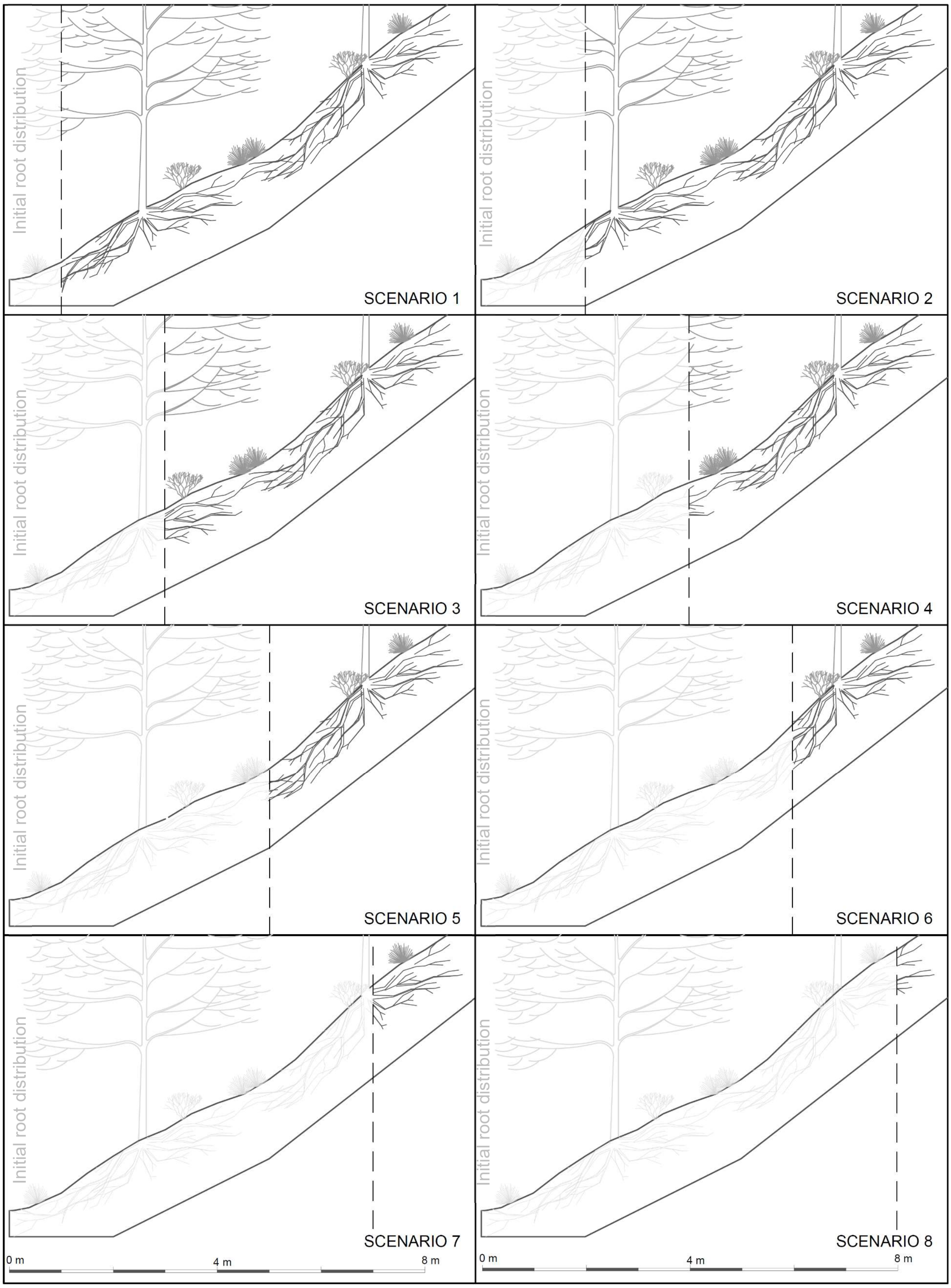

Figure 53 *Root distribution scenarios (Initial root distribution – light grey, root distribution scenario – black)*

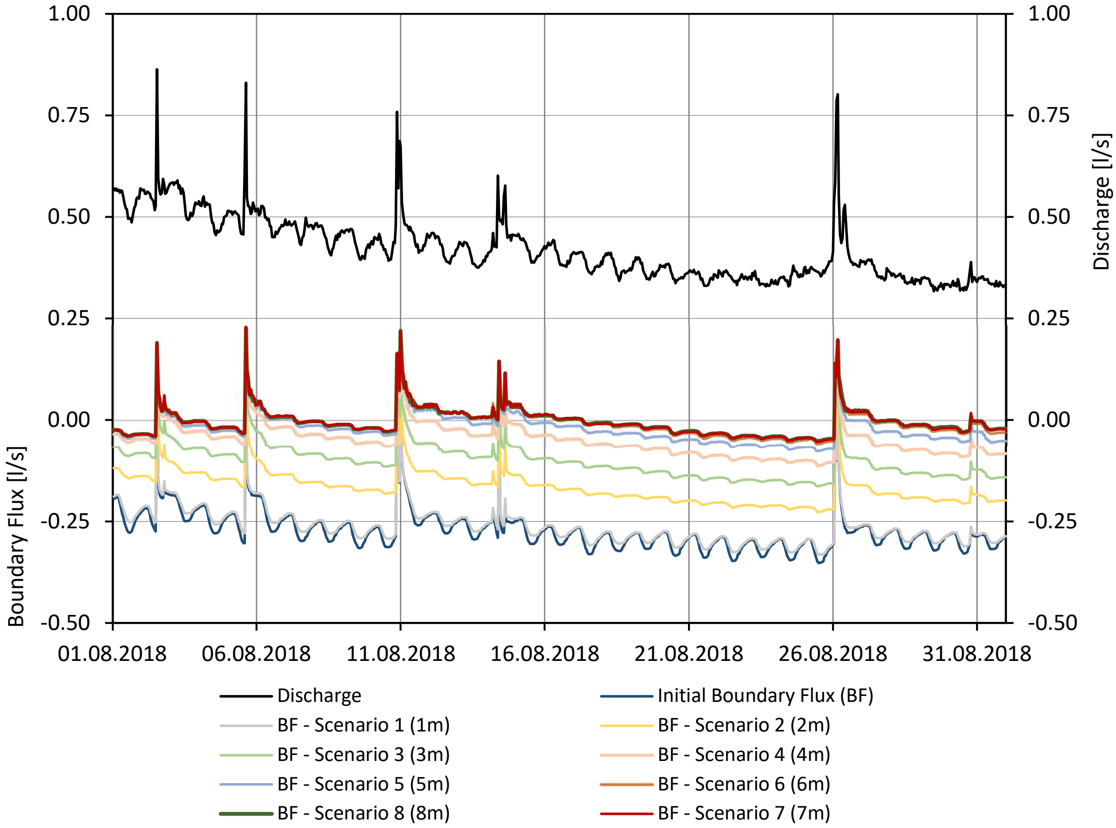

Figure 54 *Sensitivity analysis of the boundary flux on root distribution scenarios (August 2018)*

The differences of the simulated boundary fluxes (BF) of the respective scenarios and the initial simulated boundary flux (BF) are calculated as a normalised difference. Using this calculation, the magnitude of the difference can be assessed. Furthermore, the distance of the riparian roots responsible for altering the boundary flux from the stream into the soil matrix can be estimated. In Figure 55, the normalised differences [%] between the initial simulated boundary flux and the boundary flux of the scenarios are represented for each period of simulation.

Compared to the initial boundary flux, only minor differences (3-6 %) of the boundary fluxes calculated in scenario 1 are observed. Larger differences are found for subsequent scenarios (2, 3, 4). The normalised differences increase gradually, with increasing distance of the assigned root distribution. The boundary flux of scenario 4, with no roots for 4 meters, shows differences above 78% for all simulation periods, compared to the initial boundary flux. The normalised differences of scenarios 5,6,7 and 8 are always above 90%, until almost no differences can be observed between scenarios 7 and 8. This indicates that with increasing distance of the roots from the creek (5 to 8 meters), the differences in the simulated boundary fluxes become less pronounced. The normalised differences of these scenarios (5,6,7,8) do not have such a significant impact as the scenarios (2,3,4).

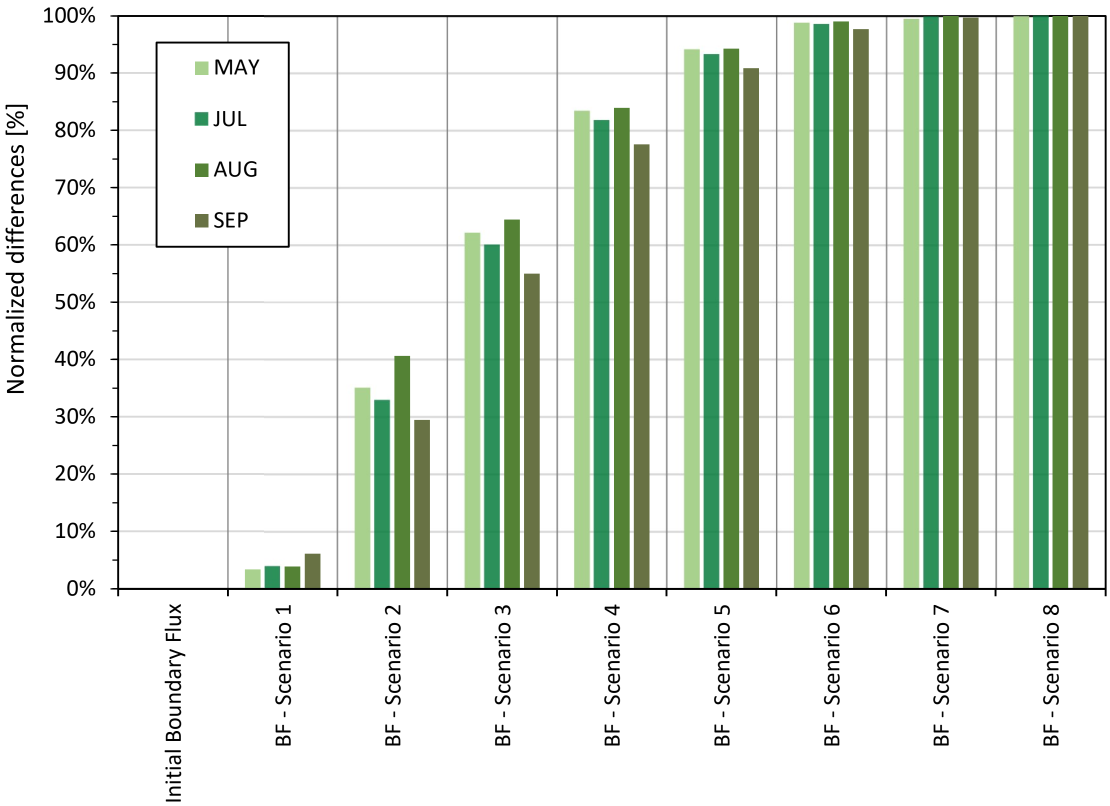

Figure 55 *Normalized differences of simulated boundary fluxes (scenarios) with the initial boundary flux*

The results show that the riparian vegetation within a distance of 8 meters (Scenario 6, 7, 8) of the creek affects discharge. In Figure 54 and Figure 55, differences of the simulated boundary flux due to a stepwise removal of the root system are clearly illustrated. However, large diurnal fluctuations are only represented in scenario 1, besides the initial scenario (Figure 54). This might suggest that only roots within a distance of 1m from the stream are responsible for the immediate water abstraction. The resulting boundary fluxes from all other scenarios still show a clear impact on discharge due to root water uptake within a distance of 8 m, but the diurnal fluctuations rapidly become small. The results indicate that plant water uptake results in a decrease in water content and depletion of the matrix potential within the vicinity of the creek, even when roots are situated further away from the stream. Therefore, stream water infiltrates into the soil matrix to replenish the soil water content in the riparian area that is lost to transpiration. The amount of water abstracted by the riparian plants for each scenario is also represented in the simulated actual transpiration rates. Based on an accompanying analysis of the actual transpiration rates calculated for each simulation period, the impact of the riparian vegetation on the water balance can be investigated. The actual transpiration sums calculated for each simulation period and scenario are presented in Figure 56 below.

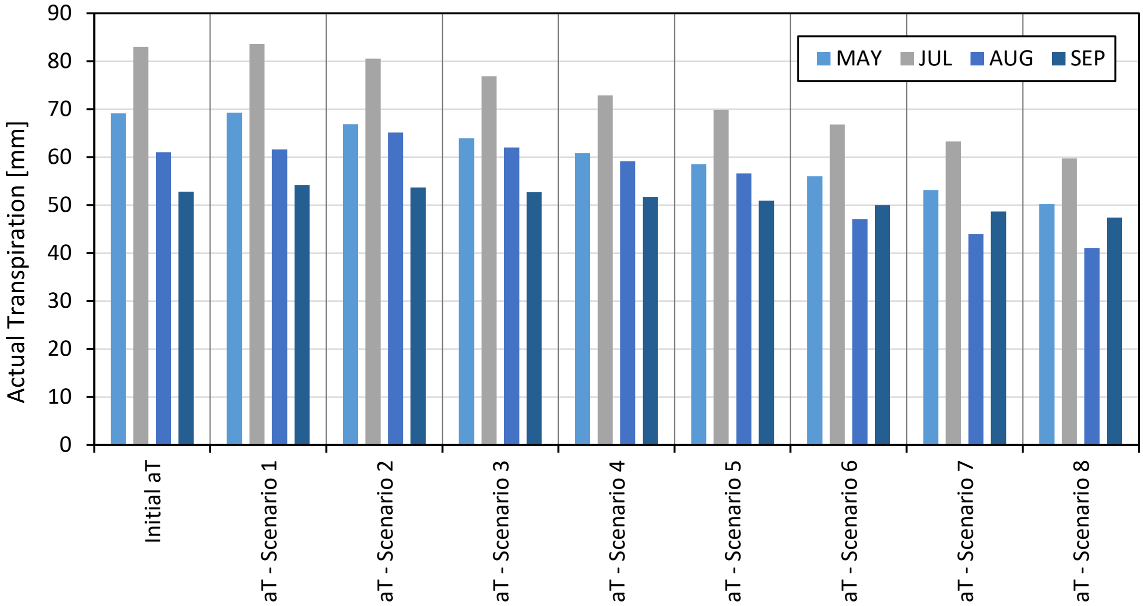

Figure 56 *Monthly actual transpiration (aT) sums [mm] for different scenarios of root distribution*

The actual transpiration sums calculated for each simulation period significantly decrease with each scenario (Figure 56) of the root distribution. The decrease of actual transpiration between the initial scenario and scenario 8 are 18.9, 23.2, 20.0, 5.4 mm in May, July, August and September, respectively. Comparing the initial scenario with scenario 8, the decrease is found to be about 10% for September. Furthermore, the actual transpiration calculated in scenario 8 led to a decrease of 27, 28, 33 %, during May, July, August compared to the initial scenario. On the other hand, actual evaporation sums do not exhibit any changes due to the different root distribution scenarios during all simulation periods. This highlights the impact of riparian vegetation and its transpiration within the vicinity of the creek.

4.3.6 Sensitivity of boundary fluxes to soil hydraulic properties

In this chapter, the effect of changing the initial soil hydraulic parameters of the van Genuchten model is investigated. The different parameter sets and their corresponding water retention curves were represented and described in 4.2.1.3. For the reference simulations, the parameters were estimated based on the textural classes (4.2.1.3.1). The other three parameter sets were derived, as explained above (4.2.1.3.2). These three parameter combinations characterise the range and the variability of the individually analysed soil samples. The impact of the different soil hydraulic parameters on the simulated boundary flux is described below.

This analysis was carried out for all simulated months. As all months show similar results in this thesis, only August 2018 is represented below (Figure 57).

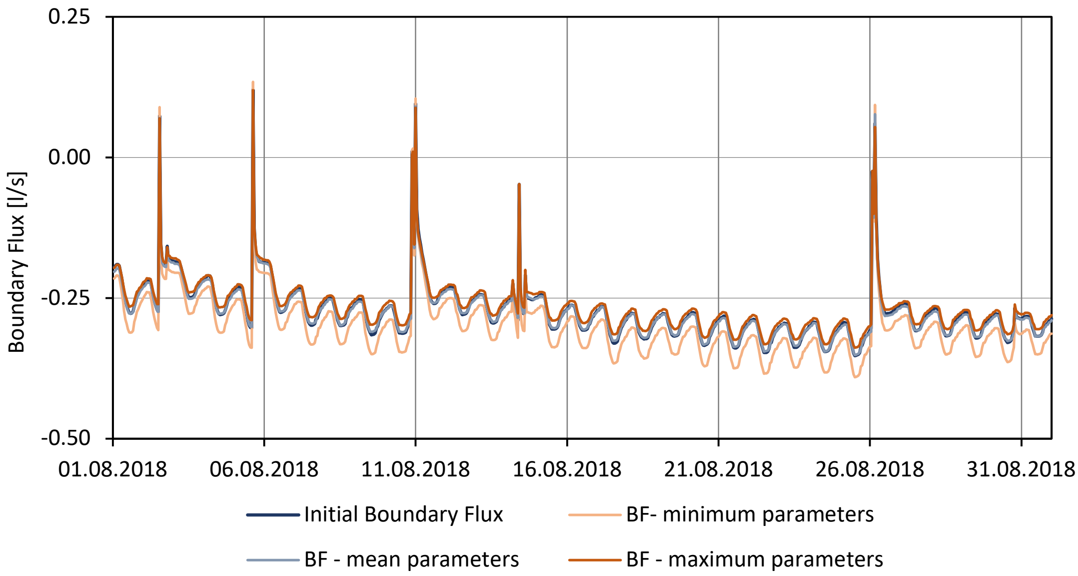

***Figure 57** Comparison of the simulated boundary flux with different soil hydraulic parameters*

The simulated boundary fluxes do not show significant differences due to changed soil hydraulic parameters. The general pattern of all boundary fluxes is similar. All fluxes consequently do exhibit peaks and pronounced diurnal fluctuations. However, the boundary flux simulated based on the minimum parameter set leads to further substantial diurnal fluctuations. The other parameter sets do not show such a significant difference compared with the initial simulated boundary flux. As a further step, the mean daily amplitudes in precipitation-free days are calculated for each simulation period. The resulting mean daily amplitudes for the respective months and different soil hydraulic parameters are plotted in Figure 58. Based on this comparison, the influence of different soil hydraulic parameters on the mean daily amplitudes can be investigated.

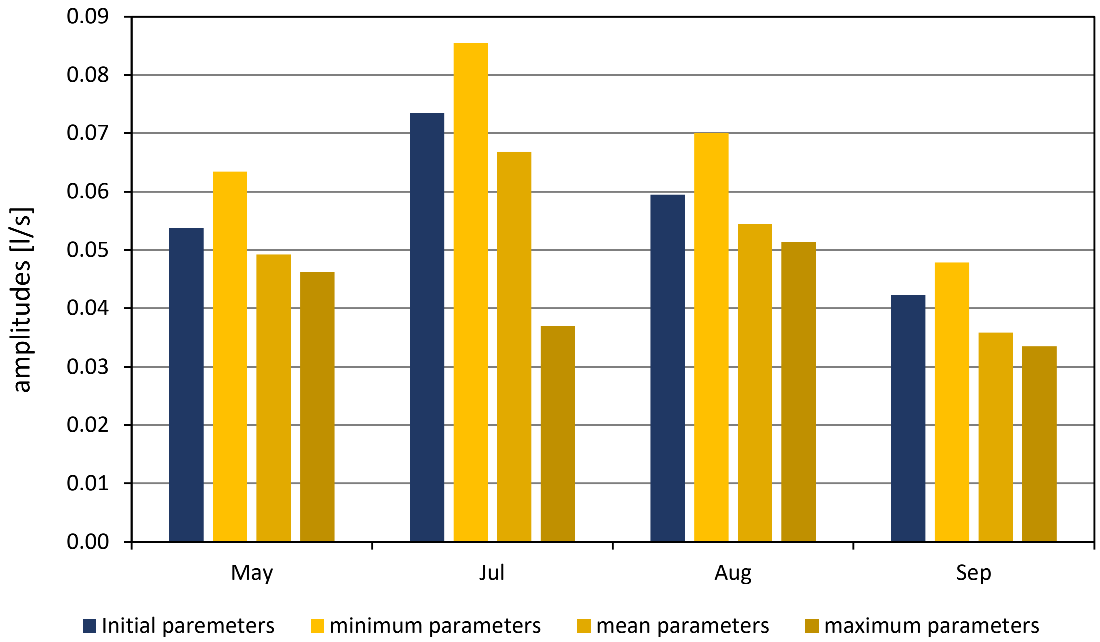

Figure 58 *Mean daily amplitudes for the respective soil hydraulic parameters*

Figure 58 reveals a clear influence of the different soil hydraulic parameters on simulated amplitudes during all simulation periods. Compared to the resulting amplitudes from the initial soil hydraulic parameter set, the minimum parameter set results in stronger daily amplitudes for all simulated months. Calculated daily amplitudes of the mean and maximum parameter sets are less pronounced. The amplitudes for the maximum parameter set show the lowest values throughout all simulation periods. However, all different boundary fluxes do show a similar general pattern, representing diurnal fluctuations adequately. Thus, only the magnitude of daily amplitudes depends on the respective soil hydraulic parameter sets.

5 Summary and discussion

This work aimed at analysing the observed diurnal discharge fluctuation in the hydrological research watershed Rosalia. The study sub-catchments cover areas of 9, 27, 146 and 222 ha. The literature study provided various explanations and processes that might cause such pronounced diurnal discharge fluctuations. Important are (i) losses due to in-stream infiltration, (ii) precipitation, (iii) Melting and freezing-thawing processes, and (iv) evapotranspiration. Gribovszki et al. (2010) stated that in temperate climates water consumption of vegetation is the most important process regarding diurnal discharge fluctuations. Following a detailed time series analysis of several hydro-meteorological obervations and to achieve a better understanding of the underlying processes causing this phenomenon, the HYDRUS model was setup for a transect in the headwaters of the catchment. HYDRUS is a software package for simulating water, heat, and solute movement in two- and three-dimensional variably saturated porous media. Several soil samples were collected and analysed to provide information on soil hydraulic parameters for the model, which is also used in scenario simulations.

To analyse the diurnal streamflow behaviour in the Rosalia, the observed discharge and runoff was analysed on a daily and seasonal temporal scale. Daily amplitudes were calculated for all gauging stations in precipitation free periods. The results showed a pronounced seasonal pattern. Maximum daily amplitudes occur during summer months throughout the area of the watershed. Only small daily amplitudes are present in winter months. In spring, amplitudes increase and decline after October. The most pronounced amplitudes are observed during the months of July and August. During these months, daily amplitudes showed diurnal fluctuations exceeding 29% of the mean daily discharge. Smallest mean amplitudes of about 13%, compared to mean daily discharge, occurred at gauge Q2 (27 ha). The maximum daily discharge is, on average, observed at about 6:00 a.m.. The minimum daily discharge occurs, on average, approximately 9 hours later at 3 p.m. at all gauges. The seasonal distribution of amplitudes and the temporal analyses suggest that the foremost process causing the diurnal fluctuations in the Rosalia is evapotranspiration.

Similar analyses for observed soil water content and air temperature were carried out in this work, as proposed by Dvořáková et al. (2014). Daily soil water content amplitudes also indicate a distinct seasonal pattern. Comparable to discharge amplitudes, the largest daily amplitudes of soil water content are detected during June and July. The median monthly soil water content and discharge amplitudes showed a particular relationship (R^2 = 0.88) over the course of the year. This highlights the distinct relationship between discharge and soil water content amplitudes during the season. The analysis of temporal occurrence of maximum and minimum values revealed a similar temporal behaviour compared to discharge observations. Maximum soil water content is observed at around 8:00 a.m. and minimum values in the later afternoon at around 6:00 p.m.. The temporal behaviour of both analysed variables also showed similar daily temporal dynamics, indicating that underlying processes causing the phenomenon are similar.

Gribovszki et al. (2010) state that climatic forcings, such as temperature, were also important factors inducing diurnal discharge fluctuations. As expected, a clear seasonal pattern of daily temperature amplitudes is evident. The analyses also indicated a clear relationship with both the temporal behaviour of soil water content and diurnal discharge fluctuations. Air temperature, a proxy having a strong connection to evapotranspiration, is one of the climatic factors regulating the plant water uptake, soil moisture content, and the transmission and release of water by plants via transpiration. Based on the amplitude and temporal analyses of discharge, soil water content and air temperature, diurnal discharge fluctuations could be indisputably attributed to evapotranspiration.

Based on these results, a HYDRUS 2D model was used to investigate and describe processes that potentially lead to diurnal discharge fluctuations. Most of the parameters used by the model were derived from literature. However, the hydraulic parameters were derived based on soil sample analyses. The results indicated highly variable soil hydraulic properties along the hillslope. Based on measured soil data collected in summer 2020, three parameter sets were determined to capture a range of potential soil hydraulic parameters.

The model was applied for four months in the vegetation period of 2018. All simulations reflected the observed low flow periods with pronounced diurnal discharge fluctuations. Generally, discharge during the selected simulation periods was mainly lower than the long-term mean discharge. Precipitation in the simulation periods was 57, 92, 64, and 93 % of the long-term monthly precipitation in May, July, August and September, respectively. This reflects the different overall hydrological conditions of the selected periods.

The simulation of the water flux between the stream and the soil domain, potentially explaining the observed diurnal discharge fluctuations, was the main focus in this study. The simulated boundary flux showed pronounced diurnal fluctuations in precipitation-free periods throughout all simulated months, very close to the observed amplitudes in discharge. The daily amplitudes of the simulated flux show similar values as the observed daily discharge amplitudes. Observed discharge peaks due to precipitation events were also present in the simulated boundary flux, since peaks in the simulated boundary flux indicated subsurface inflow to the stream. The general discharge pattern and dynamics of each respective month was mimicked successfully. In contrast, a pronounced discharge recession observed in July 2018 was not represented by the boundary flux. This is due to the fact that the lower boundary condition, representing the stream – soil matrix boundary, was set as constant. In other words, the used constant boundary head represents constant discharge conditions. Additionally, a no flux BC was used for the vertical uphill BC. This configuration does not allow any water draining into the model domain from further uphill. Therefore, possible subsurface water inflows, replenishing the soil water content along this boundary could not be represented by this configuration.

Therefore, processes that lead to a strong discharge recession after heavy rain events could not be replicated by these model settings. As this study's objective was to simulate the processes causing diurnal discharge fluctuations, the representation of such significant recession processes was not of primary interest. Nevertheless, observed diurnal discharge fluctuations during the recession period were also present in the simulated boundary flux.

As a further step, the temporal appearance of minimum and maximum discharge was compared to the temporal behaviour of the simulated boundary flux for all simulation periods. The comparison of daily minimum and maximum values of the simulated boundary flux and the observed fluctuation showed that they occurre at the same time. This indicates that the observed diurnal discharge fluctuations can be explained very well by the simulated boundary flux.

Additionally, to investigate the relationship between the simulated diurnal fluctuations and the root water uptake of the riparian vegetation, a scenario-based sensitivity analysis of the root distribution in the vicinity of the creek was performed. This was assessed by removing, in a stepwise (1m) fashion, the roots from the stream in the model domain. The sensitivity analyses clearly showed a pronounced impact on the boundary flux. In general terms, boundary fluxes and diurnal fluctuations decrease with increasing distance of the root system from the creek. Based on the simulated boundary fluxes analysis, it was shown that the root system up to a distance of 8 m has an influence on discharge . Diurnal fluctuations of the boundary fluxes were however only present, if root water uptake was assigned at nodes within 1 – 2 m distance from the creek. This indicated that only roots very close to the creek (< 2m) directly induce diurnal discharge fluctuations.

Simulated actual transpiration rates changed significantly, depending on the root distribution defined in the model. A very strong decrease of transpiration, with increasing distance of the root distribution, was observed in all simulation periods. In comparing the initial root distribution with the maximum distance of roots from the creek, as implemented in the model, the actual transpiration rates decreased up to 33 % in single months, with a mean of 25 % decrease. This demonstrated the impact of the riparian vegetation on transpiration rates along the simulated hillslope.

Due to large heterogeneity and uncertainties regarding spatio-temporal distribution, a sensitivity analyses of the boundary flux to differing soil hydraulic parameters was performed. The initial soil hydraulic parameters were estimated with pedotransfer functions available in HYDRUS based on the texture derived from a soil sample excavated in June 2015. Additionally, nine soil samples were collected in summer 2020 and analysed with the HYPROP measurement device. Based on these measurements, three characteristic soil hydraulic parameter sets for the saturated and unsaturated conditions were derived. The simulated boundary flux for the HYPROB based parameter sets was then compared to the boundary flux of the initial soil hydraulic parameters. This analysis revealed that the general pattern of diurnal fluctuations of the boundary flux was not altered significantly by using different hydraulic soil parameters. Peaks and diurnal fluctuations were reproduced adequately by all hydraulic parameter sets used. The “minimum” parameter set however showed more pronounced amplitudes. The “mean” and “maximum” parameter sets, on the other hand, showed decreasing values of daily amplitudes compared to the amplitudes simulated with the initial soil hydraulic parameters. The findings nevertheless show that soil hydraulic properties do not significantly impact the general process causing diurnal discharge fluctuations. Yet, they affect the magnitude of such.

6 Conclusion

Observation- and simulation-based evidence presented in this thesis showed that the observed diurnal discharge fluctuations within the experimental research watershed Rosalia can be attributed to root water uptake of the riparian vegetation. The processes inducing diurnal discharge fluctuations in the Rosalia were successfully simulated using HYDRUS. The simulated water flux along the stream – soil matrix boundary of a selected hillslope transect did exhibit diurnal fluctuations, adequately representing diurnal discharge fluctuations. The temporal occurrence as well as the magnitude of the diurnal discharge fluctuations were mirrored effectively by water fluxes in the model. It could be proved that diurnal discharge fluctuations in forested micro watersheds, such as the Rosalia, are dominantly caused by the riparian vegetation. Nonetheless, diurnal fluctuations in soil water content further away from the stream is also evident. However, root water uptake of such does not cause diurnal discharge fluctuations. The root water uptake in the immediate vicinity of the stream and its subsequent transpiration is proved to be the main process inducing diurnal discharge fluctuations during precipitation-free periods. Furthermore, it could be shown that transpiration rates are also highly affected by the root water uptake of the riparian vegetation. This might implicate that transpiration of the riparian vegetation plays a major role on the overall water balance. This was however not investigated in this thesis but could be assessed by further research.

List of Figures

List of Tables

REFERENCES

Baret, F., Weiss, M., 2018. Gio Global Land Component - Lot I “Operation of the Global Land Component” Algorithm Theoretical Basis Document - PRODUCT USER MANUAL 1–41.

Barnard, H.R., Graham, C.B., Van Verseveld, W.J., Brooks, J.R., Bond, B.J., McDonnell, J.J., 2010. Mechanistic assessment of hillslope transpiration controls of diel subsurface flow: a steady-state irrigation approach. Ecohydrology 130, 126–130. https://doi.org/10.1002/eco

BOKU - Forest Demonstration Centre, 2020. University Forest [WWW Document]. URL https://boku.ac.at/wabo/lehrforst/ueber-den-lehrforst (accessed 10.10.20).

BOKU - Institute of Hydrology and Water Management, 2020. Experimental research watershed Rosalia [WWW Document]. URL https://boku.ac.at/en/wau/hywa/forschungsstandorte/forsthydrologisches-versuchsgebiet-rosalia (accessed 9.10.20).

Brooks, R.H., Corey, A.T., 1964. Hydraulic properties of porous media. Hydrol. Pap. No. 3, Color. State Univ., Fort Collins.

Bursey, K.G., 2008. Quantifying hydrological fluxes of contributing hillslopes in the Weatherley Catchment. Master thesis. University of KwaZulu-Natal.

Cloke, H.L., Renaud, J.P., Claxton, A.J., McDonnell, J.J., Anderson, M.G., Blake, J.R., Bates, P.D., 2003. The effect of model configuration on modelled hillslope-riparian interactions. J. Hydrol. 279, 167–181. https://doi.org/10.1016/S0022-1694(03)00177-X

Deutscher, J., Kupec, P., Dundek, P., Holík, L., Machala, M., Urban, J., 2016. Diurnal dynamics of streamflow in an upland forested micro-watershed during short precipitation-free periods is altered by tree sap flow. Hydrol. Process. 30, 2042–2049. https://doi.org/10.1002/hyp.10771

Durner, W., 1994. Hydraulic conductivity estimation for soils with heterogeneous pore structure. Water Resour. Res. https://doi.org/10.1029/93WR02676

Dvořáková, Š., Kovář, P., Zeman, J., 2014. Impact of evapotranspiration on discharge in small catchments. J. Hydrol. Hydromechanics 62, 285–292. https://doi.org/10.2478/johh-2014-0039

ESA, 2020. PROBA-V Mission Exploitation Platform [WWW Document]. URL https://proba-v-mep.esa.int/applications/time-series-viewer/app/app.html (accessed 12.10.20).

Fürst, J., Nachtnebel, H.P., Gasch, J., Nolz, R., Stockinger, M.P., Stumpp, C., Schulz, K., 2020. Rosalia: an experimental research site to study hydrological processes in a forest catchment. Earth Syst. Sci. Data Discuss. 1–18. https://doi.org/10.5194/essd-2020-254

Gasch, J., 1985. Standortserkundung und Standortskartierung mit allgemeiner Waldbauplanung im Lehrforst Ofenbach der Universität für Bodenkultur. Master thesis. University of Natural Resources and Life Sciences, Vienna.

GBA, 1995. Geologische Karte der Republik Österreich 1:50000, 106 ASPANG-MARKT. Wien.

Gribovszki, Z., Kalicz, P., Szilágyi, J., Kucsara, M., 2008. Riparian zone evapotranspiration estimation from diurnal groundwater level fluctuations. J. Hydrol. 349, 6–17. https://doi.org/10.1016/j.jhydrol.2007.10.049

Gribovszki, Z., Szilágyi, J., Kalicz, P., 2010. Diurnal fluctuations in shallow groundwater levels and streamflow rates and their interpretation - A review. J. Hydrol. 385, 371–383. https://doi.org/10.1016/j.jhydrol.2010.02.001

Herrnegger, M., Nachtnebel, H.P., Haiden, T., 2012. Evapotranspiration in high alpine catchments - An important part of the water balance! Hydrol. Res. 43, 460–475. https://doi.org/10.2166/nh.2012.132

Hörbarth, I., 1995. Die Nebelinversionslagen im Lehrforst Rosalia als Grundlage für die Beurteilung Ihrer Wirkung auf Waldökosysteme. Dissertation.

Kosugi, K., 1999. Lognormal distribution model for unsaturated soil hydraulic properties. Water Resour. Res. 32, 2697–2703.

Liao, K.H., Lv, L.G., Yang, G.S., Zhu, Q., 2016. Sensitivity of simulated hillslope subsurface flow to rainfall patterns, soil texture and land use. Soil Use Manag. 32, 422–432. https://doi.org/10.1111/sum.12282

Lundquist, J.D., Cayan, D.R., 2002. Seasonal and spatial patterns in diurnal cycles in streamflow in the western United States. J. Hydrometeorol. 3, 591–603. https://doi.org/10.1175/1525-7541(2002)003<0591:SASPID>2.0.CO;2

Meyboom, P., 1965. Three observations on streamflow depletion by phreatophytes. J. Hydrol. 2, 248–261. https://doi.org/10.1016/0022-1694(65)90040-5

Mualem, Y., 1976. A new model for predicting the hydraulic conduc. Water Resour. Res. 12, 513–522.

Mujtaba, B., Hlaváčiková, H., Danko, M., De Lima, J.L.M.P., Holko, L., 2020. The role of stony soils in hillslope and catchment runoff formation. J. Hydrol. Hydromechanics 68, 144–154. https://doi.org/10.2478/johh-2020-0012

Pörtge, K.-H., 1996. Tagesperiodische Schwankungen des Abflusses in kleinen Einzugsgebieten als ausdruck komplexer Wasser- und Stoffflüsse. Verlag Erich Goltze GmbH KG.

Rassam, D.W., 2020. Impacts of hillslope and floodplain characteristics on groundwater dynamics: Implications for riparian denitrification. MODSIM 2005 - Int. Congr. Model. Simul. Adv. Appl. Manag. Decis. Making, Proc. 2735–2741.

Richard, A., Galle, S., Descloitres, M., Cohard, J.M., Vandervaere, J.P., Séguis, L., Peugeot, C., 2013. Interplay of riparian forest and groundwater in the hillslope hydrology of sudanian west africa (northern Benin). Hydrol. Earth Syst. Sci. 17, 5079–5096. https://doi.org/10.5194/hess-17-5079-2013

Schaap, M.G., Lej, F.J., van Genuchten, M.T., 2002. Rosetta v1.2: A computer program for estimating soil hydraulic parameters with hierarchical pedotransfer functions 251, 163–176.

Schindler, U., Durner, W., von Unold, G., Mueller, L., Wieland, R., 2010. The evaporation method: Extending the measurement range of soil hydraulic properties using the air-entry pressure of the ceramic cup. J. Plant Nutr. Soil Sci. 173, 563–572. https://doi.org/10.1002/jpln.200900201

Schmid, I., Kazda, M., 2001. Vertical distribution and radial growth of coarse roots in pure and mixed stands of Fagus sylvatica and Picea abies. Can. J. For. Res. 31, 539–548. https://doi.org/10.1139/cjfr-31-3-539

Seeger, S., Brinkmann, N., Kahmen, A., Weiler, M., 2017. Tree specific traits vs. stand leve characteristics-investigating plant water uptake in a mixed forest stand, in: Poster, EGU 2017.

Seyednasrollah, B., Young, A.M., Hufkens, K., Milliman, T., Friedl, M.A., Frolking, S., Richardson, A.D., 2019. Tracking vegetation phenology across diverse biomes using Version 2.0 of the PhenoCam Dataset. Sci. data 6, 222. https://doi.org/10.1038/s41597-019-0229-9

Šimůnek, J., Šejna, M., Saito, H., Sakai, M., van Genuchten, M.T., 2009. The HYDRUS-1D Software Package for Simulating the One-Dimensional Movement of Water, Heat, and Multiple Solutes in Variably-Saturated Media. Version 4.08.

Simunek, J., Sejna, M., van Genuchten, M.T., 1999. The HYDRUS2D software package for simulating the two-dimensional movement of water, heat, and multiple solutes in variably-saturate media 227.

Simunek, J., van Genuchten, M.T., Šejna, M., 2018. The HYDRUS Software Package for Simulating Two- and Three-Dimensional Movement of Water, Heat, and Multiple Solutes in Variably-Saturated Media. Tech. Manual, Version 3.0 274.

Stangl, K., 2013. Vergleich verschiedener Verfahren der Einheitsganglinie am Beispiel des Testeinzugsgebietes Rosalia. Master thesis. University of Natural Resources and Life Sciences, Vienna.

Széles, B., Broer, M., Parajka, J., Hogan, P., Eder, A., Strauss, P., Blöschl, G., 2018. Separation of Scales in Transpiration Effects on Low Flows: A Spatial Analysis in the Hydrological Open Air Laboratory. Water Resour. Res. 54, 6168–6188. https://doi.org/10.1029/2017WR022037

Szilágyi, J., Gribovszki, Z., Kalicz, P., Kucsara, M., 2008. On diurnal riparian zone groundwater-level and streamflow fluctuations. J. Hydrol. 349, 1–5. https://doi.org/10.1016/j.jhydrol.2007.09.014

Troxell, H.C., 1936. The diurnal fluctuation in the ground-water and flow of Santa Anna River and its meaning. Transactions. Am. Geophys. Union 17 (4), 496–504.

Ulrich, E., 1989. Abflussverhalten eines forstlichen Einzugsgebietes in der Rosalia 1983-1988 und Ansätze zu einem hydrologisch chemischen Input-Output-Modell. PhD thesis. University of Natural Resources and Life Sciences, Vienna.

UMS, 2015. Manual HYPROP, Version 2015-01. UMS GmbH, Munich, Germany.

van Genuchten, M.T., 1980. A Closed-form Equation for Predicting the Hydraulic Conductivity of Unsaturated Soils. Soil Sci. Soc. Am. J. 44, 892–898. https://doi.org/10.2136/sssaj1980.03615995004400050002x

Vogel, T., Cislerova, M., 1988. On the reliability of unsaturated hydraulic conductivity calculated from the moisture retention curve. Transp. Porous Media 3, 1–15. https://doi.org/10.1007/BF00222683

Walter, H., Lieth, H., 1967. Klimadiagramm-Weltatlas. Fischer, Jena.

Wesemann, J., 2021. Hydrologische Modellierung des natürlichen Abflussverhaltens und dessen Veränderung durch anthropogene Einflüsse. PhD thesis. University of Natural Resources and Life Sciences, Vienna.